COMPUTATIONAL 3D FRACTURE ANALYSIS IN AXISYMMETRIC MEDIA

A THESIS SUBMITTED TO
THE GRADUATE SCHOOL OF NATURAL AND APPLIED SCIENCES
OF
MIDDLE EAST TECHNICAL UNIVERSITY

BY

ÖZGE (ÜNAL) KUTLU

IN PARTIAL FULFILLMENT OF THE REQUIREMENTS
FOR
THE DEGREE OF MASTER OF SCIENCE
IN
MECHANICAL ENGINEERING

SEPTEMBER 2008

Approval of the thesis:

COMPUTATIONAL 3D FRACTURE ANALYSIS IN AXISYMMETRIC MEDIA

submitted by **ÖZGE (ÜNAL) KUTLU** in partial fulfillment of the requirements for the degree of **Master of Science in Mechanical Engineering Department, Middle East Technical University** by,

Prof. Dr. Canan Özgen _____
Dean, Graduate School of **Natural and Applied Sciences**

Prof. Dr. S. Kemal İder
Head of Department, **Mechanical Engineering** _____

Prof. Dr. Suat Kadıoğlu
Supervisor, **Mechanical Engineering Dept., METU** _____

Assoc. Prof. Dr. Serkan Dağ
Co-Supervisor, **Mechanical Engineering Dept., METU** _____

Examining Committee Members

Prof. Dr. Bülent Doyum _____
Mechanical Engineering Dept., METU

Prof. Dr. Suat Kadıoğlu _____
Mechanical Engineering Dept., METU

Assoc. Prof. Dr. Serkan Dağ _____
Mechanical Engineering Dept., METU

Prof. Dr. Haluk Darendeliler _____
Mechanical Engineering Dept., METU

Assoc. Prof. Dr. Bora Yıldırım _____
Mechanical Engineering Dept., Hacettepe Üniv.

Date: September 2, 2008

I hereby declare that all information in this document has been obtained and presented in accordance with academic rules and ethical conduct. I also declare that, as required by these rules and conduct, I have fully cited and referenced all material and results that are not original to this work.

Name, Last name: Özge (Ünal) Kutlu

Signature :

ABSTRACT

COMPUTATIONAL 3D FRACTURE ANALYSIS IN AXISYMMETRIC MEDIA

(Ünal) Kutlu, Özge

M.S., Department of Mechanical Engineering

Supervisor : Prof. Dr. Suat Kadıoğlu

Co-Supervisor: Assoc. Prof. Dr. Serkan Dağ

September 2008, 128 pages

In this study finite element modeling of three dimensional elliptic and semi-elliptic cracks in a hollow cylinder is considered. Three dimensional crack and cylinder are modeled by using finite element analysis program ANSYS.

The main objectives of this study are as follows. First, Ansys Parametric Design Language (APDL) codes are developed to facilitate modeling of different types of cracks in cylinders. Second, by using these codes the effect of some parameters of the problem like crack location, cylinder's radius to thickness ratio (R/t), the crack geometry ratio (a/c) and crack minor axis to cylinder thickness ratio (a/t) on stress intensity factors for surface and internal cracks are examined.

Mechanical and thermal loading cases are considered. Displacement Correlation Technique (DCT) is used to obtain Stress Intensity Factors.

Keywords: Fracture Mechanics, Semi-elliptic crack, Displacement Correlation Technique, Stress Intensity Factor

ÖZ

EKSENEL SİMETRİK ORTAMDA ÜÇ BOYUTLU HESAPLAMALI KIRILMA ANALİZİ

(Ünal) Kutlu, Özge
Yüksek Lisans, Makina Mühendisliği Bölümü
Tez Yöneticisi : Prof. Dr. Suat Kadıoğlu
Ortak Tez Yöneticisi: Doç. Dr. Serkan Dağ

Eylül 2008, 128 sayfa

Bu çalışmada, içi boş bir silindirdeki üç boyutlu eliptik ve yarı eliptik çatlakların sonlu elemanlar modellemesi ele alınmıştır. Üç boyutlu çatlak ve silindir sonlu elemanlar analiz programı ANSYS kullanılarak modellenmiştir.

Bu çalışmanın amaçları şöyledir: İlk olarak, silindirde değişik tipteki çatlakların modellenmesini kolaylaştırmak için Ansys Parametrik Tasarım Dili (APTD) kodları geliştirilmiştir. İkinci olarak, bu kodlar kullanılarak, problemdeki çatlak yeri, silindirin yarıçapının kalınlığına oranı (R/t), çatlak geometri oranı (a/c) ve çatlağın kısa uzunluğunun silindir kalınlığına oranı gibi parametrelerin yüzeysel ve iç çatlaklar için gerilme şiddeti faktörleri üzerindeki etkisi incelenmiştir.

Mekanik ve ısıl yüklemeler incelenmiştir. Gerilme şiddeti faktörlerinin hesaplanması için yer değiştirme korelasyon tekniği kullanılmıştır.

Anahtar Kelimeler: Kırılma Mekaniği, Yarı Eliptik Çatlak, Yer Değiştirme Korelasyon Tekniği, Gerilme Şiddeti Faktörü

To My Family

ACKNOWLEDGMENTS

I am deeply indebted to my supervisor Prof. Dr Suat Kadıoğlu for his help, guidance and patience. I would also like to express my sincere thanks to Assoc. Prof. Dr. Bora Yıldırım and to my co-supervisor Assoc. Prof. Dr Serkan Dağ for their support.

I also wish to express my thanks to my company ASELSAN Inc. for permission and supports given during this study. Finite Element Analysis was performed using the facilities in ASELSAN.

I would like to thank my family for their continuous encouragement. Especially I am thankful to my dear husband, Arda, for his support.

TABLE OF CONTENTS

LIST OF TABLES

LIST OF FIGURES

LIST OF SYMBOLS

a	: Half crack length in minor axis direction in elliptical crack
c	: Half crack length in major axis direction in elliptical crack
t	: Wall thickness of the cylinder
Ri	: Inner radius of the hollow cylinder
Ro	: Outer radius of the hollow cylinder
R	: Nominal radius of the hollow cylinder, $\frac{Ri + Ro}{2}$
L	: Length of the cylinder
KI	: Mode I Stress Intensity Factor
KI^*	: Non Dimensional Stress Intensity Factor
E	: Young's Modulus
μ	: Poisson's Ratio
P_i	: Internal Pressure
σ	: Axial Load
Φ	: Crack front angle
α	: Thermal Expansion Coefficient

CHAPTER 1

INTRODUCTION

Cylindrical structures are widely used in the industry. (Missile casings, gas and oil pipelines, pressure vessels, nuclear piping, etc.) These cylindrical structures often have severe operating conditions, such as high internal pressure, high or low operating temperatures and thermal shock. In case of pipelines also some external forces, like earthquake and wind effect these structures. Both operating conditions and external forces are important for the stress intensity factor (SIF) for longitudinal and circumferential cracks in the piping.

Crack defects are serious in these applications. To obtain the safe design conditions SIF calculations should be considered. According to have a safe design, leak-before-break (LBB) analysis is very important. Wilkowsky[1] describes this, as a methodology which ensures that a leak will be discovered prior to a fracture occurring in service. If a pressure vessel has LBB behavior, a small through-wall crack causes leakage of medium and brittle break accident will be thus prevented.

In applications mechanical and thermal loads are applied together. Application of pressure and thermal shock can cause a crack in the structure.

Fracture mechanics approach deals with the control of the fracture problem. This is possible with the calculation of the stress intensity factor (SIF).

In this study, SIF calculations of cylindrical structures for different locations of elliptic and semi-elliptic cracks are obtained using FEM.

1.1. Literature Survey

In the past there have been many studies to obtain SIF values for different types of cracks in different types of structures. There are many types of cracks for cylindrical structures; elliptic axial, fully axial, elliptic circumferential, fully circumferential, etc. Such crack problems can be solved by two or three dimensional FEM analysis. Whether 2D or 3D modelling is to be used depends on the structure, the type of the crack and the loading.

Two earlier studies relevant to the problems under consideration are as follows: In Zahoor's study [2] a number of solutions for different types of cracks in pipes are collected together. In case 1, circumferential through wall crack; in case 2, finite length circumferential part-through crack; in case 3, full circumference internal part-through crack; in case 4, finite length axial part-through crack; and in case 5, long axial part-through crack are considered and closed form SIF expressions were given. Closed formulas given for case 2 and case 4 are used for model verification in this master thesis. In verification of modeling part, the details of this comparison are given.

Raju and Newman [3] calculated stress intensity factors for internal and external circumferential semi-elliptic surface cracks in cylindrical vessels under mechanical loading.

Some of the more recent studies are briefly reviewed below. Especially Shahani and Nabavi have many studies about cracks in cylinders.

In one of the studies by Shahani and Nabavi [4] stress intensity factors are obtained for internal semi-elliptic, longitudinal cracks in a thick walled cylinder under mechanical and thermal loading. Analytical and weight function method is used for calculations. Results for the mechanically loaded internal longitudinal crack are used for model verification in this master thesis. Details of this work can be found in the following pages.

In another study of Shahani and Nabavi [5] transient thermal load is applied to a pressurized thick-walled cylinder and problem is solved analytically.

Solutions are obtained for internal longitudinal semi-elliptical crack. Thermal and mechanical boundary conditions are assumed to act on the inner and outer surfaces of the cylinder. The stress intensity factors are extracted for the deepest point and the surface points of the semi-elliptical crack using the weight function method.

In yet another study of Shahani and Nabavi [6], stress intensity factors are obtained for internal longitudinal semi-elliptical cracks in a finite length thick walled cylinder. Internal pressure is applied as a mechanical load. Especially cylinder length effect is observed in this work. The results show that the stress intensity factor increases as the cylinder length decreases, especially at the corner point of the crack compared with the deepest point.

In the study of Shahani and Habibi [7] stress intensity factors in a hollow cylinder containing a circumferential semi-elliptical crack are obtained for multi-axial loading; Axial force, bending moment and torsion. Three dimensional FEM analyses are applied.

In Miura et al. [8], a comparison of stress intensity factor solutions is made for cylinders with axial and circumferential cracks. In the study six cases of the cracked cylinders are considered. In three cases, cracks are located inside of the cylinder and in the other cases, cylinders are through-wall cracked.

Many studies are performed in METU on finite element modelling of crack problems. Five of the master theses are briefly reviewed below:

One of the earlier studies about finite element analysis of fracture mechanics problems is the study of Acar [9]. In this study, APDL codes are generated for modeling 3-D problems in Ansys. Stress Intensity Factors are calculated for different crack types in hollow and solid long cylinders. Cylinders considered are composed of either homogeneous or two dissimilar materials. Cracks studied are fully circumferential inner edge, fully circumferential outer edge, fully circumferential embedded and fully circumferential inner crack through dissimilar layers. Uniform axial and internal pressure is applied.

In another study by Atalay [10] fully longitudinal and fully circumferential cracks are considered in cylindrical and conical structures. Fully longitudinal cracks are modeled by 3-D finite element approach and fully circumferential cracks are modeled by 2-D finite element approach.

In study by İnan [11], three dimensional surface cracking problem in Functionally Graded Material (FGM) coatings bonded to homogeneous substrates is modeled by finite element analysis. The surface crack is assumed to have a semi – circular crack front profile. Mechanical and transient thermal loading is applied to the model. Structure is modeled as a plate with finite length.

In study by Sabuncuoğlu [12], crack growth analysis methods for functionally graded materials under mode I cyclic loading by using finite element technique is developed. Also the growth of an elliptical crack which is a common case in engineering applications is analyzed. The crack is assumed to be located in an infinite medium. Therefore a huge cube is modelled to simulate the infinite medium. Tension load is applied to the structure.

In study by Köşker [13], a three dimensional inclined semi-elliptic surface crack in a Functionally Graded Material coating bonded to a homogeneous substrate with a bond coat is modeled and analyzed. Transient thermal loading is applied to the model. The results obtained in this study are the peak values of mixed mode stress intensity factors and energy release rates around the crack front for various inclination angles of the semi-elliptic surface crack embedded in the FGM coating of the composite structure subjected to transient thermal loading.

1.2. Scope of the Study

In the literature, stress intensity factor solutions are obtained by different researchers for cylindrical structures. Some of them considered internal cracks and the others outer cracks. Some of them considered axial cracks and the others circumferential cracks.

In this study, different locations of elliptic and semi-elliptical cracks in a cylinder are considered. Stress intensity factors of inner surface, outer surface and embedded cracks are calculated for both axial and circumferential cracks. During the calculations, material of the cylinder is assumed to be homogeneous isotropic.

Three dimensional Finite Element Analysis (FEM) is performed by using ANSYS 11.0. To facilitate modeling for end-users, APDL codes are developed for each crack case. By using these codes, an end-user can easily model a cracked cylinder and obtain SIFs just by providing certain input values in the ANSYS environment. After solving the problem by FEM, that is, obtaining the displacement field around the crack front, SIFs are calculated by using Displacement Correlation Technique (DCT).

A number of sample results and comparisons with the existing results in the literature are provided.

CHAPTER 2

FORMULATION OF THE PROBLEM

2.1. Fracture Mechanics Basics

Fracture mechanics is the field of mechanics concerned with initiation and propagation of cracks in materials and structures. In many cases, failure of engineering structures through fracture can be fatal. For instance, growth of cracks in pressure vessels due to crack propagation could cause a fatal explosion. While designing mechanical structures, fracture mechanics analysis is needed to avoid fracture failure.

Fracture mechanics can be divided into linear elastic fracture mechanics (LEFM) and elasto-plastic fracture mechanics (EPFM). For cases where plastic zone size at the crack tip is small compared to the crack length, LEFM approach provides good results in predicting fracture.

There are three basic modes of crack tip deformations as shown in Figure 2.1; Mode I (Tension, Opening), Mode II (In-Plane Shear, Sliding), and Mode III (Out-Of-Plane Shear, Tearing)

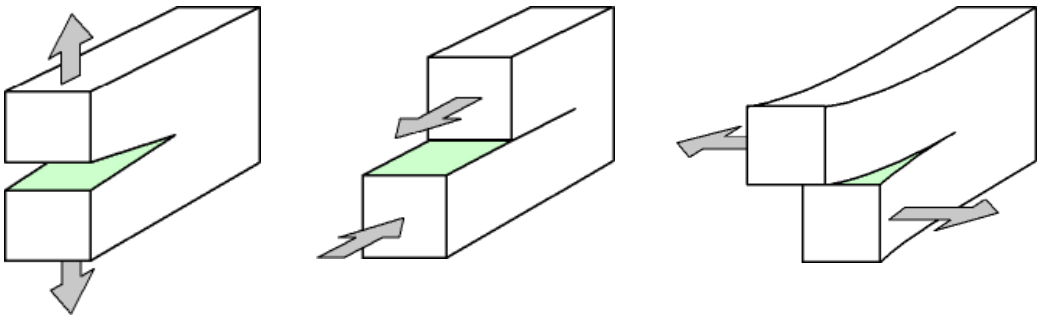

Mode I Mode II Mode III

Figure 2.1 Basic modes of crack tip deformation

In this thesis, Mode I type of loading for semi-elliptic cracks in cylinders is considered. The geometry of cracks under consideration is discussed below.

In Figure 2.2 crack face (both 2-D and 3-D), crack tip (2-D), crack front (3-D) can be seen.

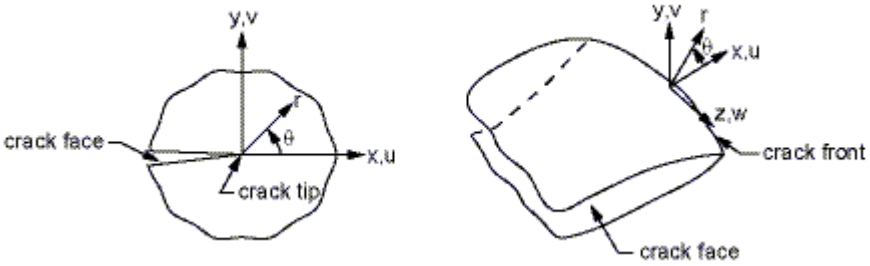

2-D Model 3-D Model

Figure 2.2 Crack face, crack front [14]

2.2. Geometry of the Problem

Six cases of semi-elliptic or elliptic cracks are examined in this study. Elliptic and semi-elliptic shapes are frequently used in the literature since good approximations to actual crack shapes can be obtained by varying a/c ratios. First three of them are axial cracks and others are circumferential cracks.

In the models, it is assumed that L>>2c to avoid free surface effects.

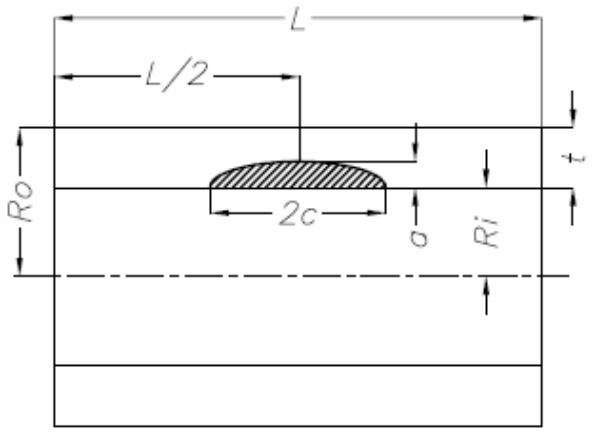

Figure 2.3 Axial inner semi-elliptic crack

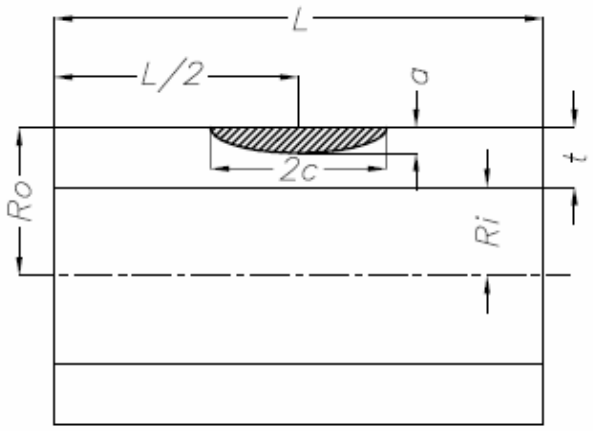

Figure 2.4 Axial outer semi-elliptic crack

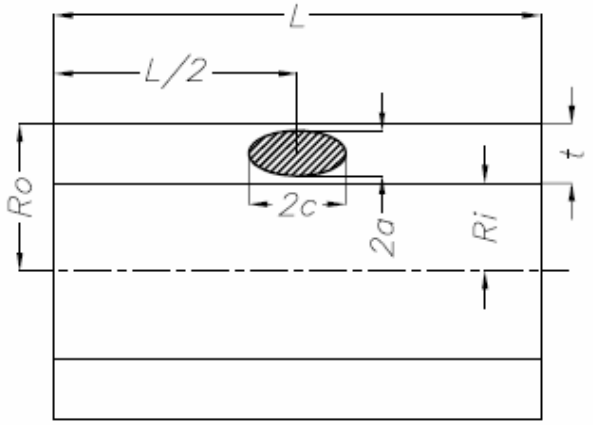

Figure 2.5 Axial embedded elliptic crack

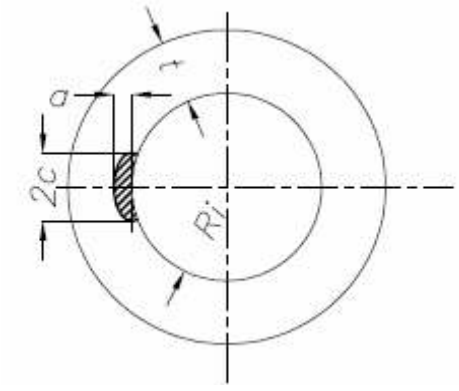

Figure 2.6 Circumferential inner semi-elliptic crack

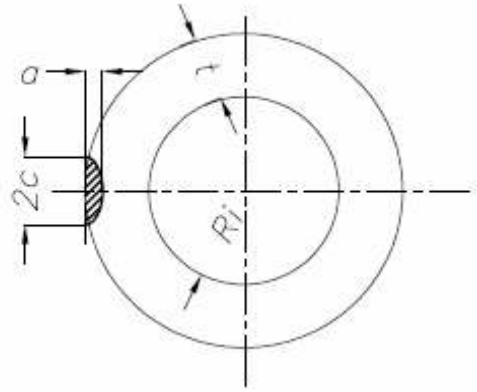

Figure 2.7 Circumferential outer semi-elliptic crack

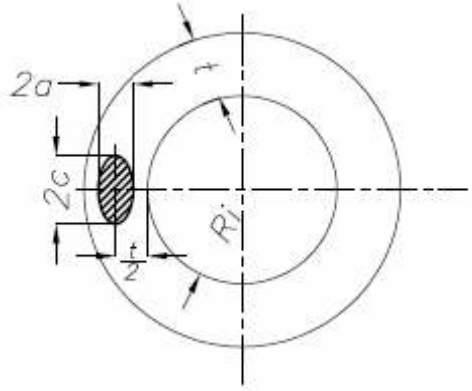

Figure 2.8 Circumferential embedded elliptic crack

In this thesis cylinders with $5 \le \frac{R}{t} \le 20$ are considered. Such cylinders are widely used as pipes, hydraulic cylinders, structural elements, etc.

2.3. Three Dimensional Crack Modeling

Finite Element analysis program ANSYS 11.0 is used for modeling. There are two ways to communicate with ANSYS program. One of them is using the ANSYS menu system, called the Graphical User Interface (GUI) and the other

way is using ANSYS commands. For the second way, either command window or APDL codes can be used. APDL codes are text documents which ANSYS commands can be written in it. From GUI, by following the instructions <*File→Read input from*>, APDL codes can be used. By the help of APDL codes, model can be changed easily. In this thesis, ANSYS Parametric Design Language (APDL) subroutines are used. Also there are some ways to interface with the GUI while using APDL. One of them is the *ASK command. By using this command, running APDL code stops to get an input from the user. In this study, *ASK command is used to get the inputs; a, c, t and R. Therefore cylinder and crack can be modeled according to different dimensions.

There are two types of modelling; top down and bottom up modelling.

Bottom up modelling: The points that define the vertices of the model are called keypoints and are the "lowest-order" solid model entities. If, in building a solid model, one first creates keypoints, and then use those keypoints to define the "higher-order" solid model entities (that is, lines, areas, and volumes), one is said to be building the model "from the bottom up." [14]

Top down modelling: The ANSYS program also gives user the ability to assemble a model using geometric primitives, which are fully-defined lines, areas, and volumes. As one creates a primitive, the program automatically creates all the "lower" entities associated with it. If the modeling effort begins with the "higher" primitive entities, one is said to be building the model "from the top down." [14]

These two methods can be combined as done in this thesis study. In this study, modelling of the crack is bottom up style and modelling of the cylinder is top down style.

MESH200, SOLID95 and SOLID 90 are used as element types for meshing.

MESH200; is a facet type meshing which means the element is subdivided into smaller portions called facets. Facets are piecewise linear surface approximations of the actual element face. MESH200 is a mesh-only element, contributing nothing to the solution. This element is used for the successive steps of meshing. More information can be found in [14].

SOLID95; is a 3-D, 20-Node structural solid element. It can tolerate irregular shapes without as much loss of accuracy. SOLID95 elements have compatible displacement shapes and are well suited to model curved boundaries. The element is defined by 20 nodes having three degrees of freedom per node: translations in the nodal x, y, and z directions. [14]. In this study prism option is used around the crack front as singular elements. According to this, O, P, W and A, B and K, L, S will be crack front nodes. X, V and T, R will be quarter nodes. Normal configuration of the element will be used for rest of the model.

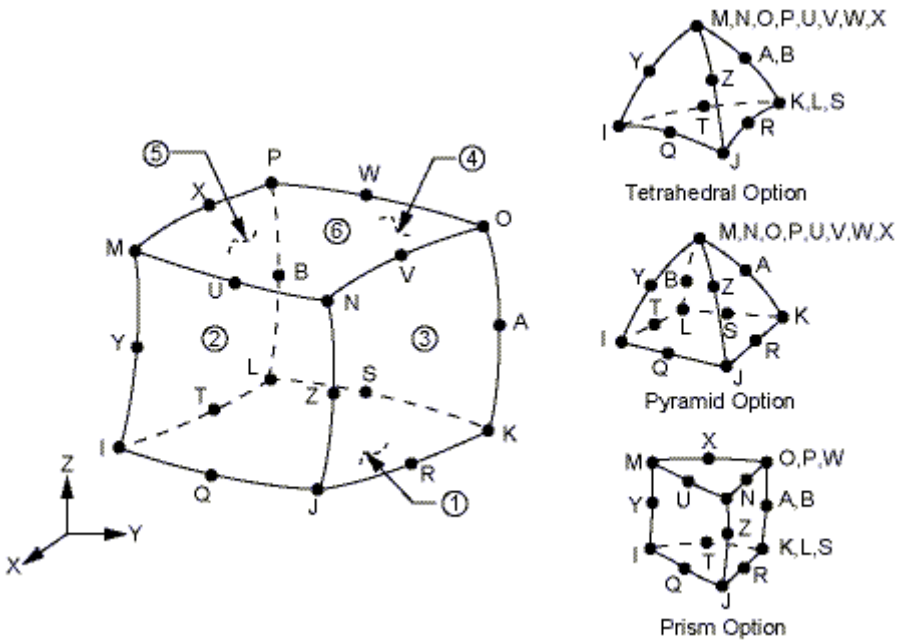

Figure 2.9 SOLID95 geometry [14]

SOLID90; is a 3-D, 20-Node thermal solid element. The element has 20 nodes with a single degree of freedom, temperature, at each node. The 20-node elements have compatible temperature shapes and are well suited to model curved boundaries. The 20-node thermal element is applicable to a 3-D, steady-state or transient thermal analysis. If the model containing this element is also to be analyzed structurally, the element should be replaced by the equivalent structural

element such as SOLID95. [14]. Prism option of SOLID90 will be used around crack front in a similar way with SOLID95. For the rest of the model regular option will be used.

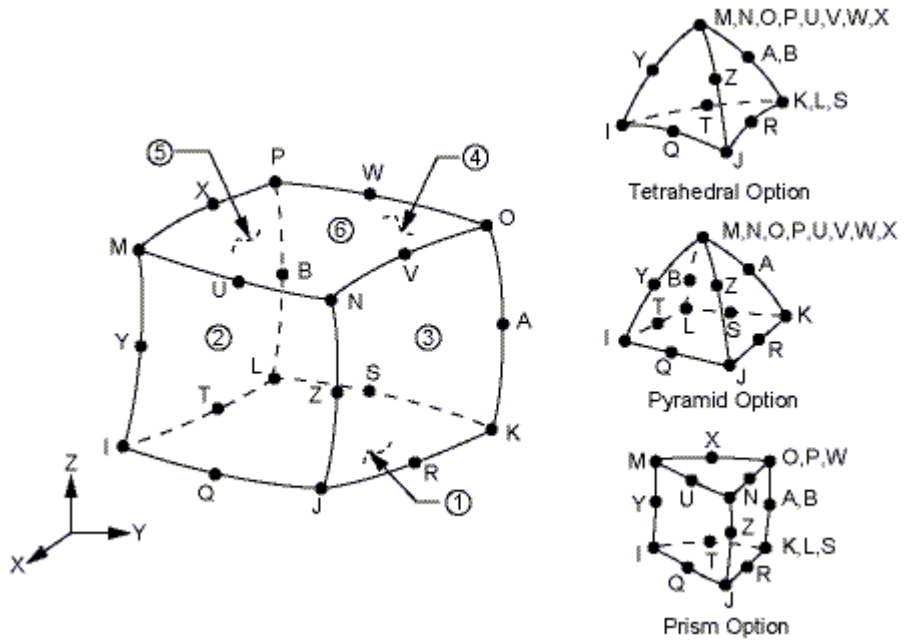

Figure 2.10 SOLID90 geometry [14]

For axial inner semi-elliptic crack, ten keypoints are generated for modelling half of the crack. Crack front is divided into eight equal parts by keypoints 1-9. 9th keypoint is at 90° and 10th keypoint is at 100°. 10th keypoint will be no more needed when cylinder is created and will be deleted.

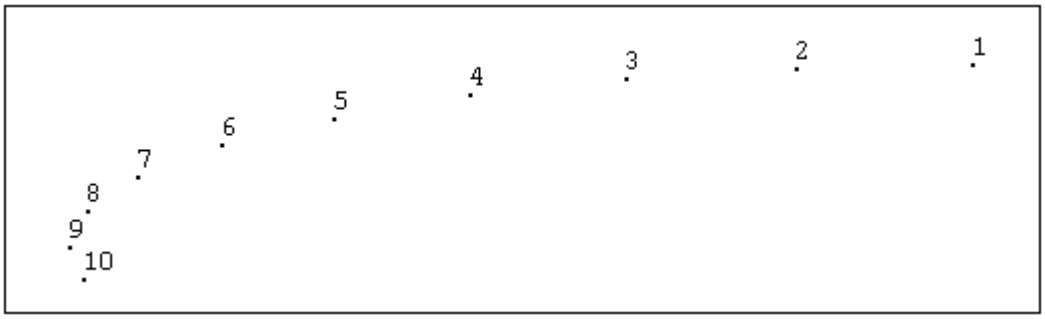

Figure 2.11 Keypoints on the crack front

A semi-circular area is created at Keypoint 1 perpendicular to the plane on which keypoints are created. This area is created to form the tubular volume around crack front in the following steps.

Then, lines are created between these keypoints following an elliptical path.

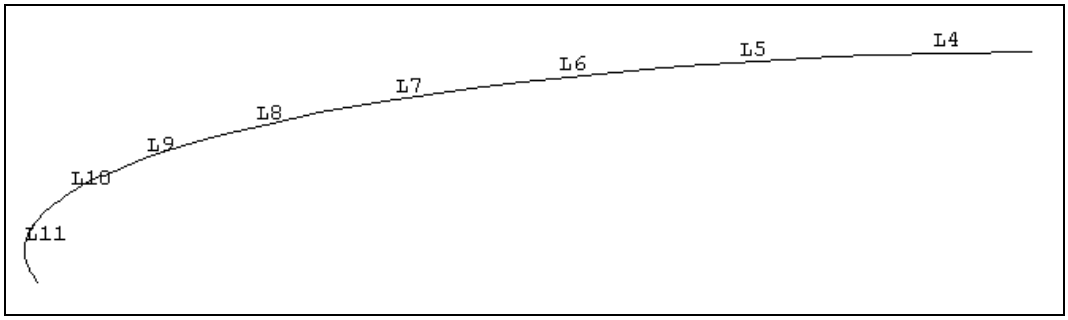

Figure 2.12 Lines on the crack front

Area created at Keypoint 1 is dragged along the lines to form a tubular volume around crack front.

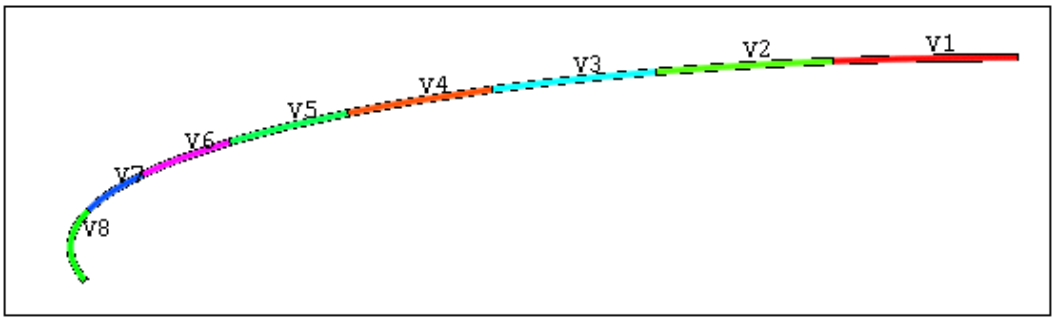

Figure 2.13 Volumes around crack front

Cylinder is generated including the crack. Cylinder is divided into sub volumes. These volumes will be meshed by different element sizes in the following steps. The smallest volume around crack will be the finest mesh. The volumes around this small volume will be less fine. Finally, rest of the cylinder

will have coarse mesh. Quarter of the cylinder is generated and symmetry boundary conditions are used at the bottom and side areas.

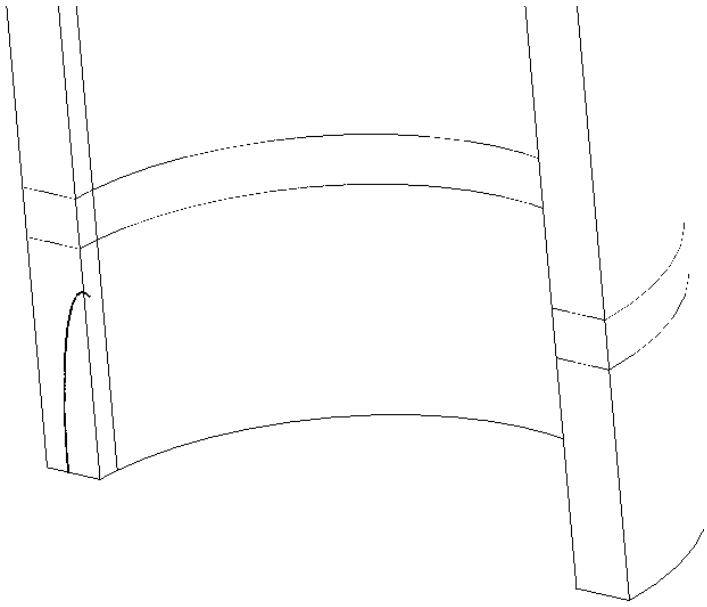

Figure 2.14 Cylindrical structure

As can be seen in Figure 2.14 there is a part of tubular volume getting out from the inner surface of the cylinder. After overlapping volumes the excess part of this volume will be deleted. The tubular volume is created for 100°. If it is created for 90°, then the volume can not reach the inner surface of the cylinder and there will be a missing volume. To avoid this situation volume is dragged along 100°, getting out of the cylinder. The situation is shown in Figure 2.15

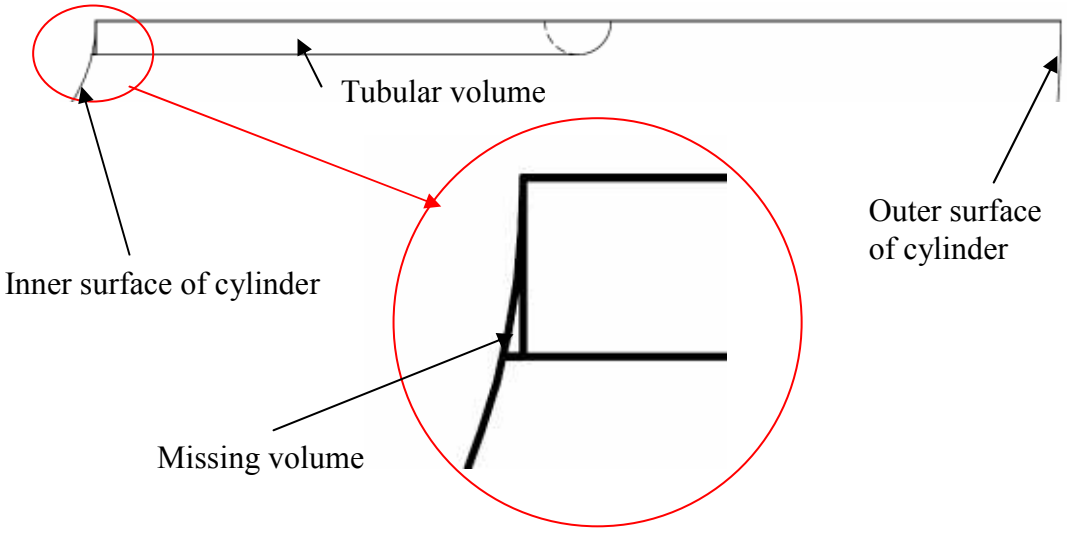

Figure 2.15 Volume around crack front and cylinder

The excess volume is deleted and now the structure is ready to be meshed.

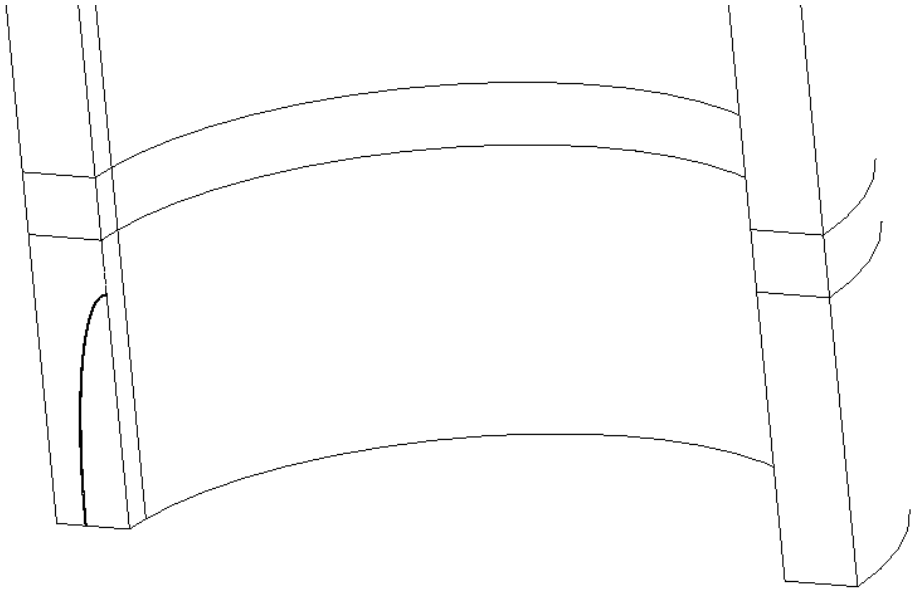

Figure 2.16 Crack and cylinder

KSCON command is used to mesh the area at the bottom of the tubular volume around crack front. KSCON, specifies a keypoint about which an area mesh will be skewed. This command defines a concentration keypoint about which an area mesh will be skewed. It is useful for modeling stress concentrations and crack tips. During meshing, elements are initially generated circumferentially about, and radially away, from the keypoint. Lines attached to the keypoint are given appropriate divisions and spacing ratios. Only one concentration keypoint per unmeshed area is allowed. The KSCON command does not support 3-D modeling. Therefore area is meshed with this command and then volumes around crack front are swept.

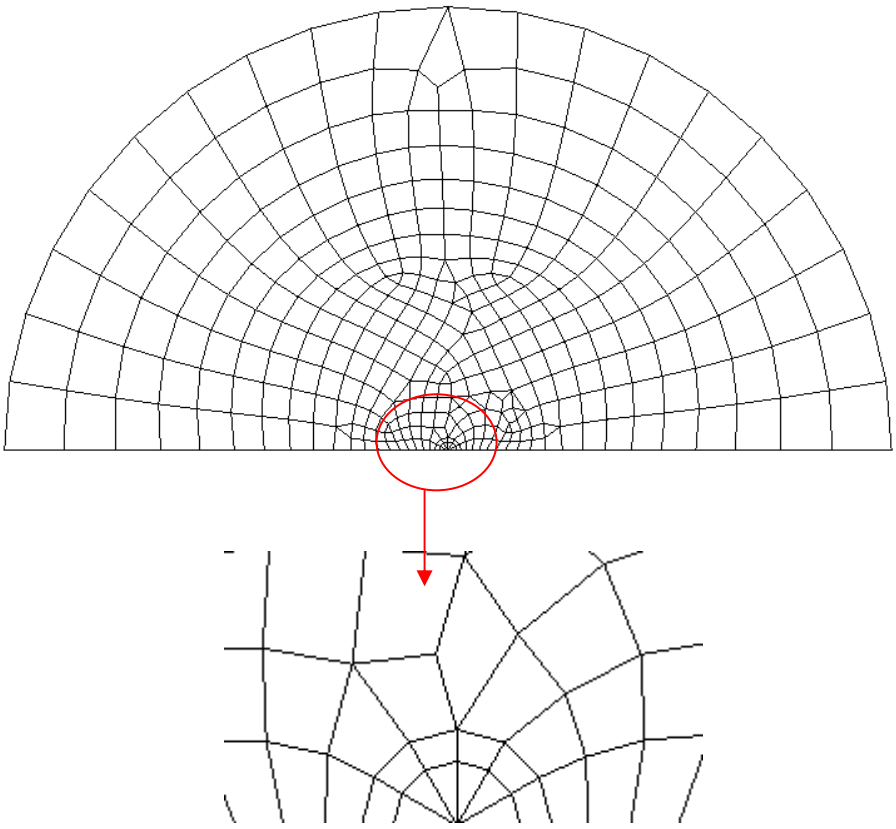

Figure 2.17 Singular elements

Singular elements around crack front can be seen in Figure 2.17. Radius of the singular elements (first row) is taken as 0.001mm. It is usually taken as a/1000 in the other thesis studies. [12], [13]

In this thesis study, working with different dimensions with one APDL code is important, so radius of singular elements is taken to be constant. Therefore after meshing, number of elements in the tubular volume for different dimensions remains constant. When calculating stress intensity factors, number of nodes at the point where SIFs are calculated will be used. Keeping the number of elements constant, makes it possible to calculate SIFs along the crack front with APDL code.

For linear elastic problems, the displacements near the crack front vary as $\sqrt{r}$, where r is the distance from the crack tip. The stresses and strains are singular at the crack tip, varying as $1/\sqrt{r}$. To produce this singularity in stresses and strains, the elements around the crack front should be quadratic, with the midside nodes placed at the quarter points. Such elements are called singular elements. [14]

Midside nodes of the elements at the first row are placed at the quarter points. These quarter point nodes are used to calculate the stress intensity factors in displacement correlation technique.

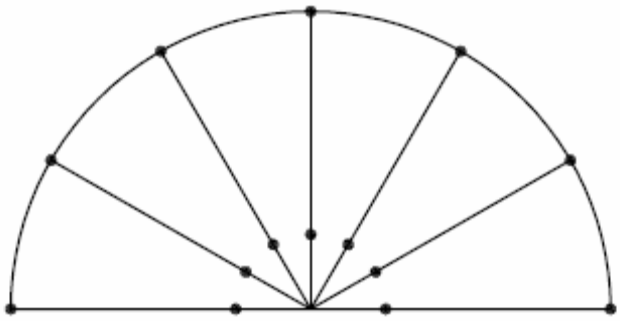

Figure 2.18 Quarter point of the singular elements

First row of elements around the crack front should be singular elements. Notice that the element shown in Figure 2.19 is wedge-shaped, with the KLPO face collapsed into the line KO. SOLID95 or SOLID 90 elements are used around crack tip.

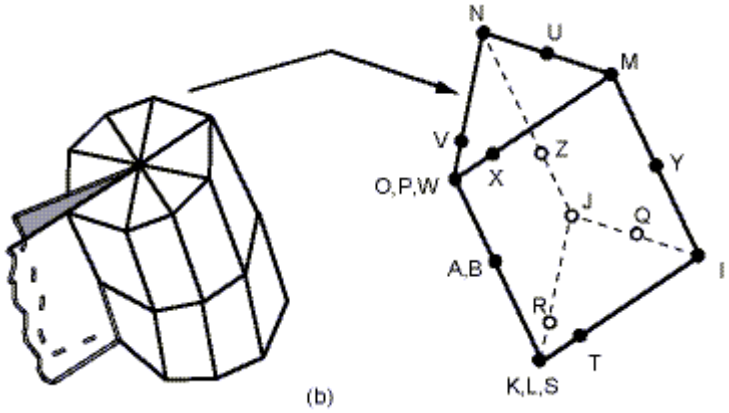

Figure 2.19 Singular elements around crack front [14]

Meshed area is swept along the crack front. Meshed tubular volume can be seen in Figure 2.20

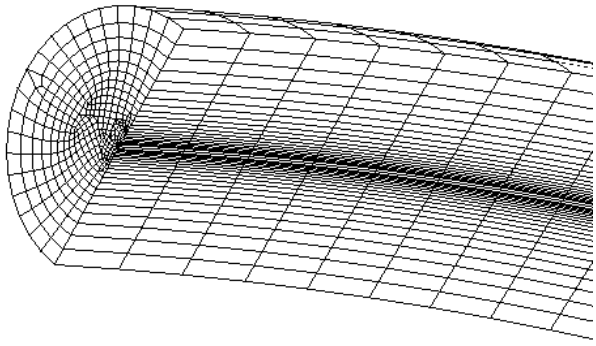

Figure 2.20 Meshing around crack front

After meshing the volume around the crack front, other volumes are meshed with different element sizes as seen in Figure 2.21.

For different a/c, a/t and R/t values, geometry of the crack and cylinder change. In some cases volumes need special effort for meshing. Different element sizes are needed with these cases.

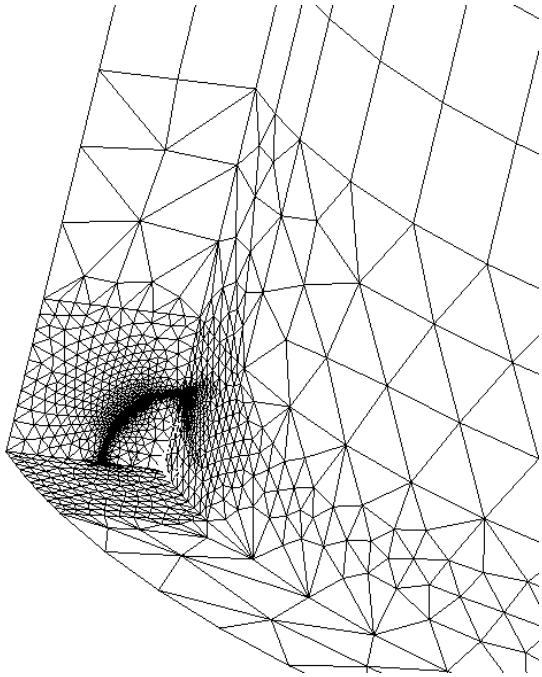

Figure 2.21 General view of the crack model

Model has two symmetry planes. Planes along longitudinal and circumferential directions are symmetry planes as seen in pink color in Figure 2.22 and 2.23. There is a point to be careful while determining symmetry areas. Crack face area should not be selected as a symmetry area. Other vise crack would not open when the load is applied to the structure.

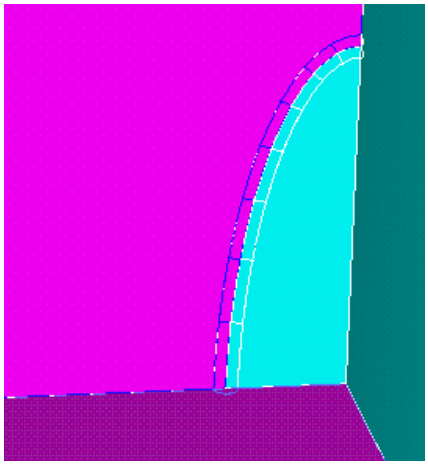

Figure 2.22 Symmetry areas around crack

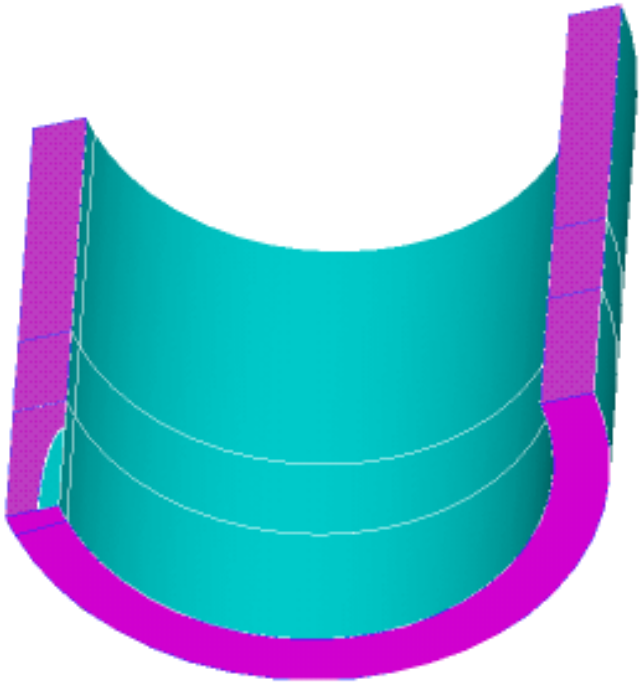

Figure 2.23 Symmetry areas of the model

The last thing before solving the problem is applying the loads. If a mechanical load is to be applied, compressive loads should be positive and tensile loads should be negative. In this study internal pressure or axial tension load is

applied according to the geometry. Therefore while internal pressure is stated as a positive amount, tensile load is stated as a negative amount.

Then the problem is solved. If it is a thermal problem, first thermal problem is solved and then thermal results file is read and structural solution is applied.

When the problem is solved, SIFs are calculated using DCT. To achieve this, formulas are written in an APDL code. After solving the problem, ANSYS calculates displacement at each node. Using this displacement values in formulas, SIFs are calculated. These formulas are given in Chapter 2.6.

Non dimensional SIFs are calculated as follows:

- Mechanical loading: $KI^* = KI / \left(\sigma * \sqrt{\pi \cdot a}\right)$

  Where σ: Internal pressure or tensile stress

- Thermal loading: $KI^* = KI / \left(E * \alpha * \Delta T * \sqrt{\pi \cdot a}\right)$

  Where ΔT: Temperature difference between inner and outer surfaces,

  α: Thermal Expansion coefficient and E: Young's modulus

Results are written to the results file at the end of this procedure.

Main steps of modeling the problem are hence listed below:

- Element types are determined.
- Keypoints along the crack front are created.
- Lines are created between these keypoints.
- Volumes around crack front are created along the lines. (as a tube)
- Cylinder is created.
- Volumes created are overlapped.
- Unneeded volumes are deleted.
- Mesh is generated.
- Symmetry planes are determined.
- Loads are applied.
- Problem is solved.
- Stress intensity factors are calculated using displacement correlation method.
- Non dimensional stress intensity factors are calculated.
- Results are written to file.

2.4.Loading Types

2.4.1.Mechanical Loading

2.4.1.1.Internal Pressure

Internal pressure is applied to the inner, outer and embedded axial cracks. Internal pressure is applied as 10 MPa in all three cases. Edges of the cylinder are stress free. This type of loading is shown in Figures 2.24 through 2.26.

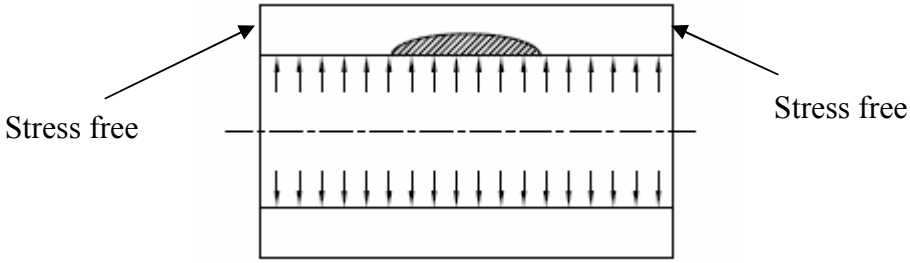

Figure 2.24 Axial inner semi-elliptic crack

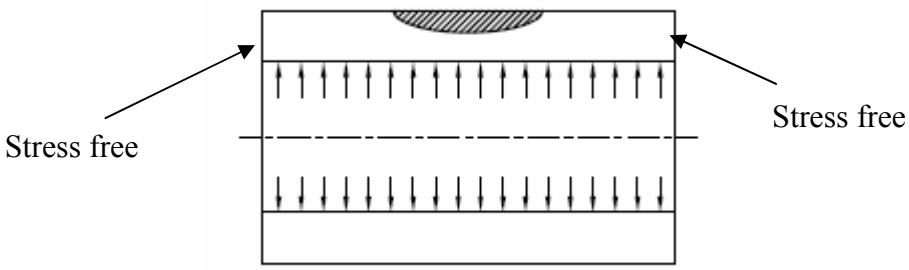

Figure 2.25 Axial outer semi-elliptic crack

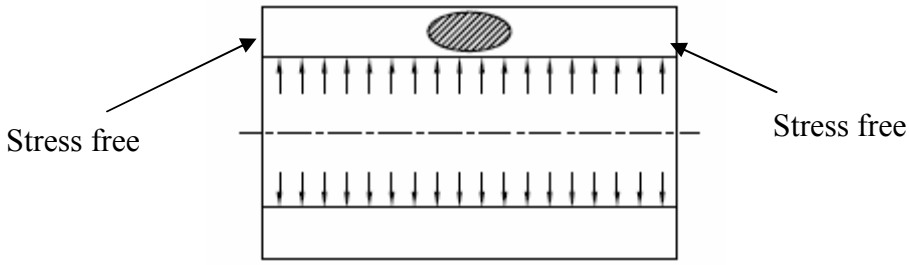

Figure 2.26 Axial embedded crack

2.4.1.2.Axial Loading (Tension)

Axial tension loading is applied to the inner, outer and embedded circumferential cracks. Axial stress applied is 10 MPa in all three cases. Crack is located in the symmetry plane. This type of loading is shown in Figure 2.27.

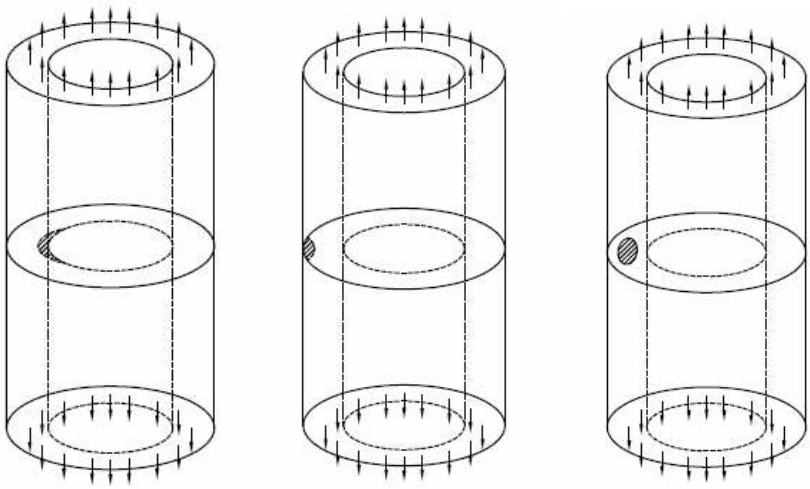

Figure 2.27 Partial circumferential cracks

2.4.2.Thermal Loading

Surface temperatures at the inner and outer wall surfaces are specified for the conduction and subsequent thermoelasticity problem. As a result a temperature profile develops across the wall thickness.

The general behaviour of a crack in the cylinder wall can be explained as follows: First assume that the crack is closed when the temperature is uniform across the walls. Upon specifying different temperatures on the inner and outer wall surfaces the cooler surface will tend to contract or expand less compared to the hotter surface. As a result cooler side will experience tension due to the

constraint applied by the hotter side and hotter side would experience compression.

Then a surface crack which is completely within the tensile surface region (cooler side) of the wall would tend to open. If the crack is deep enough, part of it would be in the compressive stress zone, hence it would close. Such problems are known as crack contact problems, but they are not addressed in this thesis. In this thesis study, thermal loads are applied to semi-elliptic surface cracks only.

As stated before, in this thesis, steady-state thermal loading is applied to the structure. Inside temperature is lower than the outer temperature for structures with inside surface crack for both axial and circumferential cracks. Vice versa, inside temperature is greater than the outer temperature for structures with external surface crack for both axial and circumferential cracks. Thermal boundary conditions are shown in Figure 2.28.

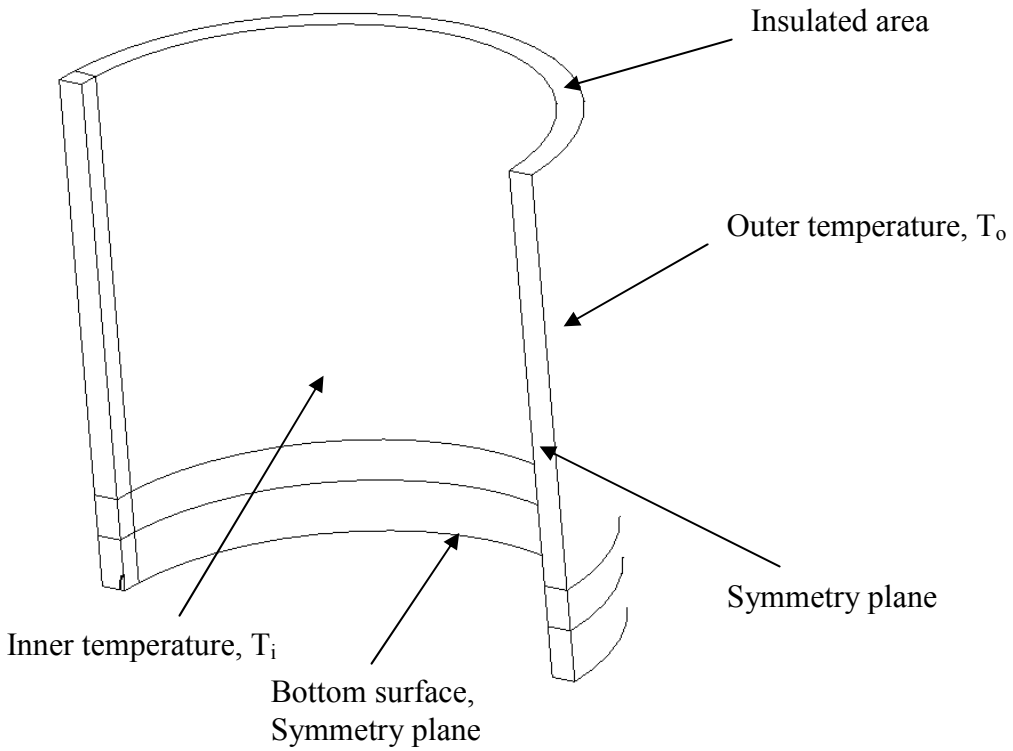

Figure 2.28 Boundary conditions of thermal loading

In Figure 2.29 thermal analysis results of an axial inner semi-elliptical crack is shown. In this problem dimensions are; a=0.5mm, c=1.25mm, t=2.5mm, R=50mm and L=500mm. Temperature of -100°C is applied inner surface of the cylinder while temperature of 100°C is applied at the outer surface.

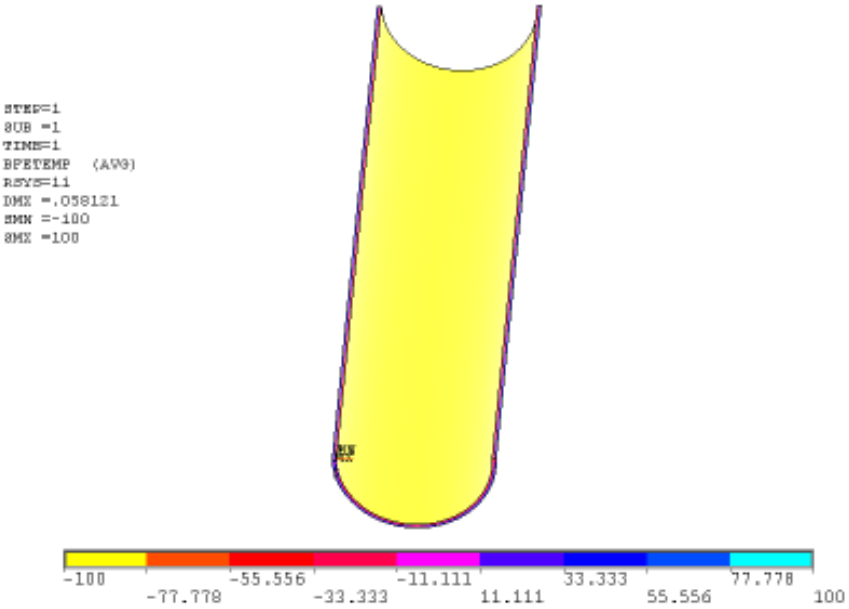

Figure 2.29 Results plot of thermal analysis

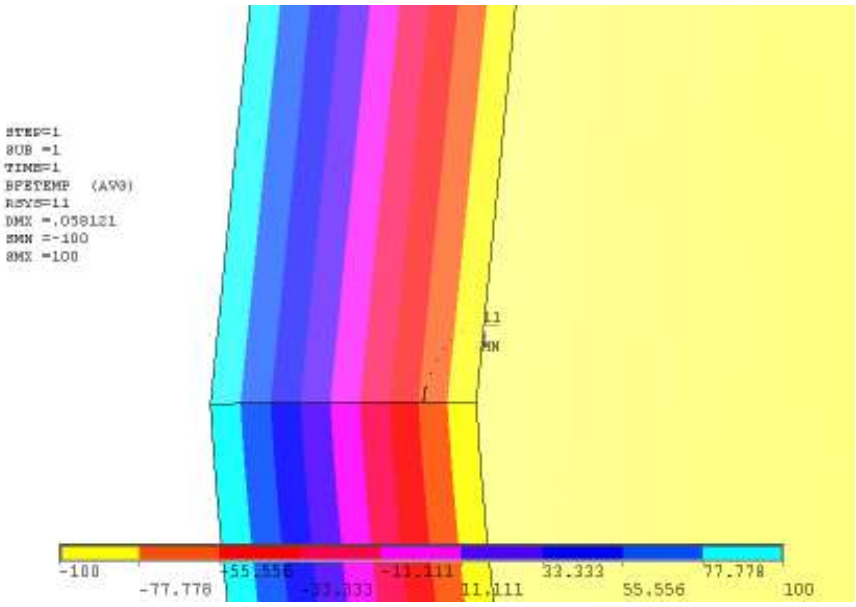

Figure 2.30 Closer view of Figure 2.29

2.5.Displacement Correlation Technique

By solving the problem, displacements of nodes are calculated by ANSYS. Then stress intensity factors are calculated by using displacement correlation technique. This technique has been used earlier in [11], [12], and [13]. Displacements of three nodes are used for this calculation. First one is a point on the crack front. Second and third nodes are the nodes next to the first one. They are on the crack face. The line passes through these three nodes is perpendicular to crack front.

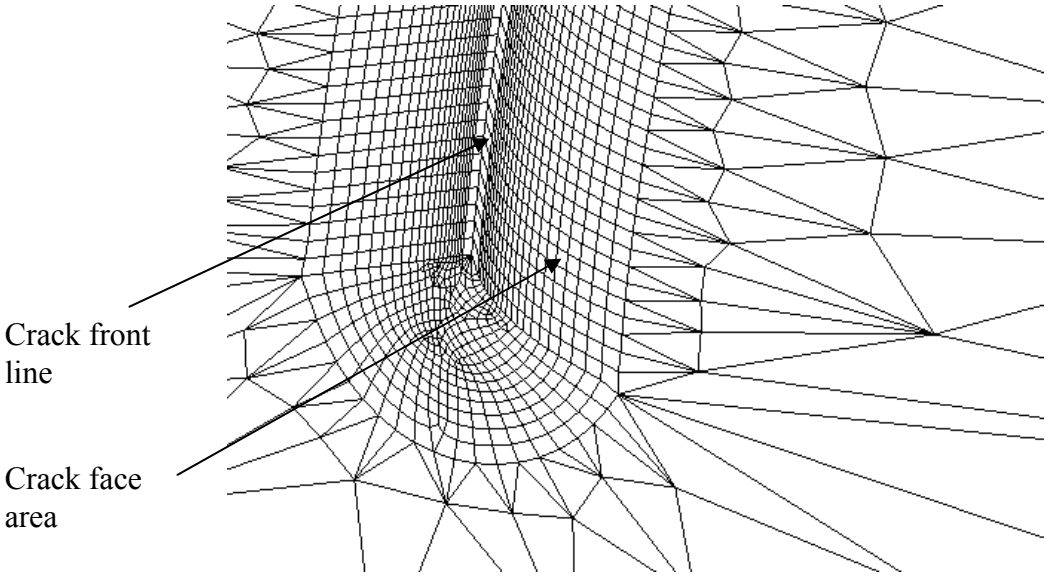

Figure 2.31 Opened crack view after loading

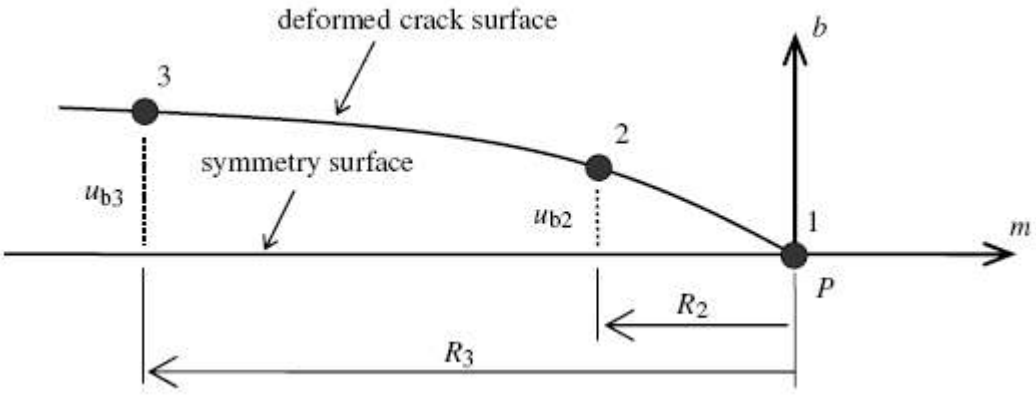

Figure 2.32 Nodes used in DCT

Then SIF is obtained as follows:

$$X = \frac{R_3^{3/2} u_{b2} - R_2^{3/2} u_{b3}}{\sqrt{R_2}\sqrt{R_3}\left(R_3 - R_2\right)} \tag{4}$$

$$K_I = \frac{\sqrt{2\pi} \times E}{4\left(1-\nu^2\right)} \cdot X \tag{5}$$

$$K_I = \frac{\sqrt{2\pi} \times E}{4\left(1-\nu^2\right)} \cdot \left[\frac{R_3^{3/2} u_{b2} - R_2^{3/2} u_{b3}}{\sqrt{R_2}\sqrt{R_3}\left(R_3 - R_2\right)} \right] \tag{6}$$

The expressions above are taken from [13]

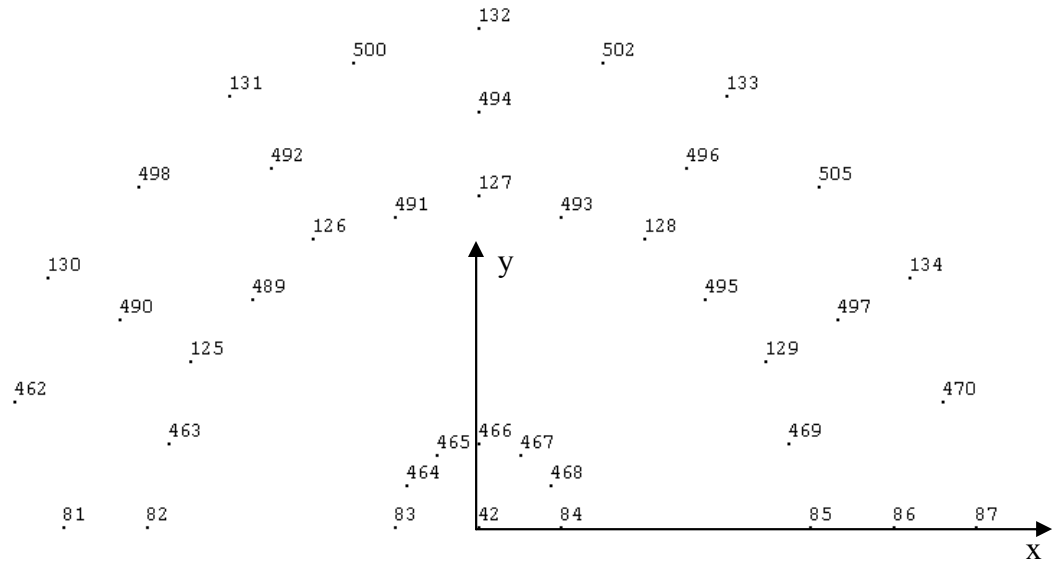

Figure 2.33 Schematic view of nodes

To find the SIF along the crack front, a coordinate system is placed at a crack tip node, for example Node 42. X axis should be along the crack face and y axis should be perpendicular to the crack face area. Nodes 42, 84, and 466 should be used to place the coordinate system. These nodes are shown in Figure 2.33. The nodes to be used in SIF calculations are Nodes 42, 84 and 85. u_{b2} and u_{b3} is calculated by using displacements of these three nodes.

2.6.Verification of Modeling

2.6.1.Embedded crack in an infinite medium

At first, stress intensity factors for an embedded crack in a homogeneous infinite plate are calculated to verify the model. Closed form equations from [15] are used as benchmark solution. SIF is given as follows:

$$K_1 = \sigma\sqrt{\frac{\pi \cdot a}{Q}} f(\Phi) \tag{1}$$

$$Q = 1 + 1.464\left(\frac{a}{c}\right)^{1.65} \tag{2}$$

$$f(\Phi) = \left[\sin^2(\Phi) + \left(\frac{a}{c}\right)^2 \cos^2(\Phi)\right]^{1/2} \tag{3}$$

In order to obtain the problem of a crack in an infinite medium, with the current modelling approach, a huge cylinder with an embedded crack is modelled as shown in Figure 2.34.

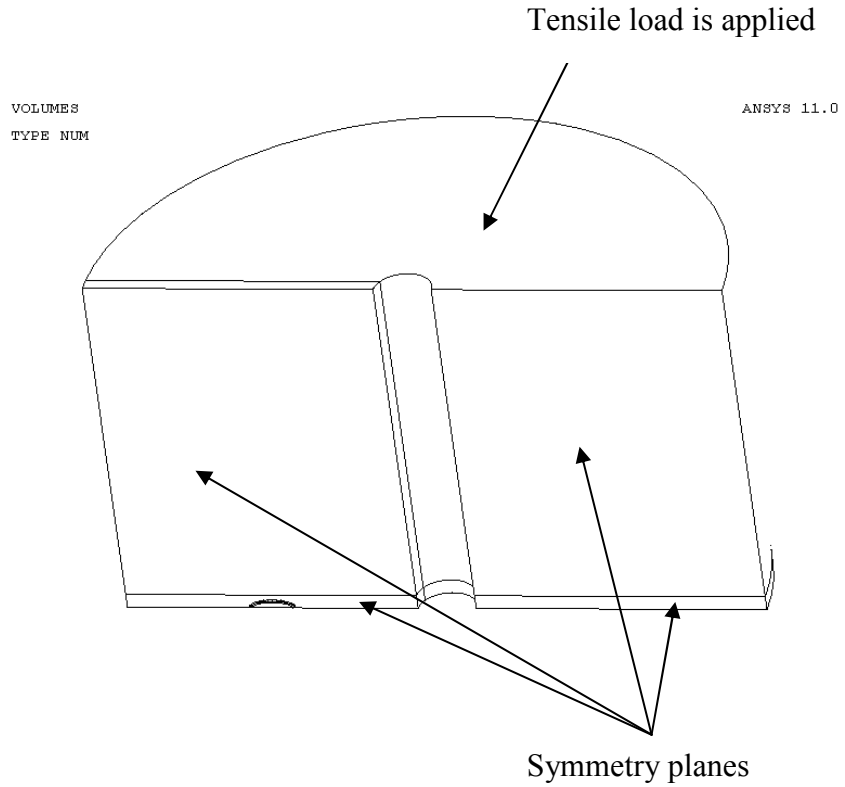

Figure 2.34 Model of an elliptic crack in a huge cylinder

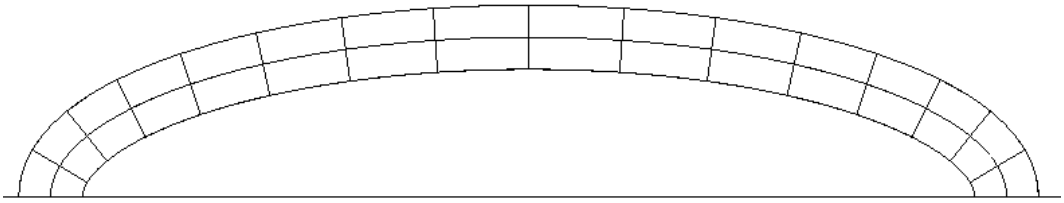

Figure 2.35 Closer view of the crack

Then, half of an elliptic crack is modeled in the huge cylinder to eliminate free surface effects as seen in Figure 2.35. Symmetry planes are defined. 50073 elements and 160351 nodes are used for the model. SIFs are calculated from finite element model using DCT.

Dimensions of the model:

a =0.5mm, minor radius of the crack

c =1.5mm, major radius of the crack

σ =10Mpa, tension load applied

Ri=4 mm, Inner diameter of the cylinder

Ro=44 mm, Outer diameter of the cylinder

L/2=25mm, Half length of the cylinder

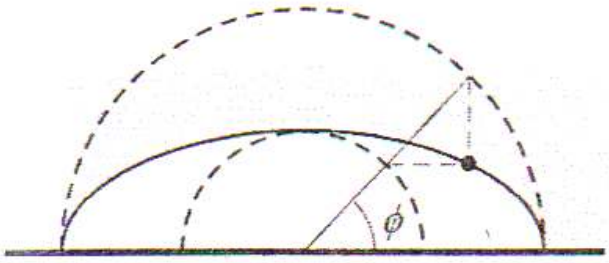

Figure 2.36 Description of Φ angle

SIF values calculated from closed form equation and FEM model are compared in Table 2.1.

Table 2.1 SIFs for embedded crack in an infinite medium

ϕ	Closed formula, KI $MPa\sqrt{mm}$	FEM Analysis,KI $MPa\sqrt{mm}$	Error (%)
0,00	6,5000	6,4762	0,3662
11,25	6,9473	6,9227	0,3541
22,50	7,8916	7,8697	0,2775
33,75	8,8722	8,8270	0,5095
45,00	9,7211	9,6858	0,3631
56,25	10,3923	10,3250	0,6476
67,50	10,8740	10,8140	0,5518
78,75	11,1634	11,0950	0,6127
90,00	11,2599	11,1910	0,6119
101,25	11,1634	11,1020	0,5500
112,50	10,8740	10,8280	0,4230
123,75	10,3923	10,3420	0,4840
135,00	9,7211	9,6829	0,3930
146,25	8,8722	8,8385	0,3798
157,50	7,8916	7,8628	0,3649
168,75	6,9473	6,9229	0,3512
180,00	6,5000	6,4667	0,5123

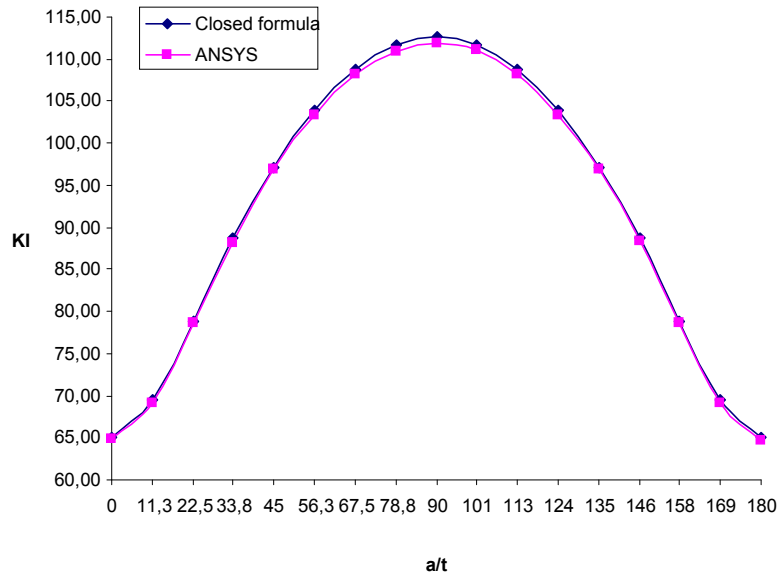

Figure 2.37 Comparison of results with closed formula

2.6.2.Axially cracked cylinder, Nabavi [4]

As a second benchmark solution, SIFs for an axially cracked cylinder are considered.

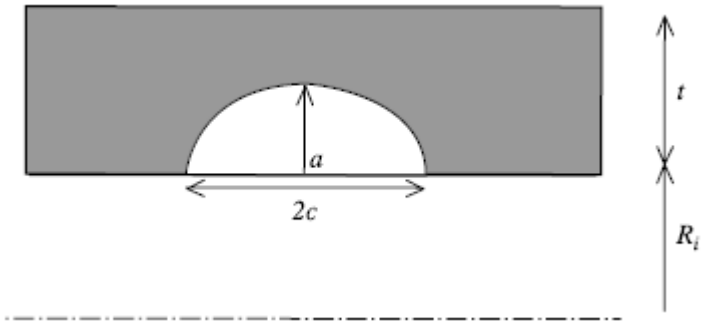

Figure 2.38 Geometry used by Nabavi [4]

In Nabavi's study [4], SIFs are obtained for internal semi-elliptic, longitudinal cracks in a thick walled cylinder. Analytical and weight function method is used for calculations. 10Mpa internal pressure is applied in the problem. Internal pressure is applied both on the inner surface of the cylinder and the crack face. Results are given as a graph in Nabavi's study [4].

SIF values calculated at the deepest points are compared for the following geometries.

Table 2.2 Comparison of KI* Nabavi[4] and ANSYS model

a (mm)	R/t	a/c	a/t	KI*, NABAVI [4]	KI*, ANSYS	ERROR %
2	4.5	0.2	0.2	5.80	5.75	0.86
3	4.5	0.2	0.3	6.20	6.03	2.74
4	4.5	0.2	0.4	6.70	6.51	2.84
5	4.5	0.2	0.5	7.25	7.15	1.38
6	4.5	0.2	0.6	8.00	7.91	1.13
7	4.5	0.2	0.7	8.90	8.78	1.35
8	4.5	0.2	0.8	9.90	9.88	0.20
2	4.5	0.4	0.2	5.70	5.00	12.28
3	4.5	0.4	0.3	5.75	5.09	11.48
4	4.5	0.4	0.4	5.90	5.23	11.36
5	4.5	0.4	0.5	6.20	5.44	12.26
6	4.5	0.4	0.6	6.40	5.71	10.78
7	4.5	0.4	0.7	6.80	6.03	11.32
8	4.5	0.4	0.8	7.20	6.47	10.14
2	4.5	1.0	0.2	5.30	3.49	34.15
3	4.5	1.0	0.3	5.30	3.45	34.91
4	4.5	1.0	0.4	5.30	3.43	35.28
5	4.5	1.0	0.5	5.30	3.42	35.47
6	4.5	1.0	0.6	5.30	3.42	35.47
7	4.5	1.0	0.7	5.30	3.45	34.91
8	4.5	1.0	0.8	5.30	3.52	33.58

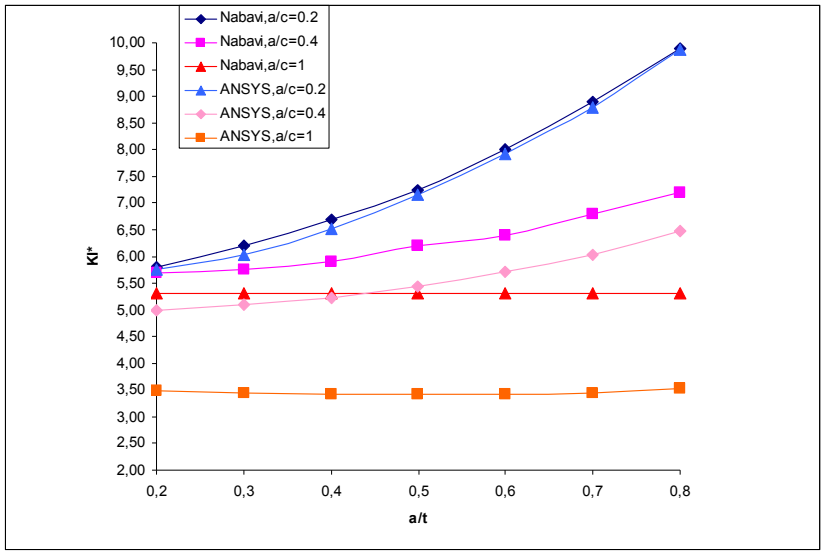

Figure 2.39 Comparison of results with Nabavi [4]

As it can be seen in the Figure 2.39, results follow similar paths. However as a/c aproaches to 1, ANSYS analysis results get lower than Nabavi's results.

2.6.3.Axially cracked cylinder, Zahoor-case 4 [2]

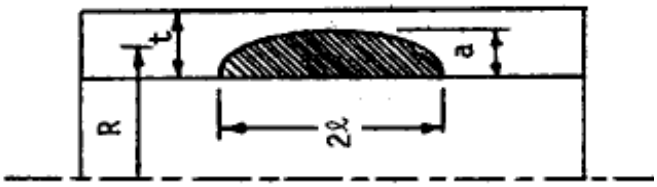

Figure 2.40 Geometry used by Zahoor-case 4 [2]

In Zahoor's study [2] a number of solutions for different types of cracks in pipes are collected together. At first longitudinal crack will be investigated. 10MPa internal pressure is applied in this case. R/t is considered as 5,10 and 20.

Table 2.3 Comparison of KI* Zahoor-case 4 [2] and ANSYS model

a (mm)	R/t	a/l	a/t	KI*, Zahoor-case4 [2]	KI*, ANSYS	ERROR %
2	5	0.2	0.2	6.80	6.41	5.68
2	5	0.4	0.2	5.85	5.57	4.78
2	5	0.8	0.2	4.62	4.34	6.06
4	5	0.2	0.4	7.82	7.25	7.30
4	5	0.4	0.4	6.21	5.84	5.89
4	5	0.8	0.4	4.74	4.32	8.89
6	5	0.2	0.6	9.17	8.82	3.84
6	5	0.4	0.6	6.64	6.36	4.16
6	5	0.8	0.6	4.88	4.39	10.01
1	10	0.2	0.2	12.64	11.91	5.09
1	10	0.4	0.2	10.89	10.40	4.52
1	10	0.8	0.2	8.60	8.07	6.18
2	10	0.2	0.4	14.46	13.88	4.04
2	10	0.4	0.4	11.54	11.12	3.68
2	10	0.8	0.4	8.83	8.20	7.13
3	10	0.2	0.6	16.81	16.73	0.46
3	10	0.4	0.6	12.32	12.14	1.43
3	10	0.8	0.6	9.08	8.37	7.84
1	20	0.2	0.2	23.77	22.89	3.69
1	20	0.4	0.2	20.49	20.02	2.31
1	20	0.8	0.2	16.18	15.47	4.39
1	20	0.2	0.4	27.04	25.87	2.01
1	20	0.4	0.4	21.70	21.68	0.10
1	20	0.8	0.4	16.61	15.82	4.77
2	20	0.2	0.6	31.16	32.37	-1.10
2	20	0.4	0.6	23.10	23.58	-2.07
2	20	0.8	0.6	17.08	16.26	4.82

In this case, similar to the Nabavi's study [4], internal pressure is applied both on the inner surface of the cylinder and the crack face. Difference of this study from Nabavi's is the length parameters of the cylinder and the crack. Nabavi's study is applicable only for R/t is 4.5. The study of Zahoor is valid for R/t is 5, 10 and 20. In Zahoor's study it is remarked that the closed form expression gives better than 4 percent accuracy but when 2a/l=12 and a/t<0.4, this expression gives results that are overestimated by as much as 8 percent.

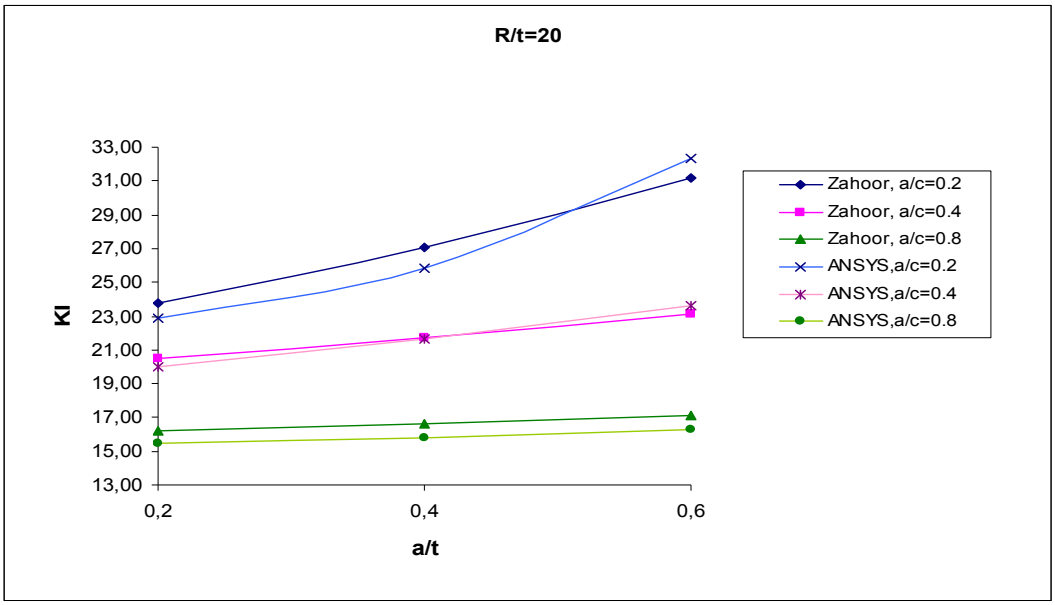

Figure 2.41 Comparison of results for R/t=20

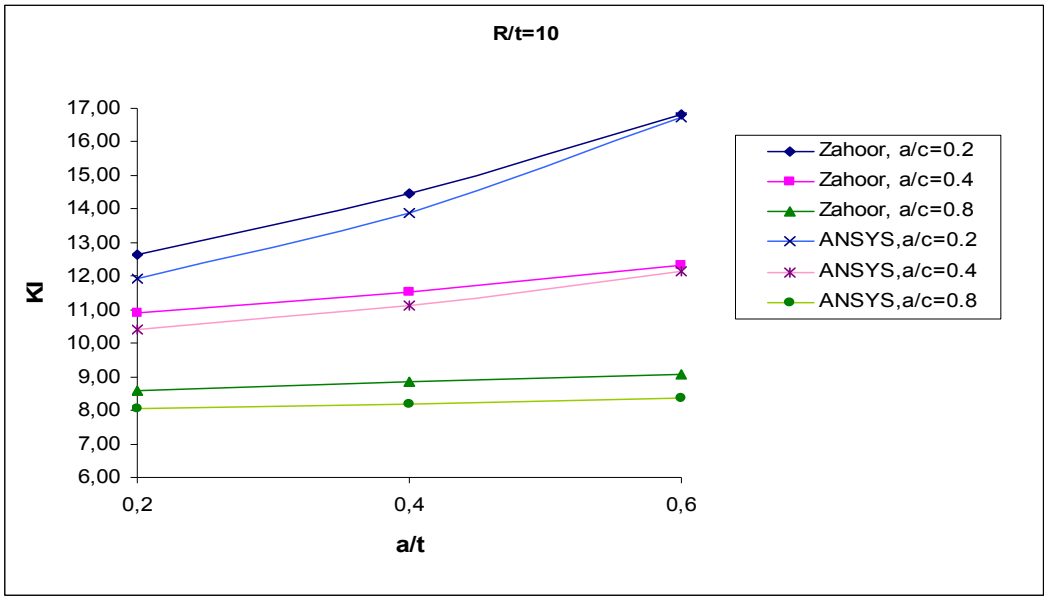

Figure 2.42 Comparison of results for R/t=10

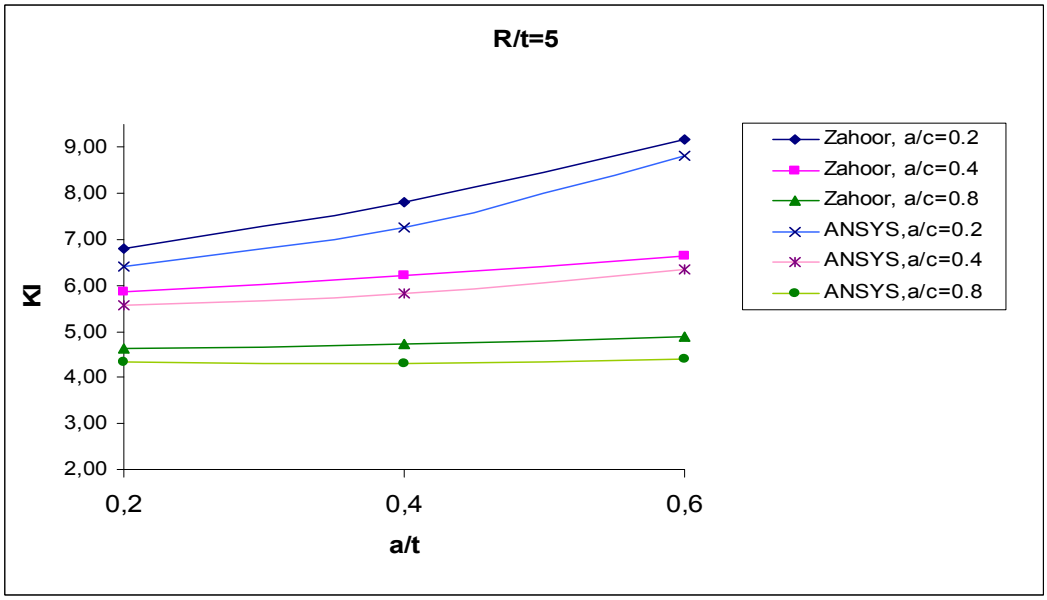

Figure 2.43 Comparison of results for R/t=5

When R/t=20, results of Zahoor's study and ANSYS model are closer but as R/t decreases, results get different. For all R/t values graphics follow parallel lines. As a result, when crack aspect ratio (a/c) is not close to 1, the difference between results from ANSYS model and literature is acceptable. Therefore in the sample cases the maximum value for a/c is taken as 0.8.

2.6.4.Circumferentially cracked cylinder, Zahoor-case 2 [2]

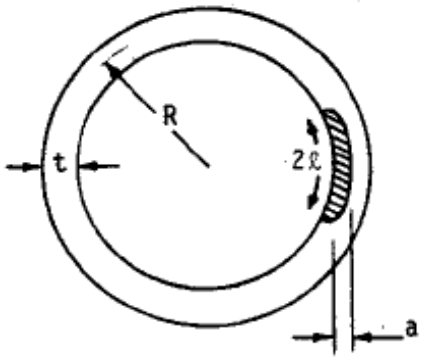

Figure 2.44 Geometry used by Zahoor-case 2 [2]

In Zahoor's study [2], circumferential semi-elliptic crack is considered as case 2. In this case, 10MPa tensile load is applied to the cylinder. R/t is considered as 5,10 and 20.

SIF values for semi-elliptic circumferential crack at the inner surface of the cylinder are compared for ANSYS and Zahoor's results[2].

Table 2.4 Comparison of KI* Zahoor-case 2 [2] and ANSYS model

a (mm)	R/t	a/c	a/t	KI*, Zahoor-case2 [2]	KI*, ANSYS	ERROR %
2	5	0.2	0.2	1.03	1.13	-10.28
2	5	0.4	0.2	0.92	0.97	-4.81
2	5	0.8	0.2	0.78	0.75	4.25
4	5	0.2	0.4	1.14	1.22	-6.96
4	5	0.4	0.4	0.97	1.00	-3.71
4	5	0.8	0.4	0.81	0.76	6.41
6	5	0.2	0.6	1.30	1.33	-1.99
6	5	0.4	0.6	1.03	1.05	-1.68
6	5	0.8	0.6	0.85	0.77	9.20
1	10	0.2	0.2	1.06	1.12	-5.74
1	10	0.4	0.2	0.95	0.98	-2.37
1	10	0.8	0.2	0.82	0.75	8.69
2	10	0.2	0.4	1.18	1.21	-2.32
2	10	0.4	0.4	1.01	1.00	0.64
2	10	0.8	0.4	0.86	0.75	12.42
3	10	0.2	0.6	1.37	1.34	2.07
3	10	0.4	0.6	1.08	1.05	2.68
3	10	0.8	0.6	0.91	0.77	15.08
1	20	0.2	0.2	1.09	1.11	-1.96
1	20	0.4	0.2	0.99	0.96	2.18
1	20	0.8	0.2	0.87	0.74	14.68
1	20	0.2	0.4	1.24	1.21	2.48
1	20	0.4	0.4	1.05	1.00	5.00
1	20	0.8	0.4	0.92	0.76	18.11
2	20	0.2	0.6	1.44	1.33	8.06
2	20	0.4	0.6	1.14	1.06	7.22
2	20	0.8	0.6	0.98	0.77	21.75

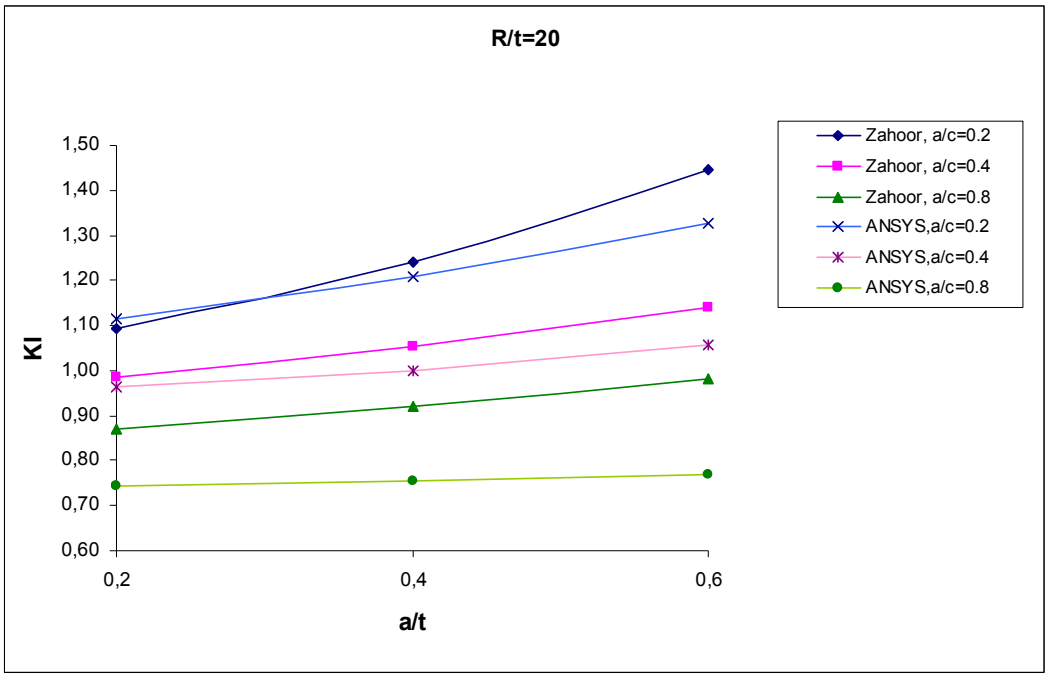

Figure 2.45 Comparison of results for R/t=20

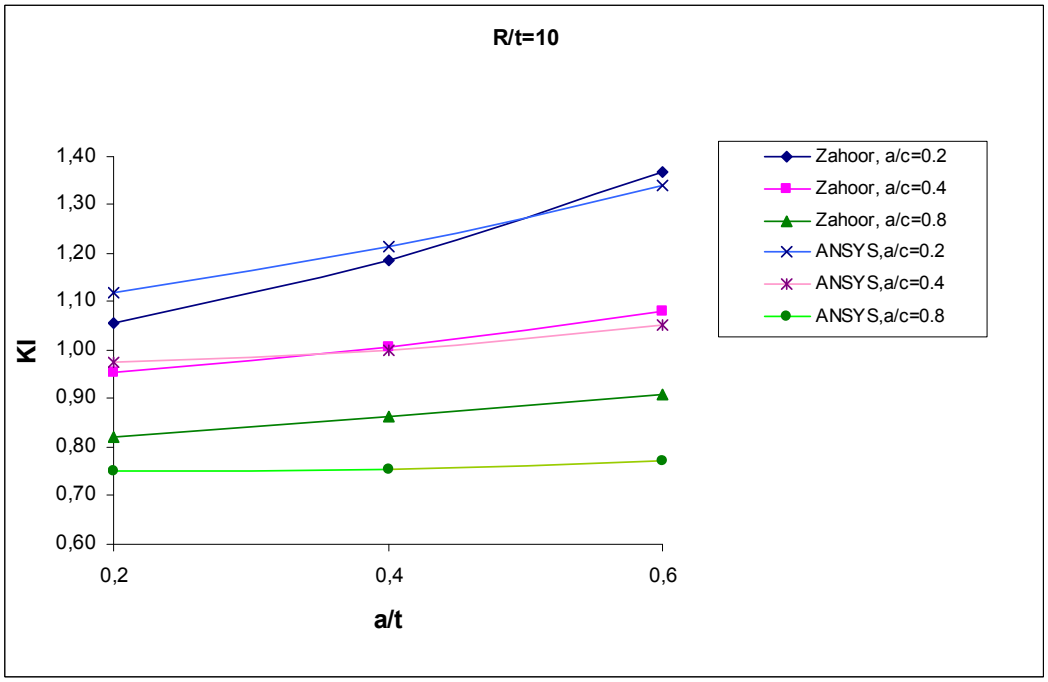

Figure 2.46 Comparison of results for R/t=10

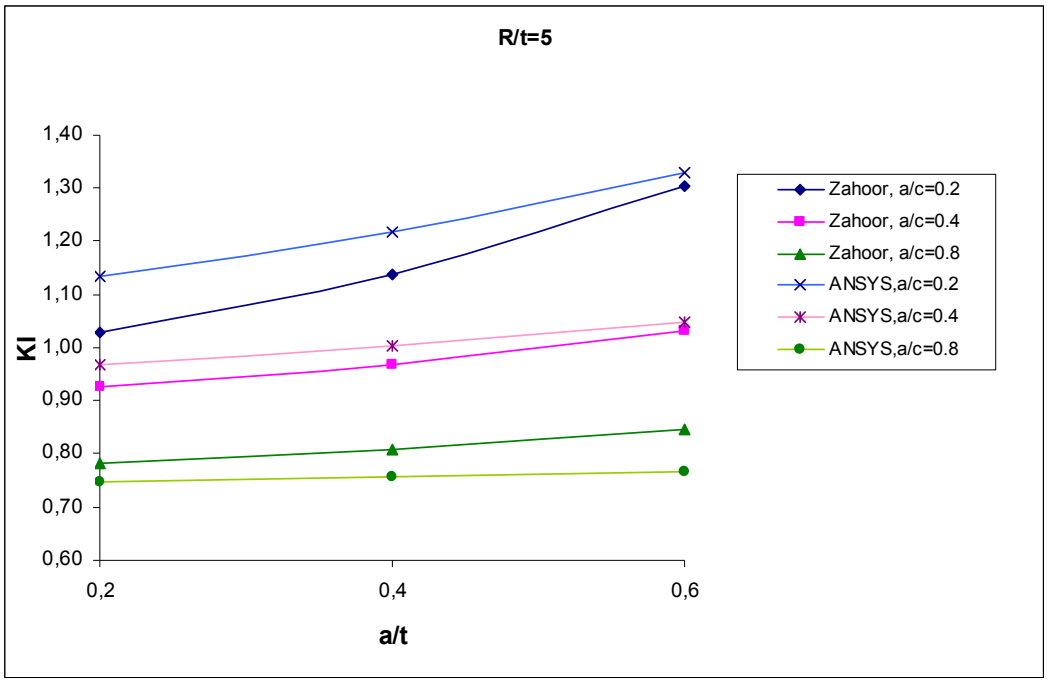

Figure 2.47 Comparison of results for R/t=5

As R/t increases, the difference between the results of Zahoor[2] and ANSYS model increases for a/c=0.8. Similar to the axial inner crack case (case 4), as crack aspect ratio (a/c) increases, difference between the results increases. It is noticed that when a/c=0.8 and R/t=20, the error is as much as 15-20 percent. As R/t and a/c decreases, also error decreases.

CHAPTER 3

NUMERICAL RESULTS

Ten types of analysis are performed in this study.

TYPE1: Partial Inner Axial Semi-elliptic crack, inner pressure is applied

TYPE2: Partial Outer Axial Semi-elliptic crack, inner pressure is applied

TYPE3: Embedded Axial Elliptic crack, inner pressure is applied

TYPE4: Partial Inner Circumferential Semi-elliptic crack, tensile load is applied

TYPE5: Partial Outer Circumferential Semi-elliptic crack, tensile load is applied

TYPE6: Embedded Circumferential Elliptic crack, tensile load is applied

TYPE7: Partial Inner Axial Semi-elliptic crack, thermal load is applied

TYPE8: Partial Outer Axial Semi-elliptic crack, thermal load is applied

TYPE9: Partial Inner Circumferential Semi-elliptic crack, thermal load is applied

TYPE10: Partial Outer Circumferential Semi-elliptic crack, thermal load is applied

Material is assumed to be a homogeneous isotropic material. Stainless steel is considered in this analysis. Material properties are:

Young's modulus: 200 GPa
Poissons ratio: 0.3
Coefficient of thermal expansion: 1.2 E-5 1/K
Thermal Conductivity: 25 W/m.K
Mass Density: 7600 kg/m3
Specific Heat: 460 J/kg.K

3.1.MECHANICAL LOADING

3.1.1.Inner Pressurized Partial Inner Axial Semi-elliptic Crack

Crack front angle 0 is the deepest point and angle 90 is the surface point. Inner pressure of magnitude 10Mpa is applied to the structure. Results are obtained for different R/t, a/t and a/c values. R is 50mm for all cases but a, c and t change. Results are obtained for the following values;

R/t = 5, 10 and 20

a/t = 0.2, 0.4 and 0.6

a/c = 0.2, 0.4 and 0.8

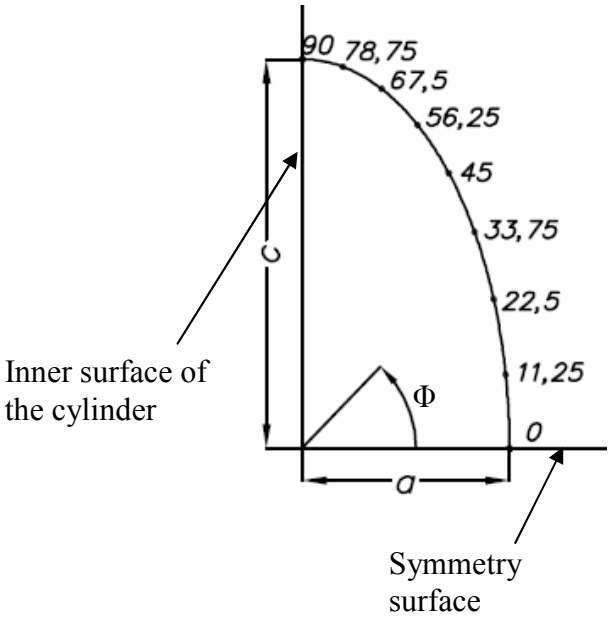

Figure 3.1 Crack front angles for Type1 and Type7

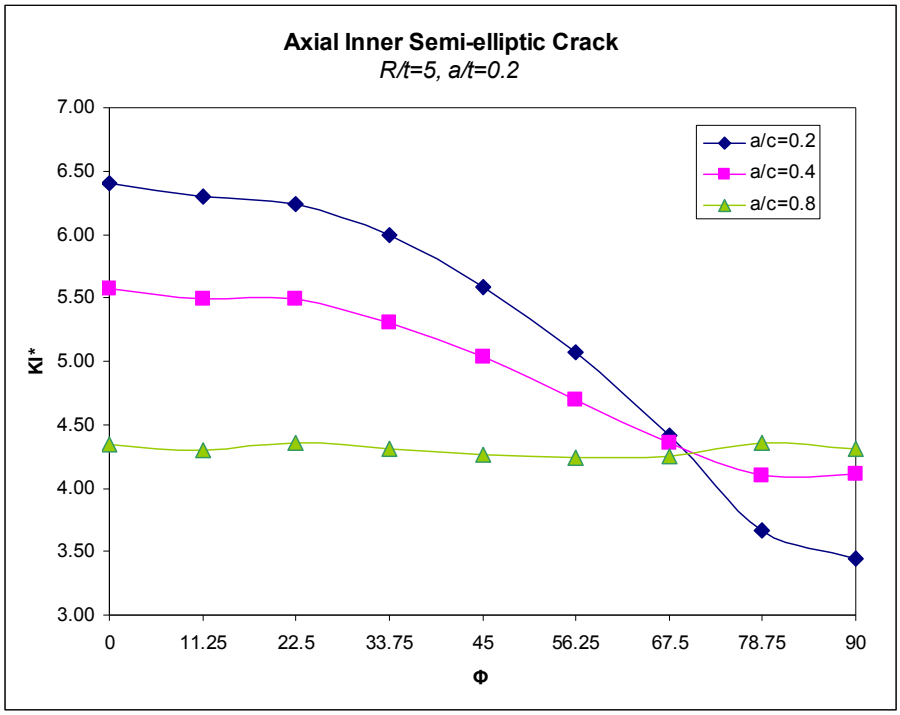

Figure 3.2 KI* versus Φ, Type1, R/t=5, a/t=0.2

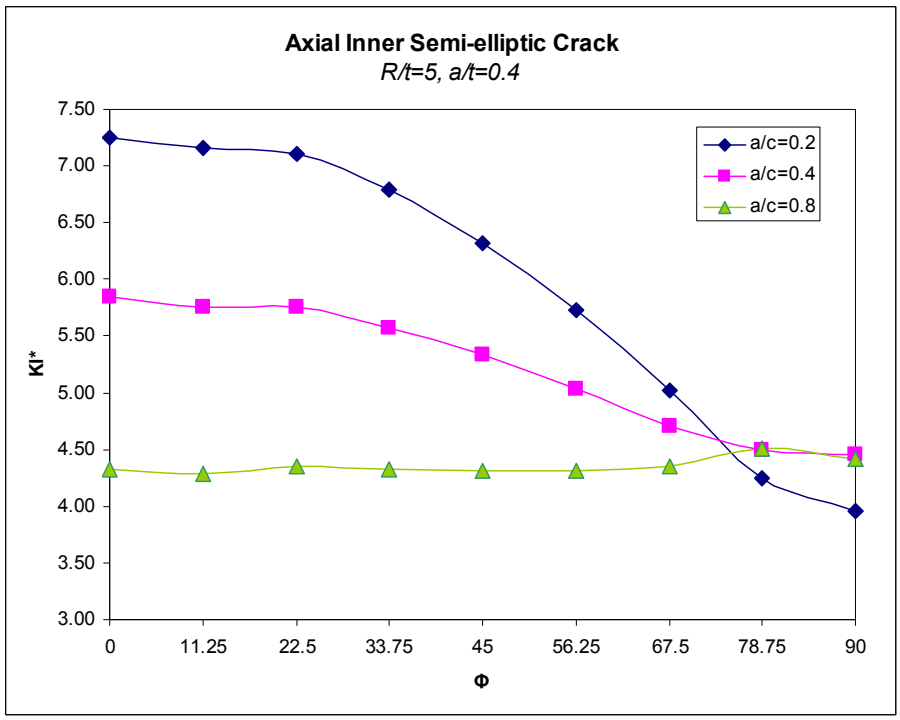

Figure 3.3 KI* versus Φ, Type1, R/t=5, a/t=0.4

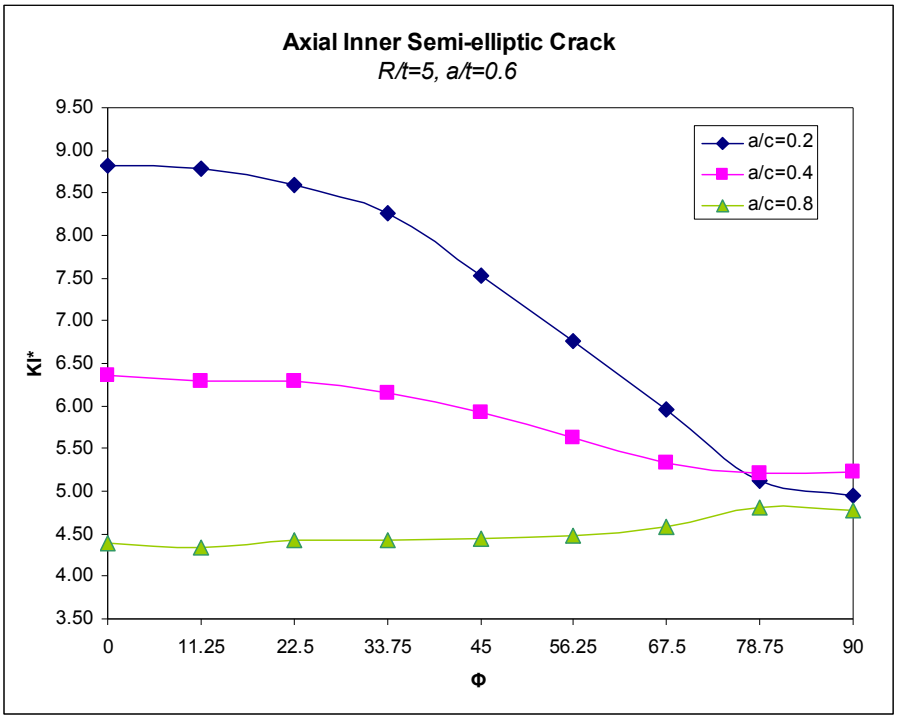

Figure 3.4 KI* versus Φ, Type1, R/t=5, a/t=0.6

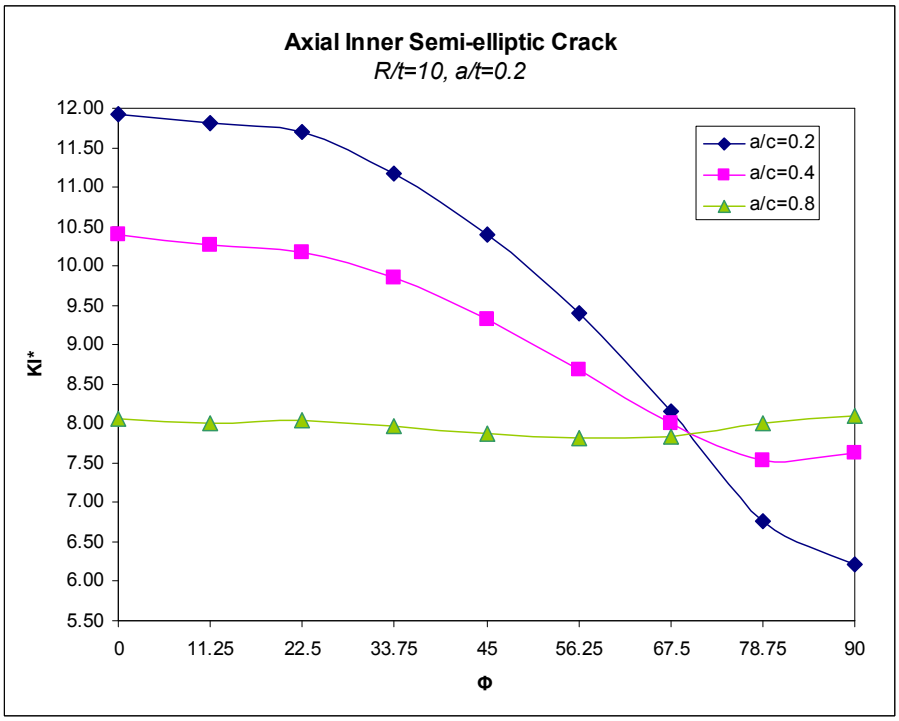

Figure 3.5 KI* versus Φ, Type1, R/t=10, a/t=0.2

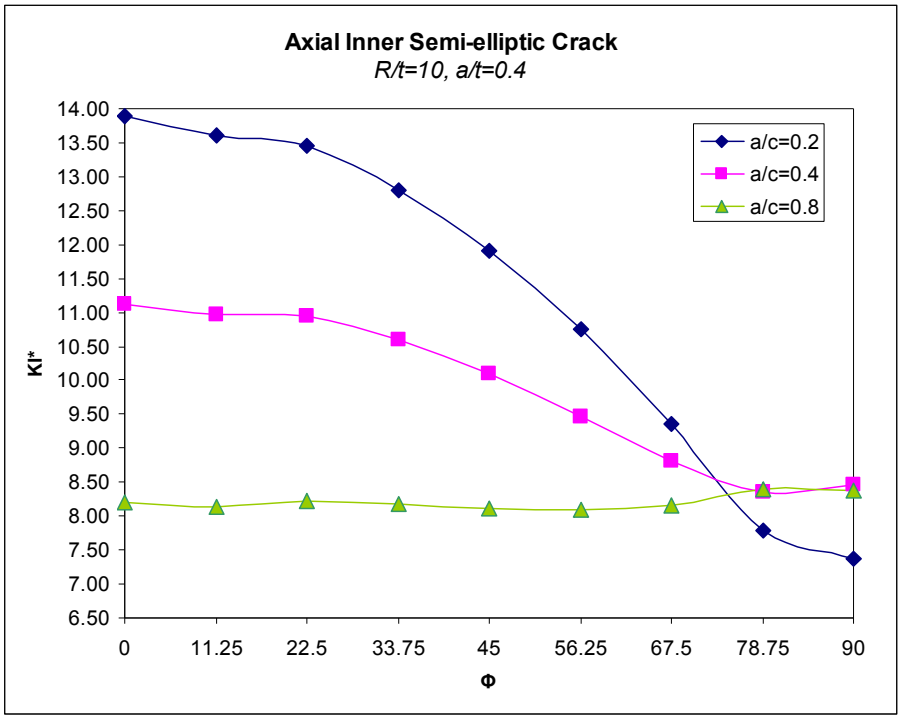

Figure 3.6 KI* versus Φ, Type1, R/t=10, a/t=0.4

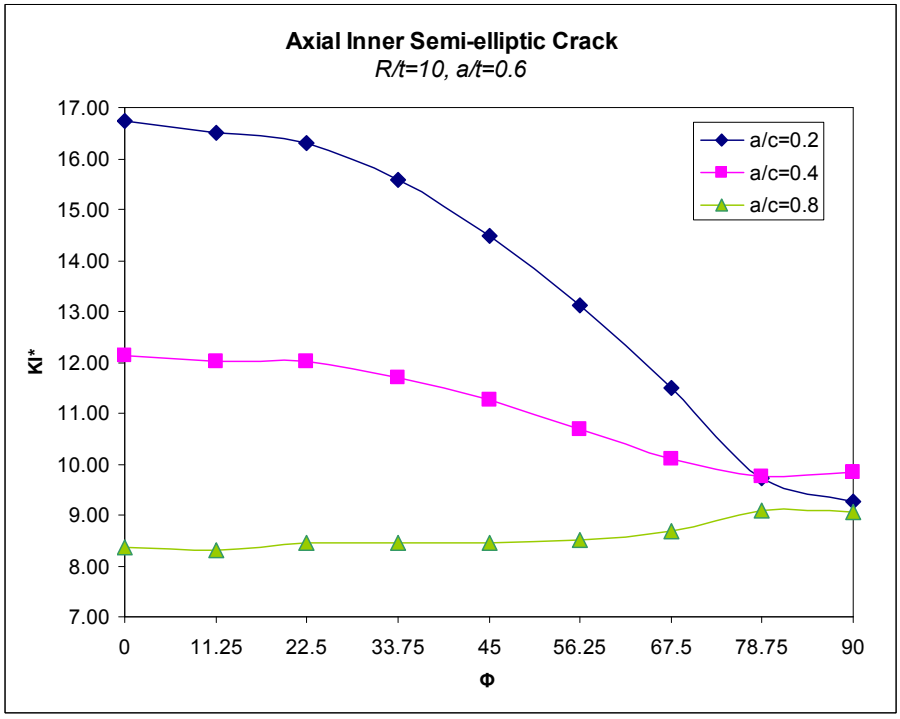

Figure 3.7 KI* versus Φ, Type1, R/t=10, a/t=0.6

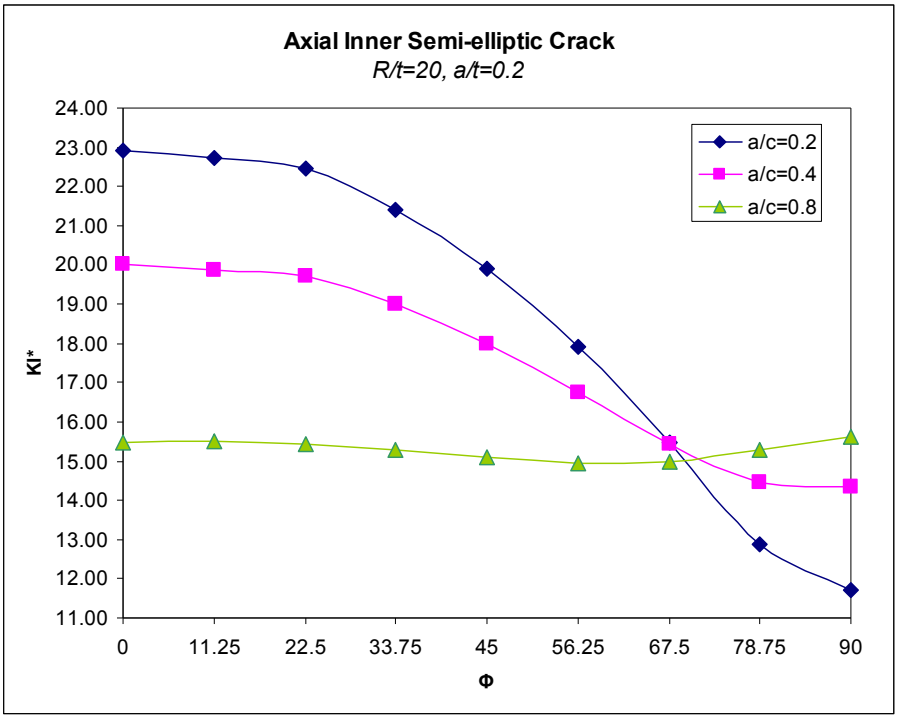

Figure 3.8 KI* versus Φ, Type1, R/t=20, a/t=0.2

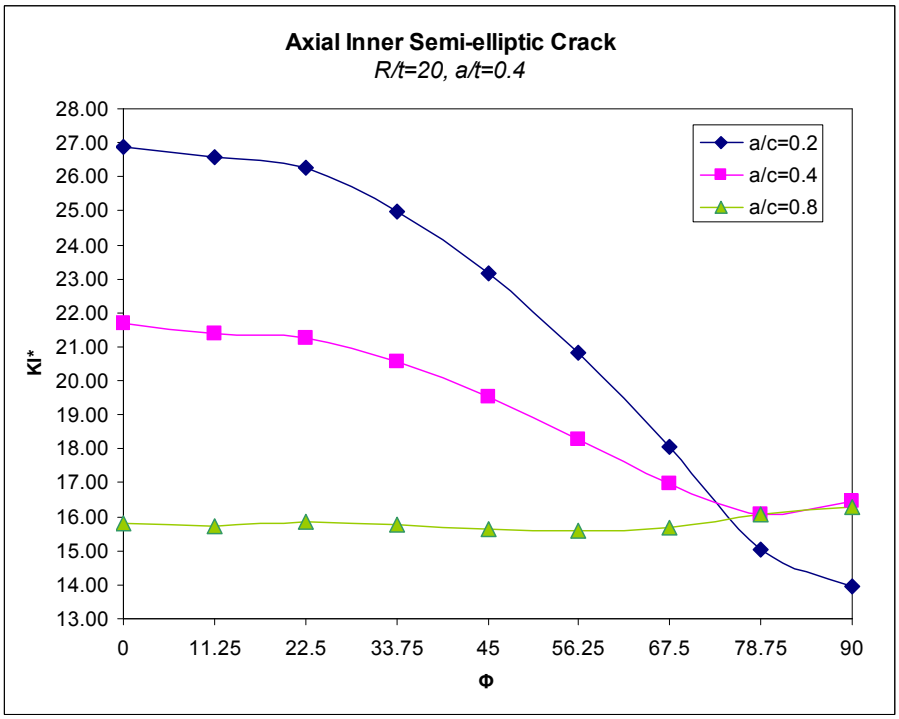

Figure 3.9 KI* versus Φ, Type1, R/t=20, a/t=0.4

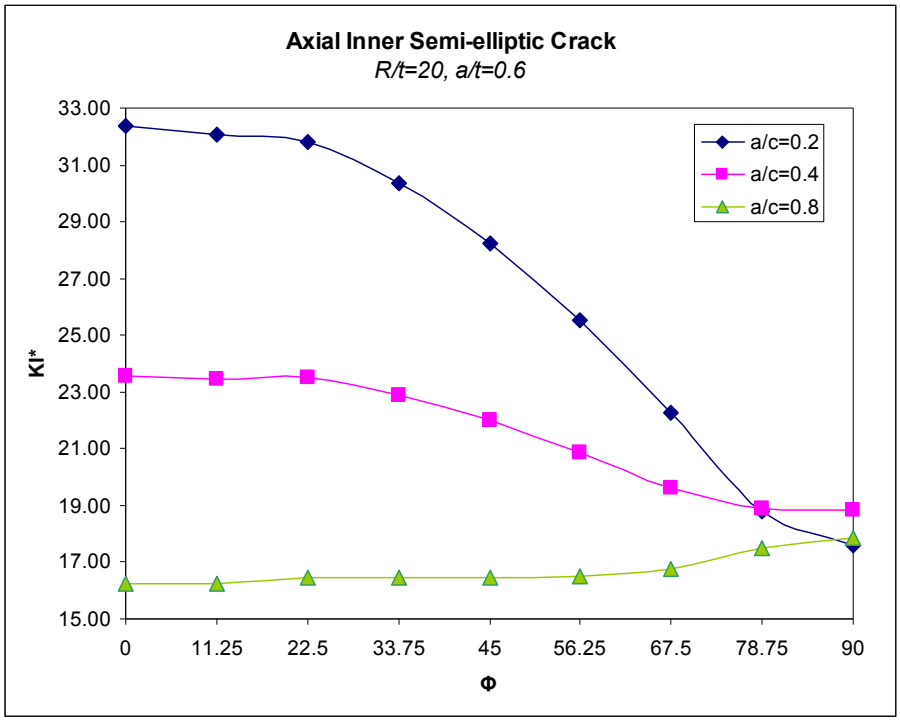

Figure 3.10 KI* versus Φ, Type1, R/t=20, a/t=0.6

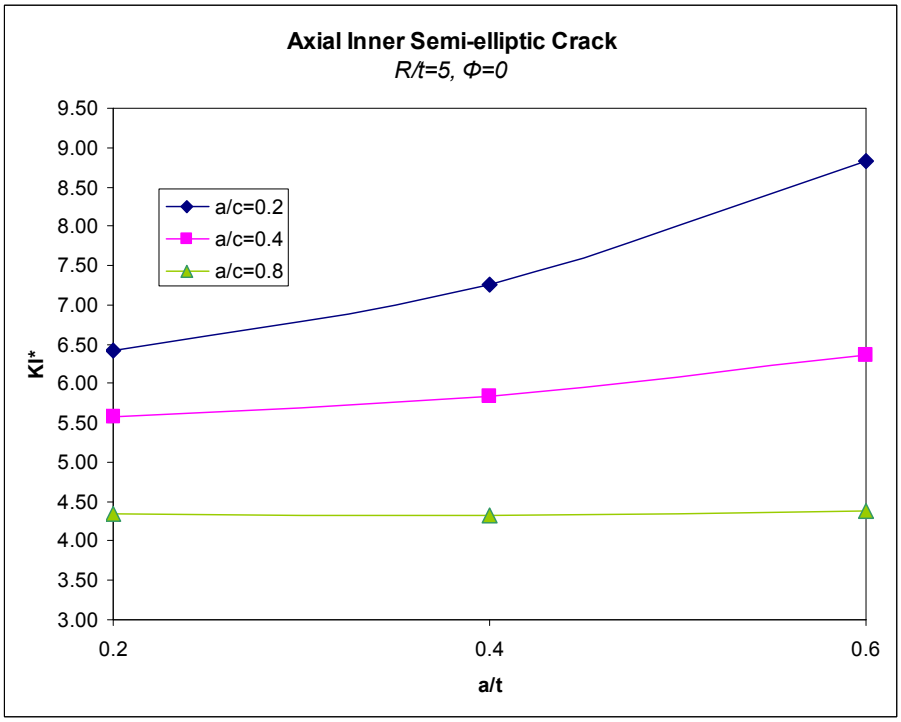

Figure 3.11 KI* at the deepest point versus a/t, Type1, R/t=5

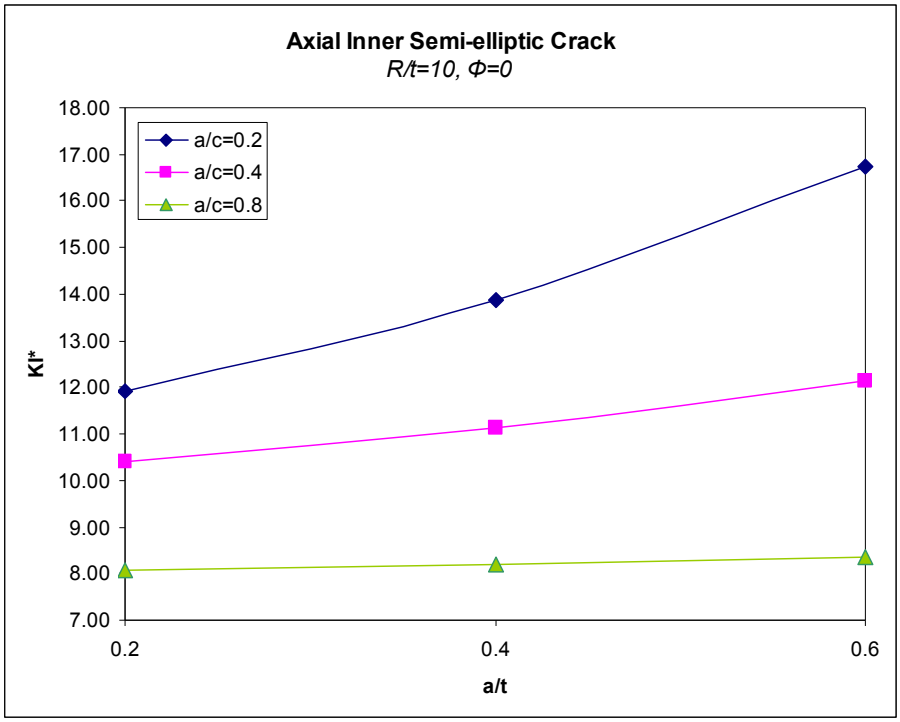

Figure 3.12 KI* at the deepest point versus a/t, Type1, R/t=10

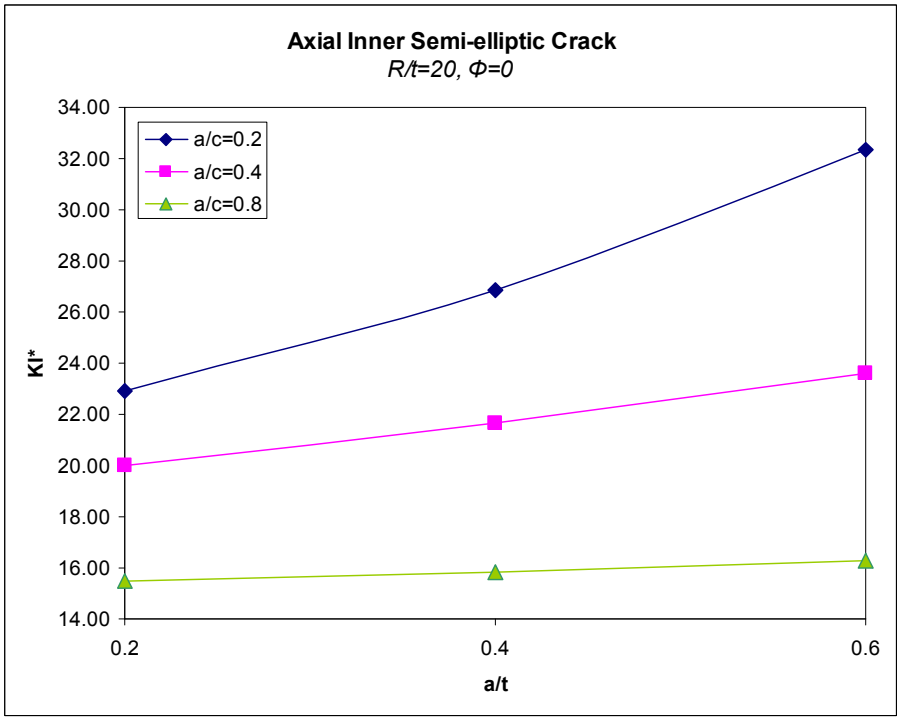

Figure 3.13 KI* at the deepest point versus a/t, Type1, R/t=20

Table 3.1 KI* for mechanical loaded partial inner axial crack

R/t	a/t	a/c	a (mm)	Φ=0	11.25	22.5	33.75	45	56.25	67.5	78.75	90
5	0.2	0.2	2	6.41	6.30	6.25	5.99	5.59	5.07	4.41	3.67	3.44
		0.4	2	5.58	5.50	5.49	5.30	5.03	4.70	4.35	4.10	4.11
		0.8	2	4.34	4.30	4.35	4.31	4.27	4.24	4.25	4.36	4.31
	0.4	0.2	4	7.25	7.16	7.11	6.79	6.32	5.73	5.02	4.24	3.96
		0.4	4	5.84	5.76	5.76	5.58	5.34	5.03	4.71	4.50	4.45
		0.8	4	4.33	4.28	4.35	4.33	4.31	4.31	4.35	4.51	4.42
	0.6	0.2	6	8.82	8.78	8.59	8.26	7.53	6.77	5.95	5.12	4.95
		0.4	6	6.37	6.28	6.29	6.15	5.93	5.63	5.34	5.20	5.23
		0.8	6	4.39	4.34	4.42	4.43	4.44	4.48	4.58	4.81	4.77
10	0.2	0.2	1	11.92	11.80	11.70	11.16	10.40	9.40	8.15	6.76	6.21
		0.4	1	10.40	10.27	10.18	9.85	9.33	8.69	8.01	7.53	7.64
		0.8	1	8.07	8.00	8.05	7.97	7.87	7.81	7.83	8.01	8.10
	0.4	0.2	2	13.89	13.61	13.46	12.80	11.90	10.75	9.36	7.79	7.38
		0.4	2	11.12	10.96	10.96	10.59	10.09	9.46	8.80	8.36	8.45
		0.8	2	8.20	8.14	8.23	8.18	8.11	8.09	8.15	8.40	8.37
	0.6	0.2	3	16.73	16.50	16.29	15.57	14.48	13.12	11.48	9.74	9.27
		0.4	3	12.14	12.00	12.01	11.71	11.25	10.69	10.09	9.74	9.85
		0.8	3	8.37	8.30	8.45	8.45	8.45	8.52	8.68	9.07	9.05
20	0.2	0.2	0.5	22.90	22.71	22.46	21.41	19.89	17.92	15.48	12.88	11.72
		0.4	0.5	20.02	19.85	19.72	18.99	17.98	16.74	15.43	14.46	14.34
		0.8	0.5	15.47	15.51	15.45	15.28	15.09	14.96	14.97	15.30	15.62
	0.4	0.2	1	26.87	26.59	26.28	24.96	23.14	20.83	18.06	15.04	13.94
		0.4	1	21.68	21.38	21.28	20.56	19.52	18.27	16.96	16.05	16.44
		0.8	1	15.82	15.73	15.86	15.77	15.64	15.58	15.67	16.09	16.29
	0.6	0.2	1.5	32.37	32.05	31.82	30.34	28.23	25.52	22.27	18.77	17.58
		0.4	1.5	23.58	23.45	23.51	22.90	22.00	20.86	19.64	18.88	18.82
		0.8	1.5	16.26	16.23	16.46	16.44	16.44	16.52	16.79	17.49	17.88

KI* at the deepest point is greater than KI* at the surface point for the cases a/c is equal to 0.2 and 0.4. For the cases a/c is equal to 0.8, KI* values along the crack front are almost constant. Also KI* values increases as R/t increases.

When a/c is equal to 0.2 and 0.4, KI* values increases as a/t increases. Nevertheless, when a/c is equal to 0.8, KI* does not change so much as a/t increases. So a/t does not affect KI* when a/c is 0.8.

3.1.2.Inner Pressurized Partial Outer Axial Semi-elliptic Crack

Crack front angle 0 is the deepest point and angle 90 is the surface point. Inner pressure of magnitude 10Mpa is applied to the structure. Results are obtained for different R/t, a/t and a/c values. R is 50mm for all cases but a, c and t change. Results are obtained for the following ranges;

R/t = 5, 10 and 20

a/t = 0.2, 0.4 and 0.6

a/c = 0.2, 0.4 and 0.8

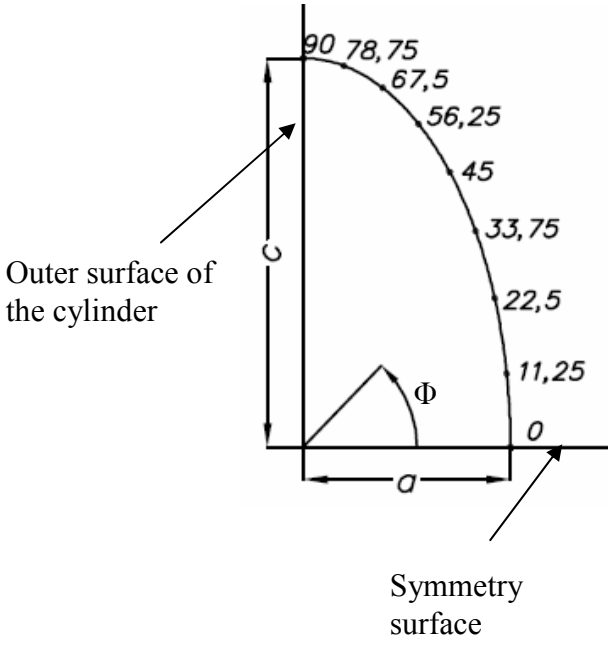

Figure 3.14 Crack front angles for Type2 and Type8

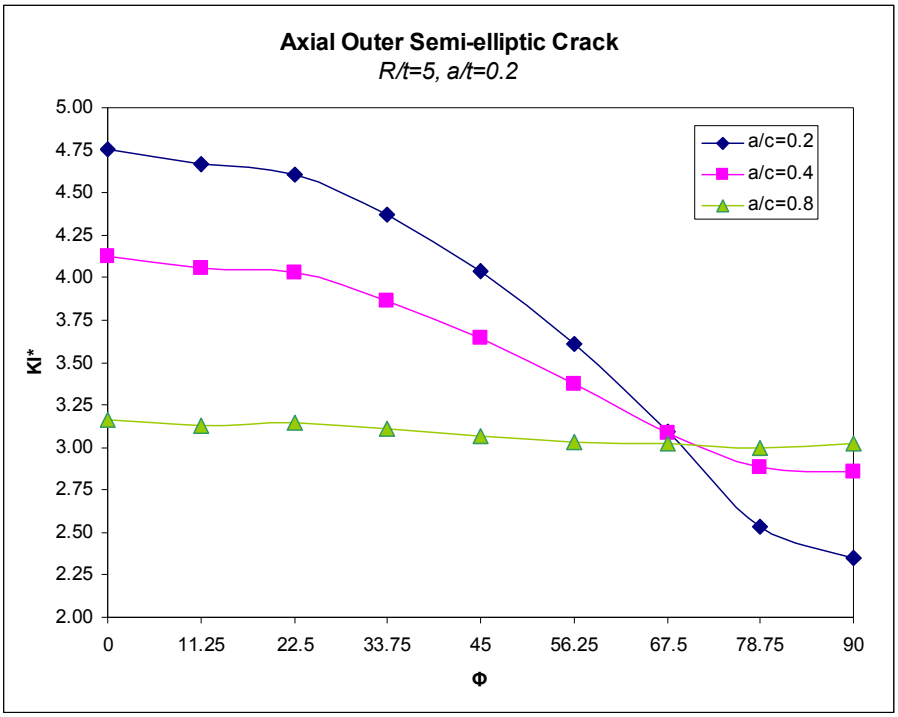

Figure 3.15 KI* versus Φ, Type2, R/t=5, a/t=0.2

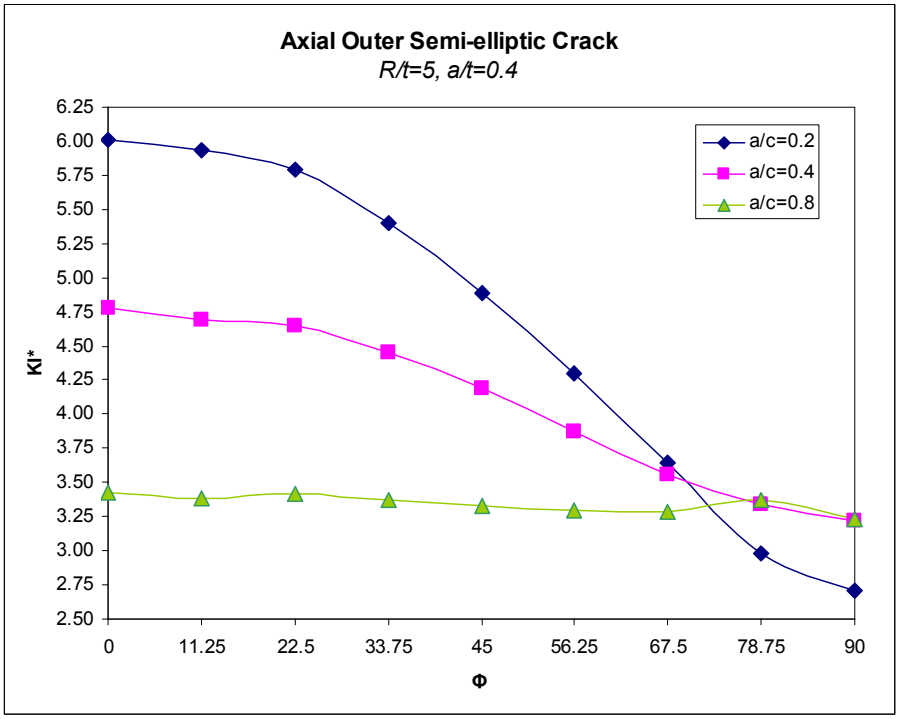

Figure 3.16 KI* versus Φ, Type2, R/t=5, a/t=0.4

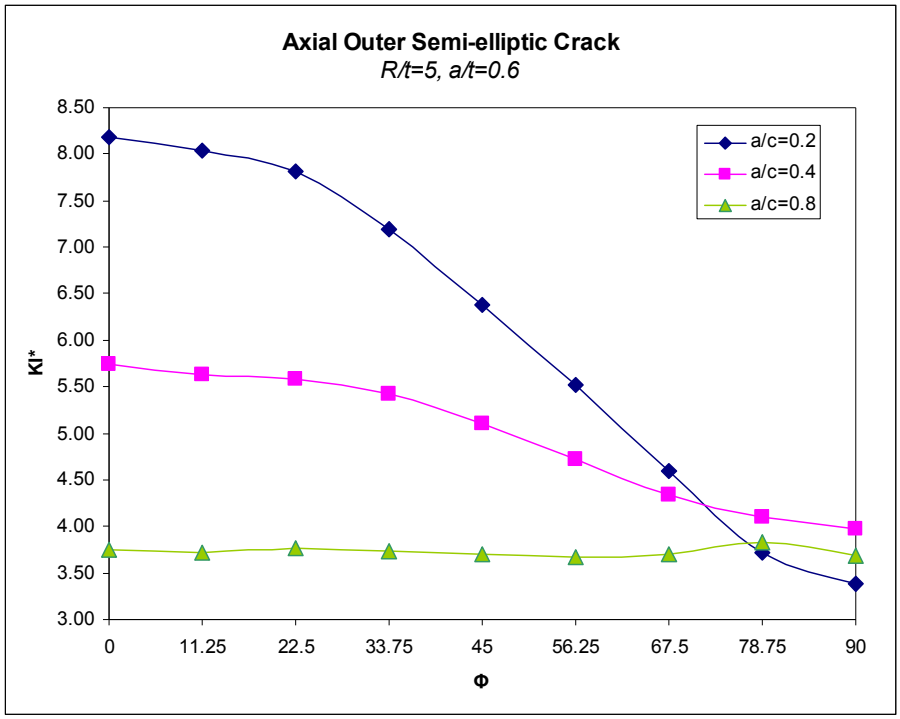

Figure 3.17 KI* versus Φ, Type2, R/t=5, a/t=0.6

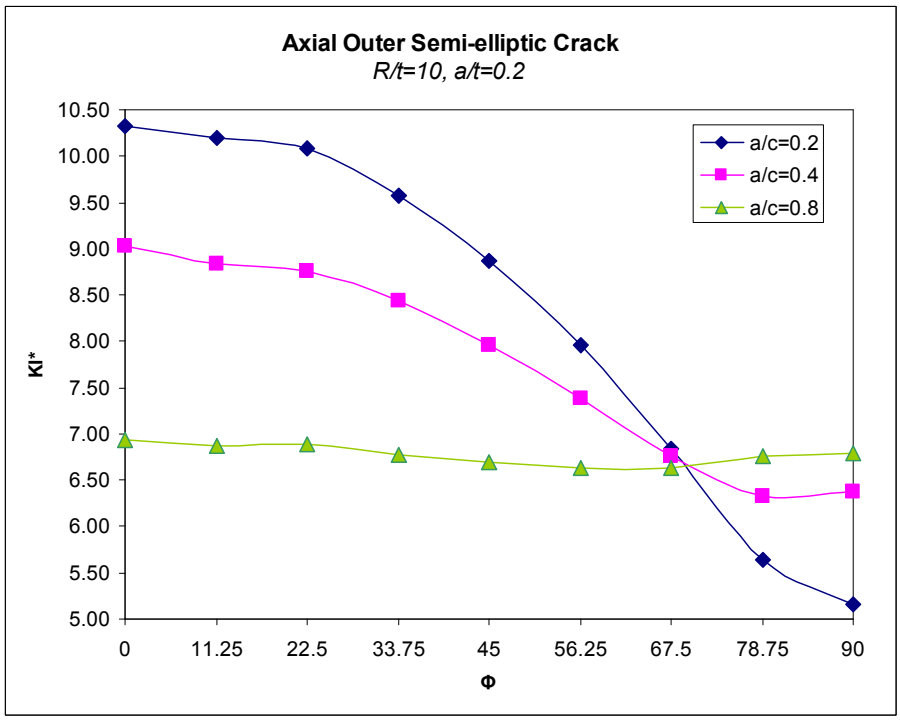

Figure 3.18 KI* versus Φ, Type2, R/t=10, a/t=0.2

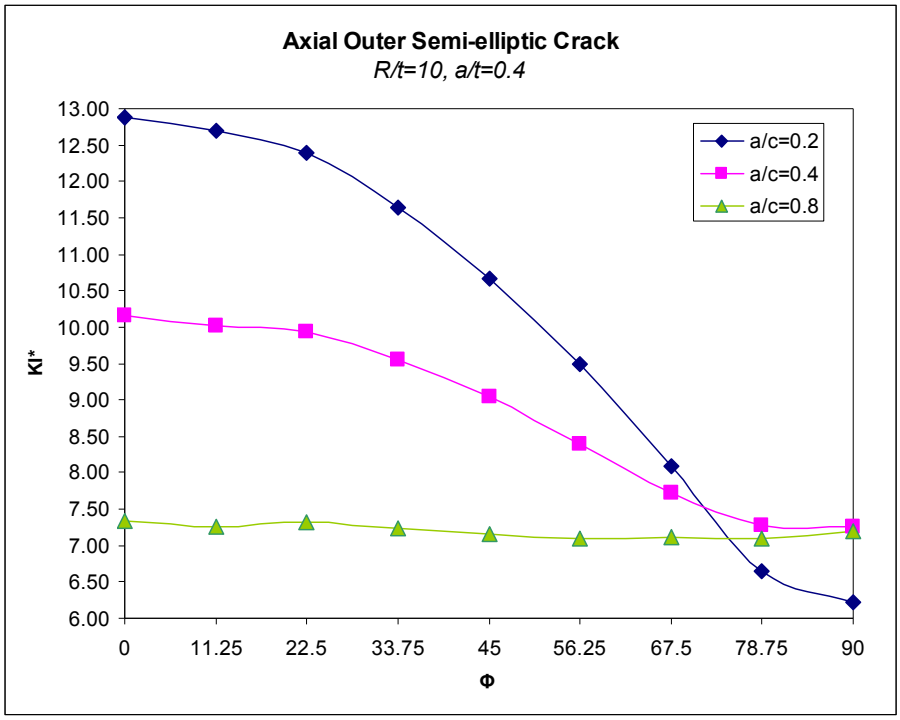

Figure 3.19 KI* versus Φ, Type2, R/t=10, a/t=0.4

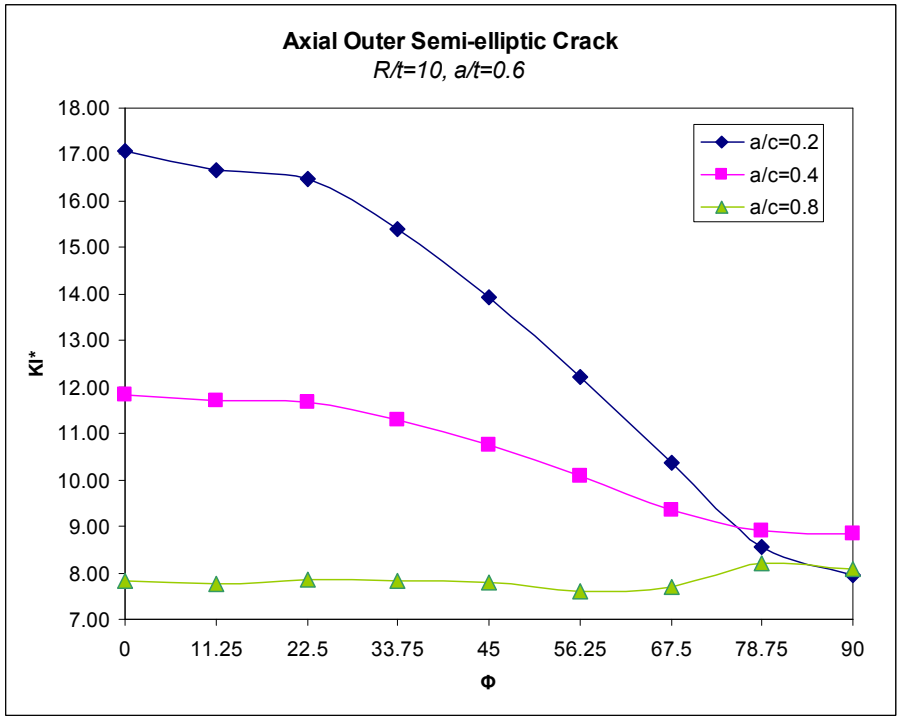

Figure 3.20 KI* versus Φ, Type2, R/t=10, a/t=0.6

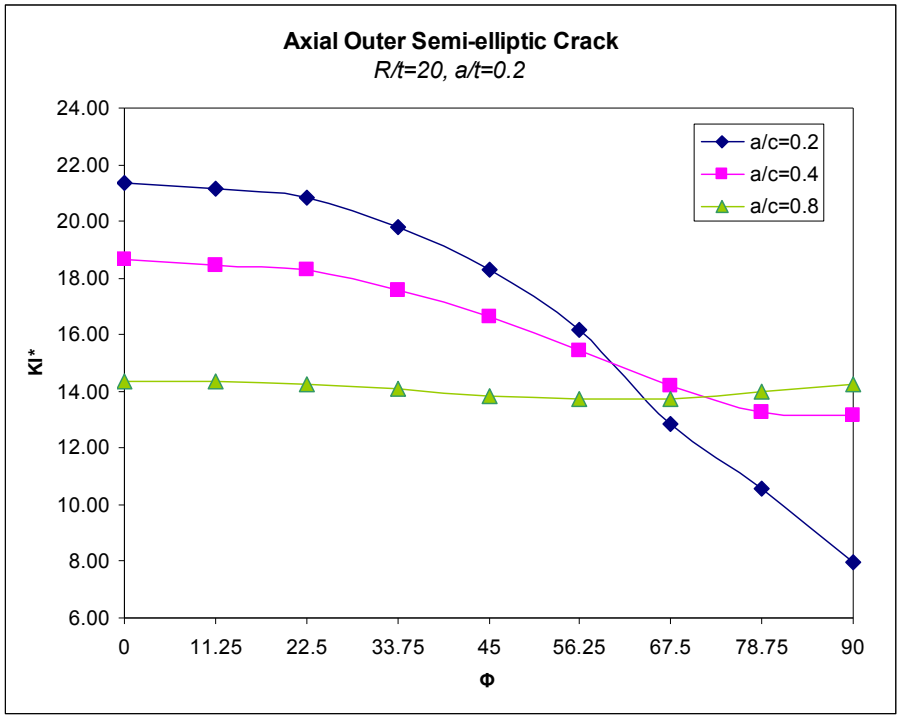

Figure 3.21 KI* versus Φ, Type2, R/t=20, a/t=0.2

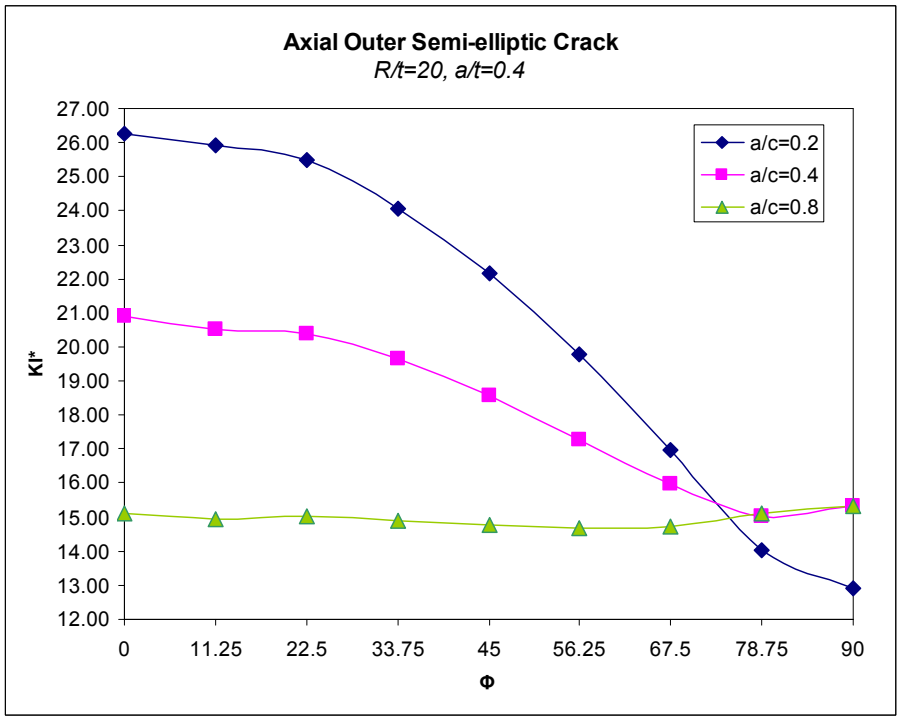

Figure 3.22 KI* versus Φ, Type2, R/t=20, a/t=0.4

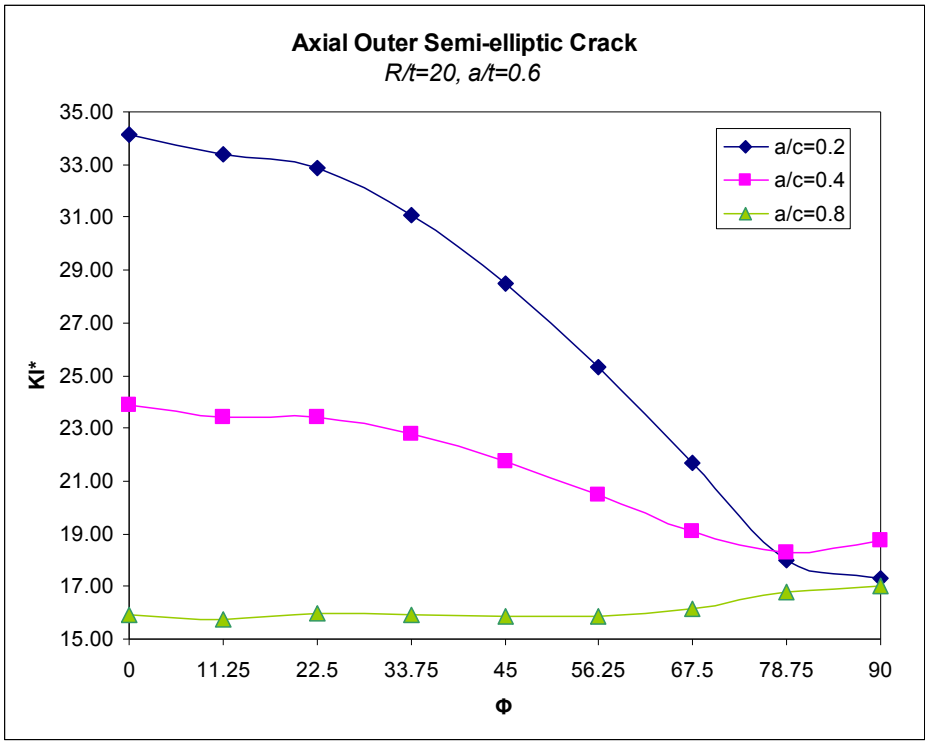

Figure 3.23 KI* versus Φ, Type2, R/t=20, a/t=0.6

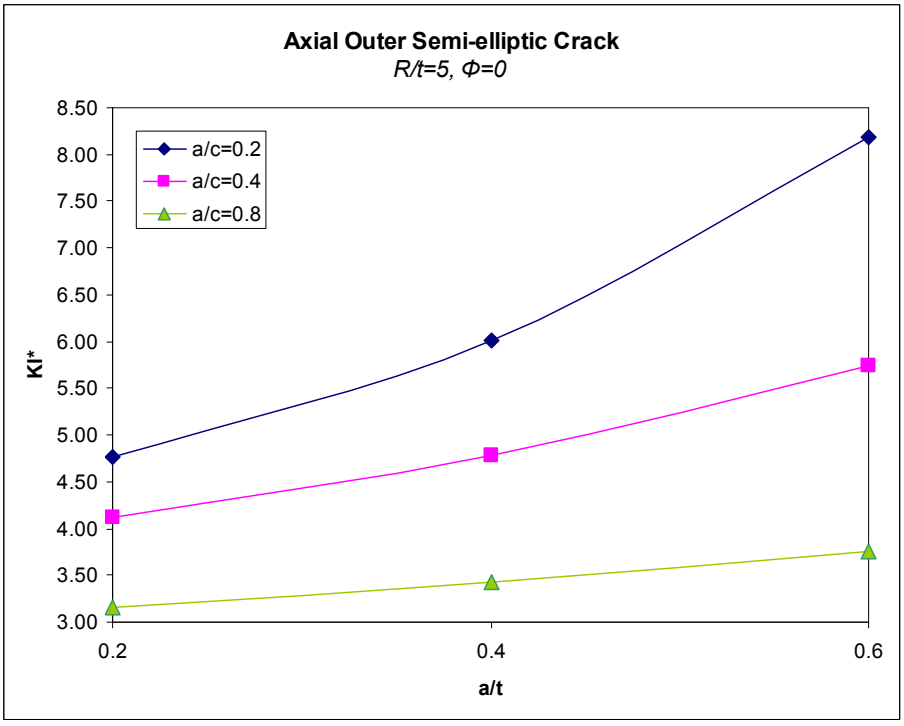

Figure 3.24 KI* at the deepest point versus a/t, Type2, R/t=5

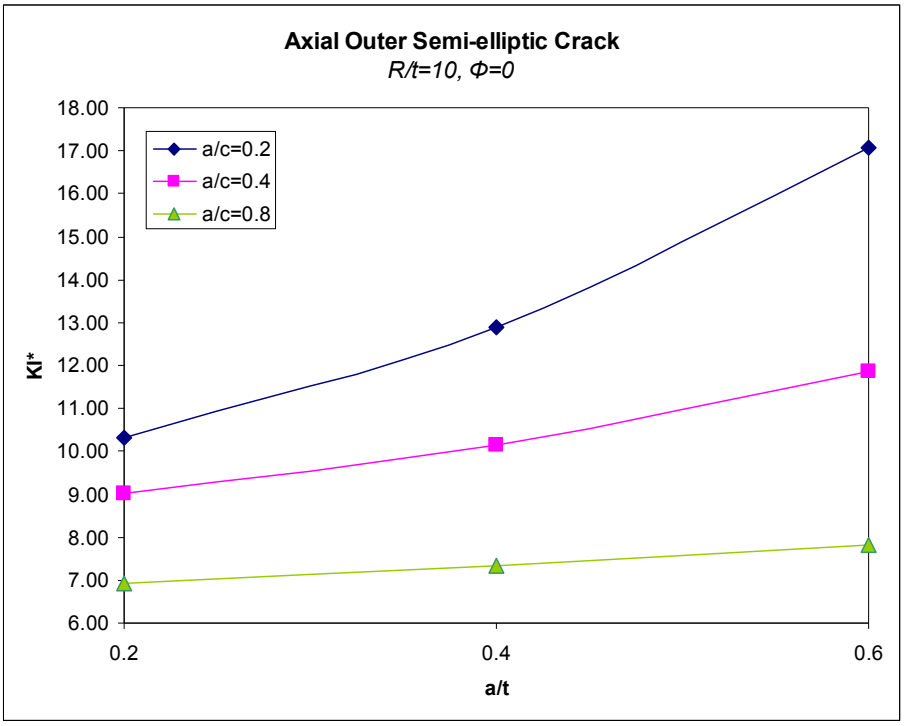

Figure 3.25 KI* at the deepest point versus a/t, Type2, R/t=10

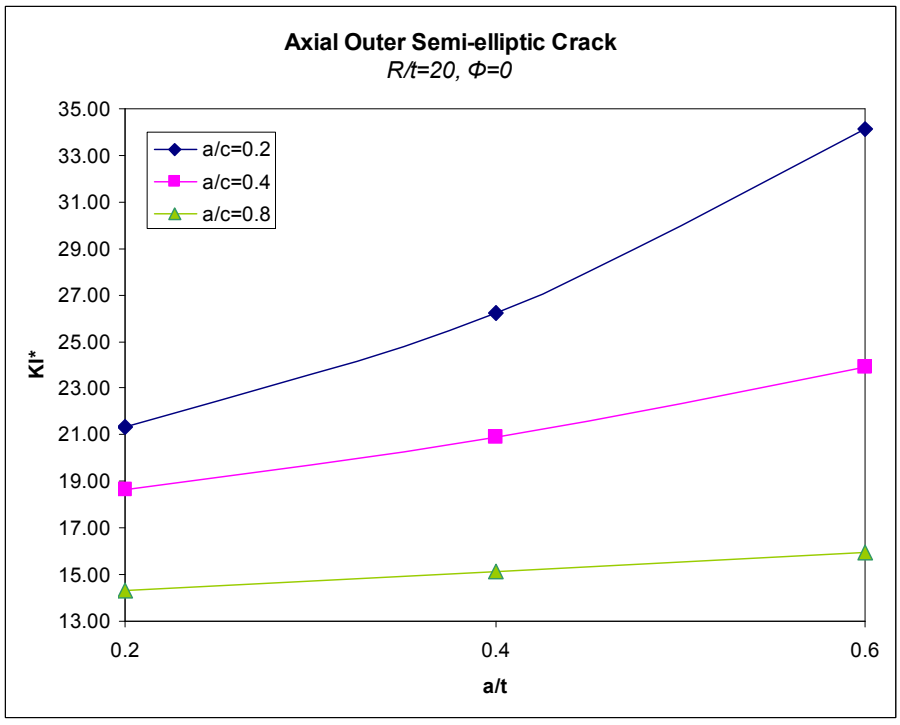

Figure 3.26 KI* at the deepest point versus a/t, Type2, R/t=20

Table 3.2 KI* for mechanical loaded partial outer axial crack

R/t	a/t	a/c	a (mm)	Φ=0	11.25	22.5	33.75	45	56.25	67.5	78.75	90
5	0.2	0.2	2	4.76	4.67	4.61	4.37	4.03	3.61	3.09	2.53	2.35
		0.4	2	4.12	4.06	4.03	3.87	3.64	3.37	3.09	2.88	2.86
		0.8	2	3.16	3.13	3.15	3.11	3.07	3.03	3.02	3.00	3.03
	0.4	0.2	4	6.01	5.93	5.80	5.40	4.89	4.30	3.65	2.98	2.71
		0.4	4	4.78	4.69	4.65	4.46	4.19	3.88	3.56	3.34	3.21
		0.8	4	3.43	3.38	3.42	3.38	3.33	3.29	3.29	3.37	3.23
	0.6	0.2	6	8.18	8.05	7.82	7.19	6.38	5.52	4.59	3.72	3.38
		0.4	6	5.74	5.63	5.58	5.42	5.10	4.72	4.34	4.10	3.98
		0.8	6	3.75	3.71	3.76	3.73	3.69	3.67	3.70	3.83	3.68
10	0.2	0.2	1	10.32	10.20	10.08	9.58	8.87	7.96	6.84	5.63	5.15
		0.4	1	9.02	8.84	8.76	8.43	7.95	7.37	6.77	6.33	6.38
		0.8	1	6.94	6.86	6.88	6.78	6.69	6.63	6.62	6.76	6.79
	0.4	0.2	2	12.88	12.69	12.39	11.64	10.66	9.49	8.09	6.65	6.21
		0.4	2	10.16	10.01	9.94	9.56	9.03	8.39	7.73	7.27	7.26
		0.8	2	7.34	7.25	7.32	7.25	7.16	7.11	7.11	7.09	7.19
	0.6	0.2	3	17.07	16.65	16.47	15.40	13.93	12.21	10.37	8.55	7.94
		0.4	3	11.85	11.70	11.66	11.29	10.74	10.07	9.36	8.91	8.86
		0.8	3	7.83	7.76	7.87	7.83	7.79	7.60	7.69	8.20	8.07
20	0.2	0.2	0.5	21.36	21.17	20.86	19.82	18.29	16.18	12.83	10.55	7.96
		0.4	0.5	18.64	18.45	18.29	17.58	16.61	15.44	14.19	13.27	13.14
		0.8	0.5	14.34	14.35	14.26	14.07	13.84	13.70	13.72	14.00	14.24
	0.4	0.2	1	26.25	25.90	25.51	24.07	22.14	19.76	16.98	14.02	12.93
		0.4	1	20.91	20.53	20.39	19.64	18.56	17.29	15.97	15.04	15.31
		0.8	1	15.11	14.96	15.03	14.90	14.75	14.66	14.72	15.11	15.32
	0.6	0.2	1.5	34.11	33.36	32.85	31.07	28.51	25.33	21.67	17.98	17.29
		0.4	1.5	23.88	23.43	23.43	22.78	21.72	20.48	19.12	18.30	18.75
		0.8	1.5	15.94	15.77	15.97	15.92	15.88	15.89	16.13	16.76	17.01

Similar to the inner axial crack case, KI* at the deepest point is greater than KI* at the surface point for the cases a/c is equal to 0.2 and 0.4. For the cases a/c is equal to 0.8, KI* values along the crack front are almost constant. Also KI* values increases as R/t increases.

When a/c is equal to 0.2 and 0.4, KI* values increases as a/t increases. Nevertheless, when a/c is equal to 0.8, KI* does not change so much as a/t increases. So a/t does not affect KI* when a/c is 0.8.

3.1.3.Inner Pressurized Embedded Axial Crack

Crack front angle 0 is closer to the outer surface of the cylinder. Inner pressure of magnitude 10Mpa is applied to the structure. Results are obtained for different R/t, a/t and a/c values. R is 50mm for all cases but a, c and t change. Results are obtained for the following ranges;

R/t = 5, 10 and 20

a/t = 0.2, 0.3 and 0.4

a/c = 0.2, 0.4 and 0.8

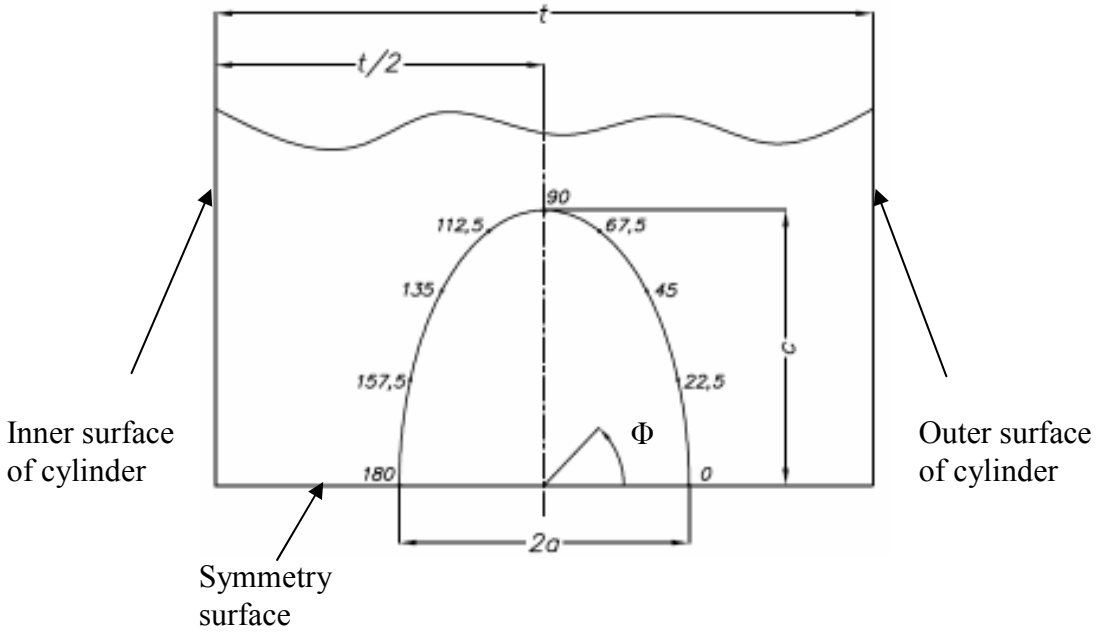

Figure 3.27 Crack front angles for Type3

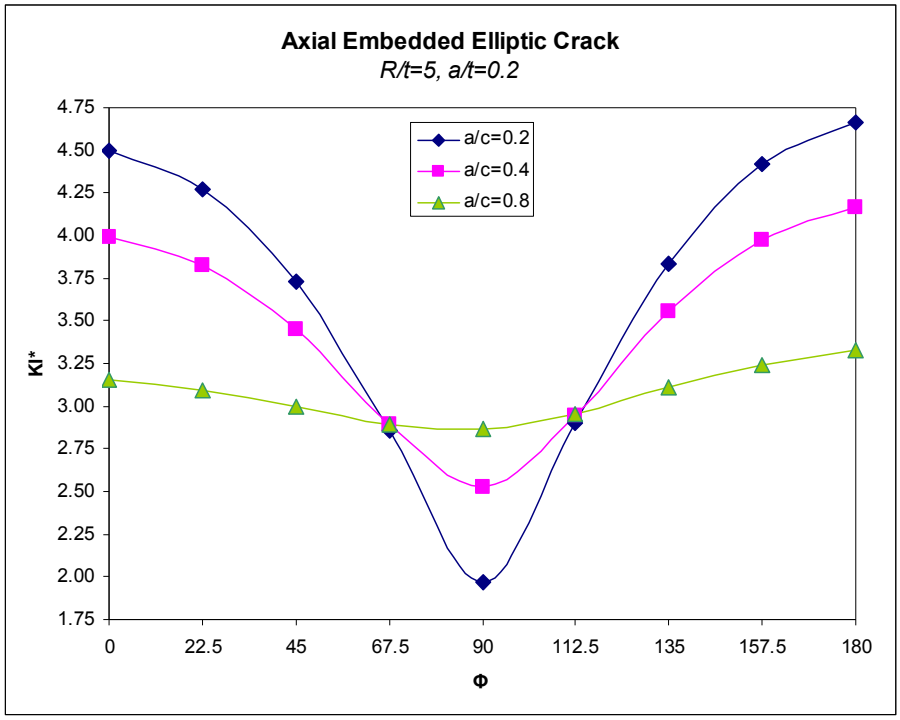

Figure 3.28 KI* versus Φ, Type3, R/t=5, a/t=0.2

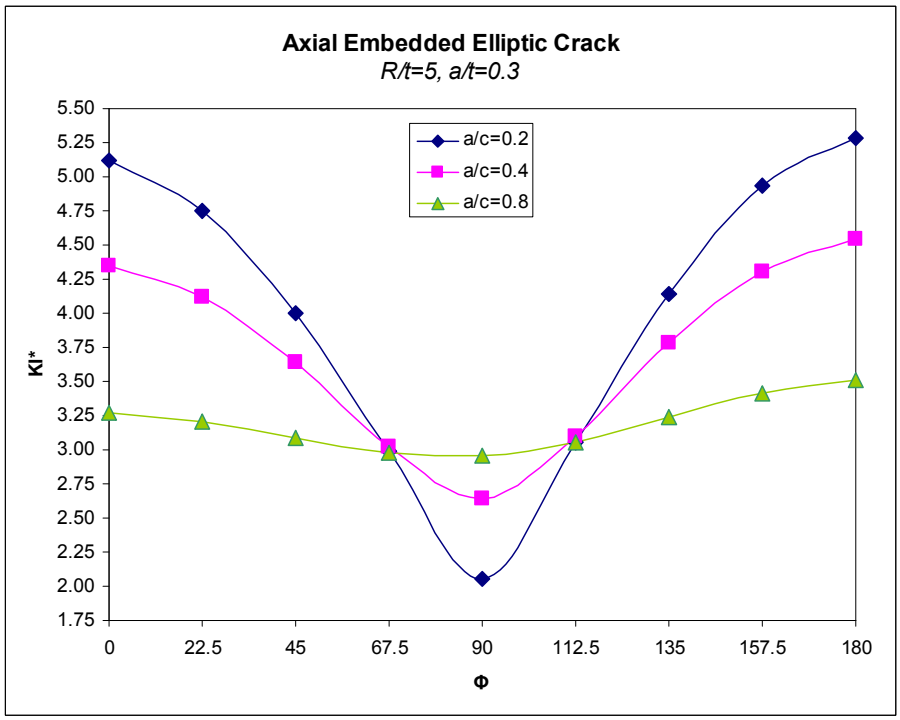

Figure 3.29 KI* versus Φ, Type3, R/t=5, a/t=0.3

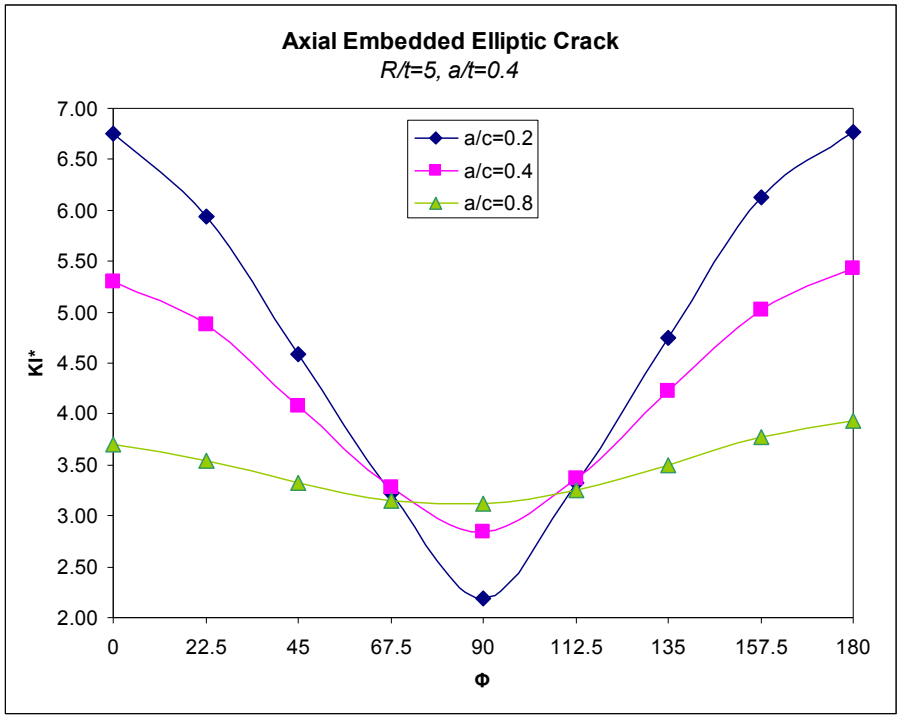

Figure 3.30 KI* versus Φ, Type3, R/t=5, a/t=0.4

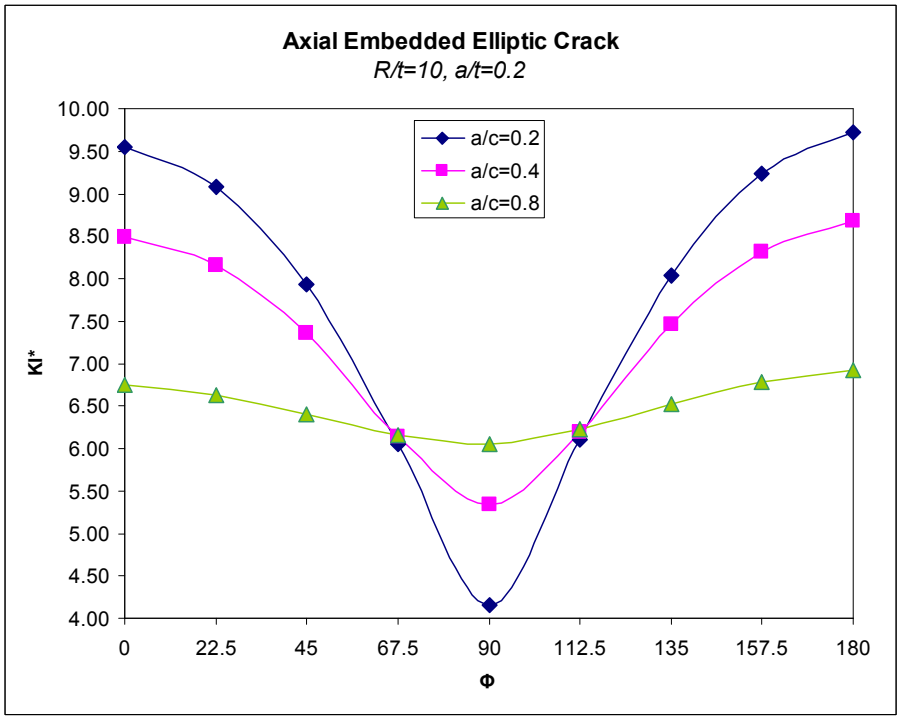

Figure 3.31 KI* versus Φ, Type3, R/t=10, a/t=0.2

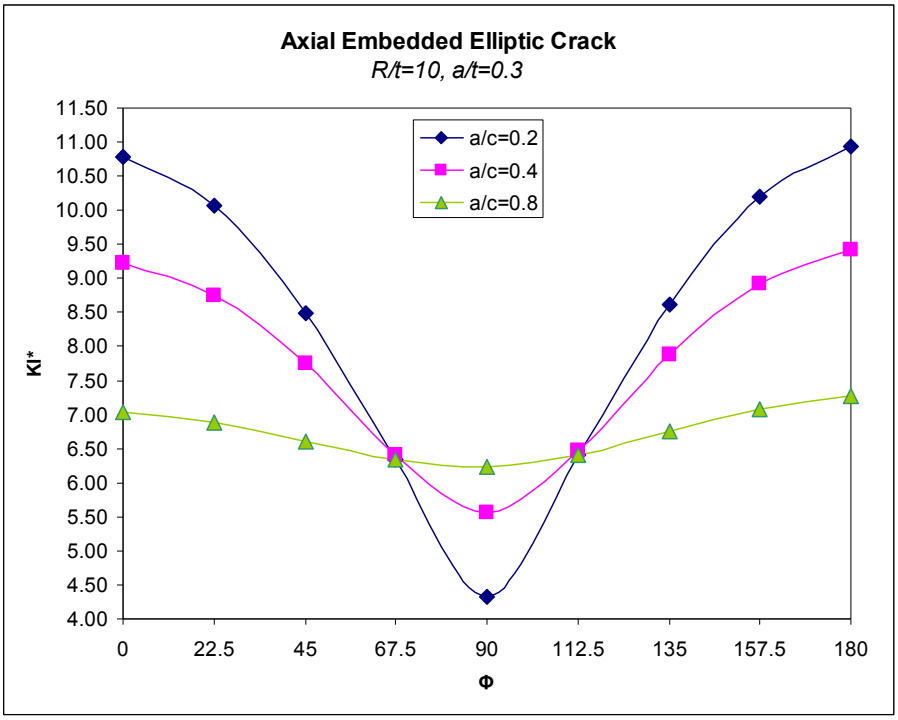

Figure 3.32 KI* versus Φ, Type3, R/t=10, a/t=0.3

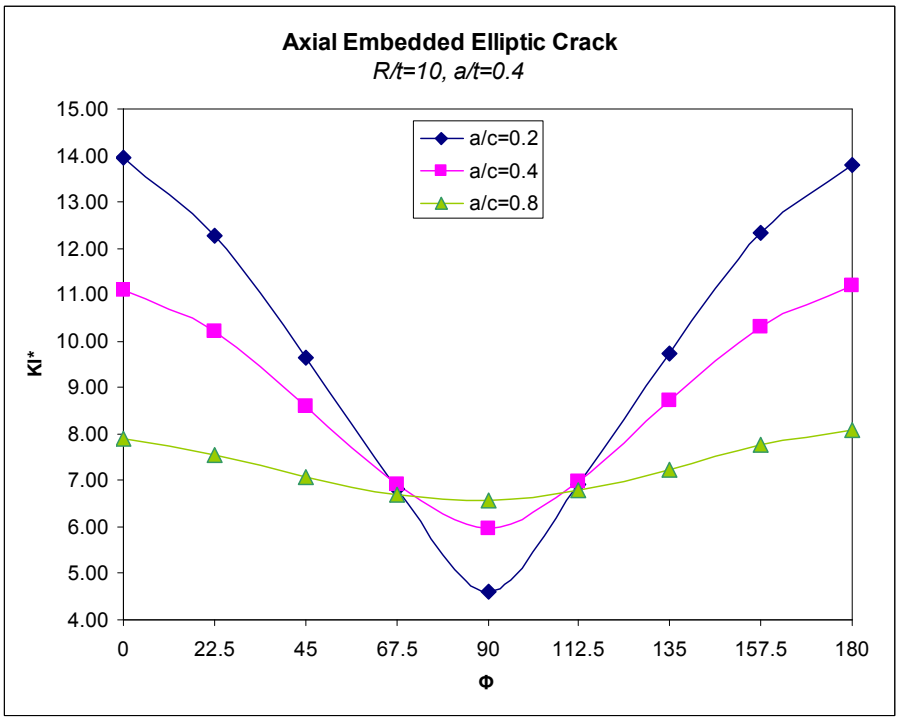

Figure 3.33 KI* versus Φ, Type3, R/t=10, a/t=0.4

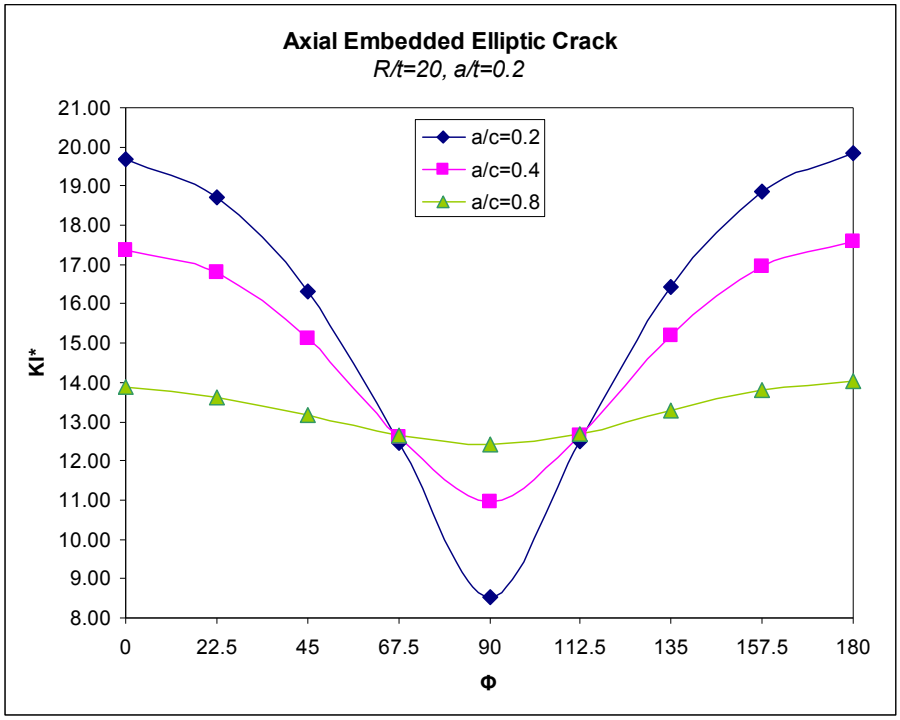

Figure 3.34 KI* versus Φ, Type3, R/t=20, a/t=0.2

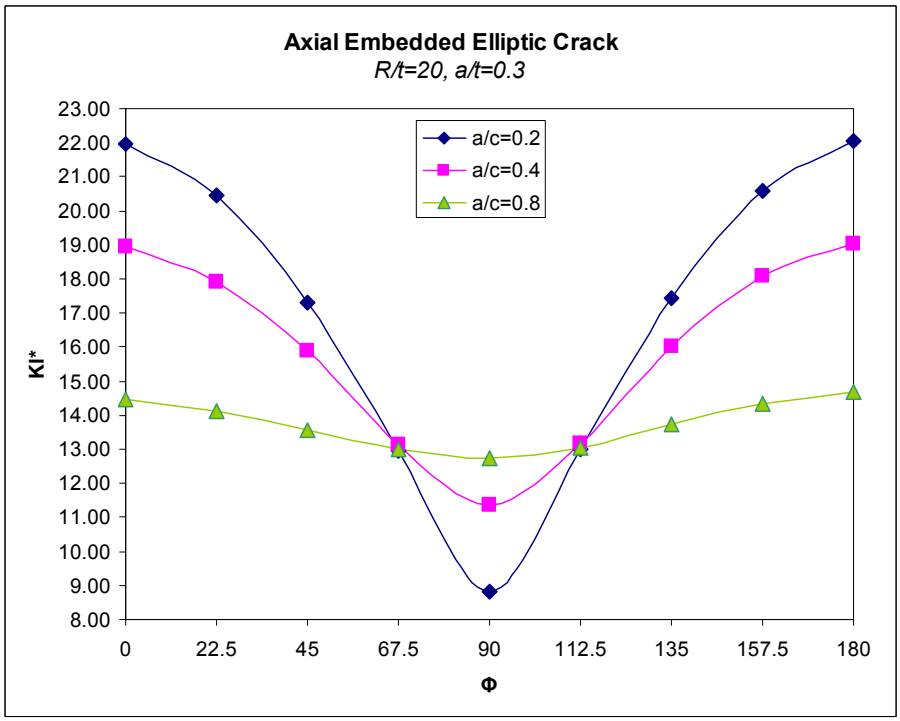

Figure 3.35 KI* versus Φ, Type3, R/t=20, a/t=0.3

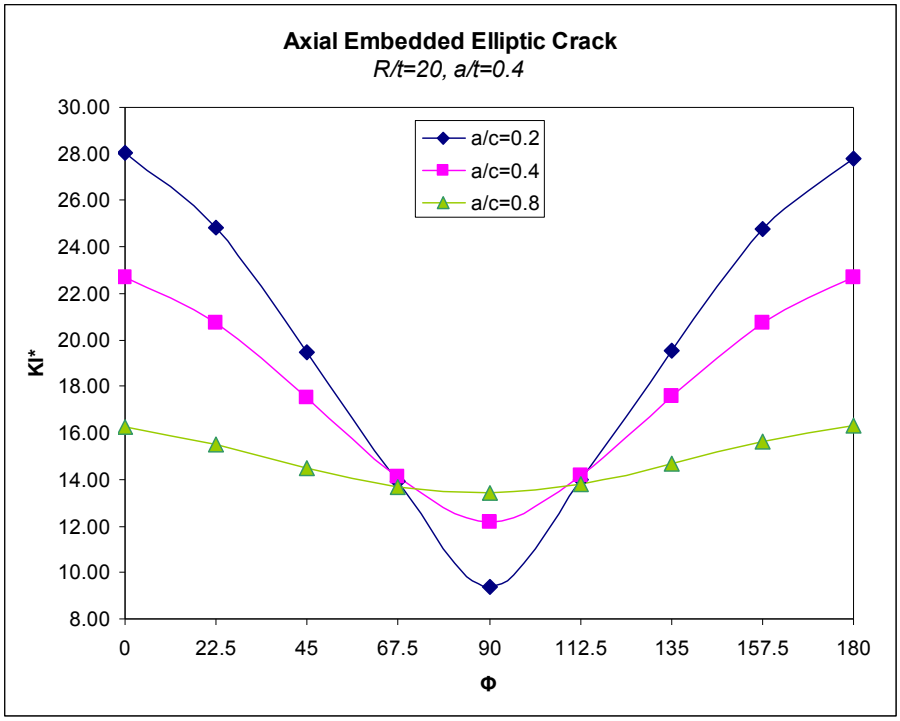

Figure 3.36 KI* versus Φ, Type3, R/t=20, a/t=0.4

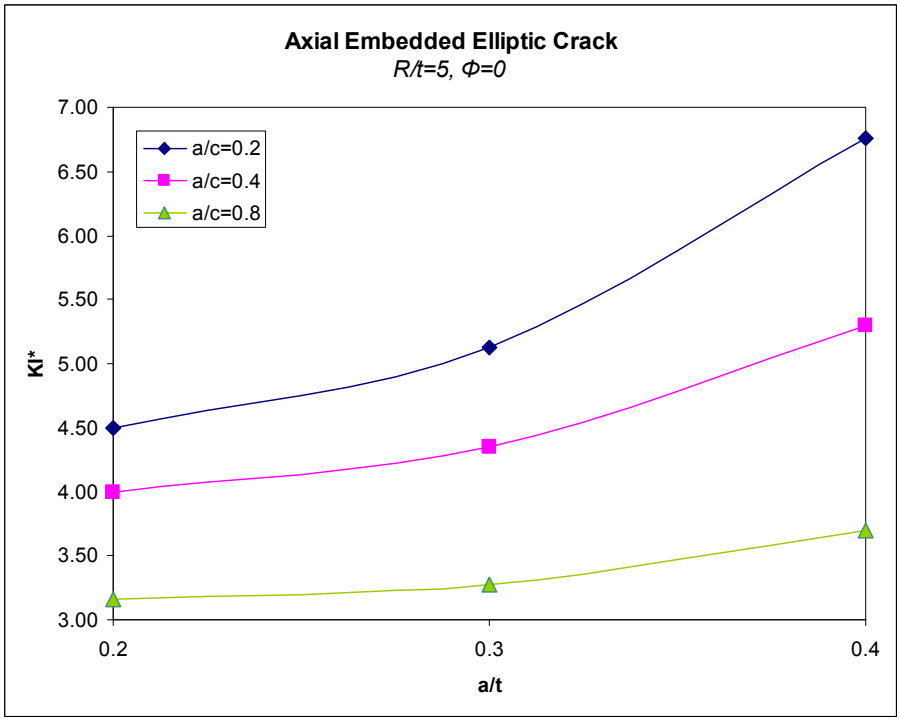

Figure 3.37 KI* at Φ=0 versus a/t, Type3, R/t=5

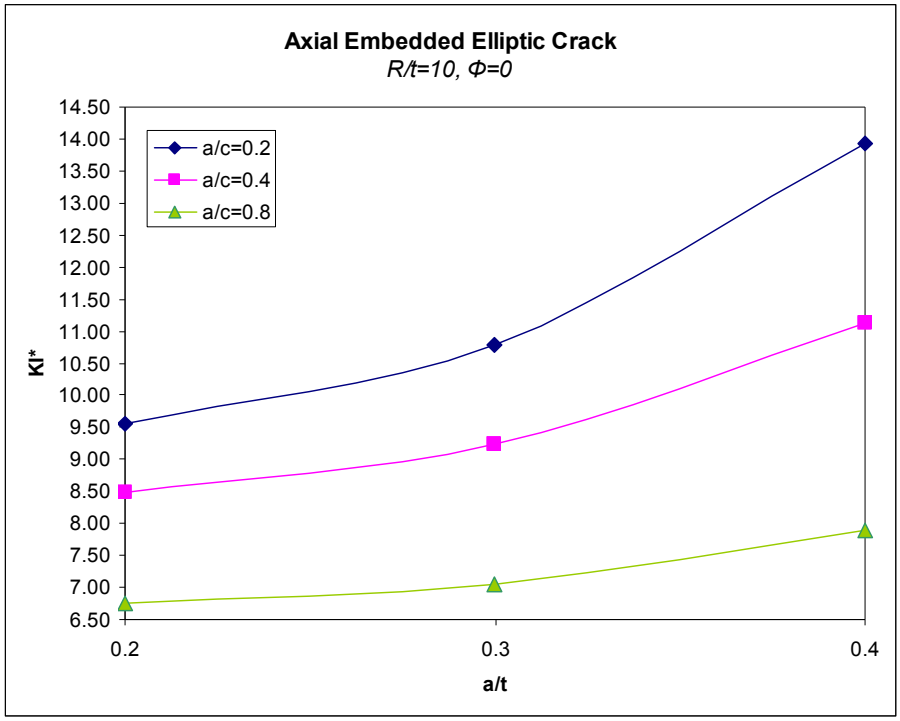

Figure 3.38 KI* at Φ=0 versus a/t, Type3, R/t=10

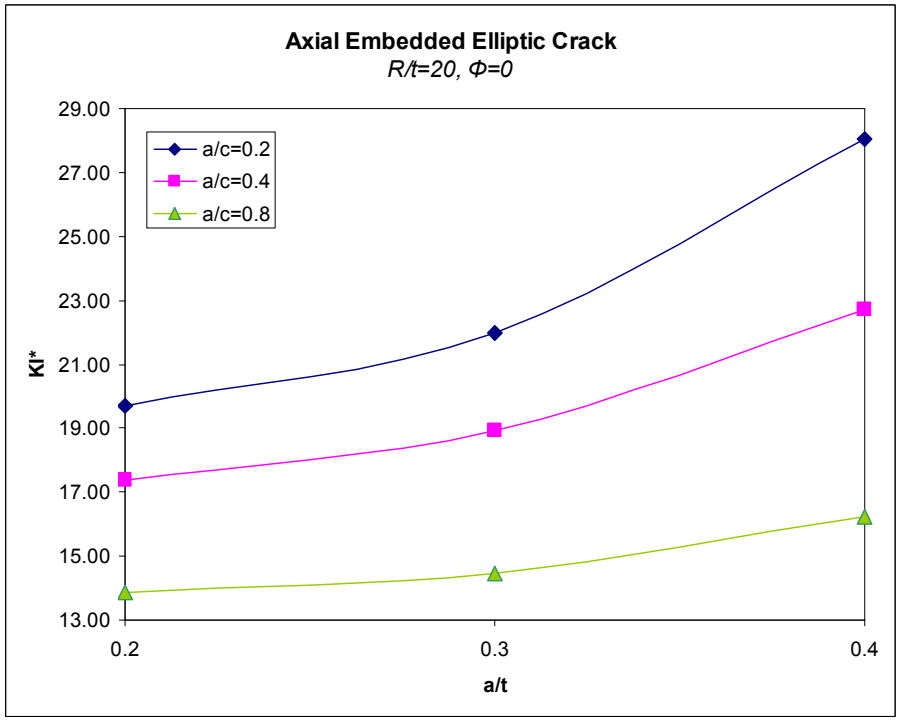

Figure 3.39 KI* at Φ=0 versus a/t, Type3, R/t=20

Table 3.3 KI* for mechanical loaded embedded axial crack

R/t	a/t	a/c	a (mm)	Φ=0	22.50	45	67.5	90	112.5	135	157.5	180
5	0.2	0.2	2	4.50	4.27	3.73	2.85	1.97	2.90	3.84	4.41	4.66
		0.4	2	3.99	3.82	3.45	2.89	2.53	2.94	3.56	3.98	4.17
		0.8	2	3.16	3.09	3.00	2.90	2.87	2.95	3.11	3.25	3.33
	0.3	0.2	3	5.12	4.75	4.00	2.99	2.05	3.05	4.15	4.94	5.28
		0.4	3	4.35	4.12	3.64	3.03	2.64	3.09	3.79	4.31	4.54
		0.8	3	3.28	3.20	3.09	2.98	2.95	3.06	3.24	3.41	3.51
	0.4	0.2	4	6.76	5.93	4.59	3.22	2.18	3.32	4.75	6.13	6.77
		0.4	4	5.30	4.87	4.08	3.28	2.84	3.37	4.23	5.03	5.43
		0.8	4	3.70	3.54	3.33	3.15	3.12	3.25	3.50	3.77	3.94
10	0.2	0.2	1	9.54	9.08	7.94	6.06	4.16	6.10	8.04	9.23	9.72
		0.4	1	8.49	8.16	7.35	6.15	5.35	6.20	7.46	8.32	8.68
		0.8	1	6.74	6.62	6.40	6.15	6.06	6.22	6.52	6.78	6.92
	0.3	0.2	1.5	10.79	10.06	8.49	6.33	4.33	6.40	8.61	10.20	10.94
		0.4	1.5	9.23	8.75	7.75	6.41	5.57	6.48	7.89	8.92	9.43
		0.8	1.5	7.04	6.88	6.61	6.33	6.24	6.41	6.76	7.08	7.26
	0.4	0.2	2	13.94	12.29	9.63	6.83	4.61	6.91	9.74	12.32	13.78
		0.4	2	11.12	10.20	8.60	6.92	5.96	6.99	8.71	10.31	11.18
		0.8	2	7.90	7.56	7.08	6.69	6.56	6.78	7.24	7.76	8.10
20	0.2	0.2	0.5	19.70	18.71	16.33	12.45	8.54	12.50	16.43	18.85	19.86
		0.4	0.5	17.36	16.79	15.12	12.62	10.95	12.66	15.20	16.94	17.60
		0.8	0.5	13.89	13.63	13.17	12.64	12.41	12.70	13.28	13.81	14.04
	0.3	0.2	0.8	21.96	20.46	17.32	12.95	8.84	13.01	17.45	20.61	22.04
		0.4	0.8	18.94	17.91	15.87	13.13	11.37	13.19	16.00	18.10	19.01
		0.8	0.8	14.48	14.12	13.57	12.99	12.75	13.06	13.72	14.34	14.67
	0.4	0.2	1	28.04	24.82	19.47	13.90	9.37	13.96	19.56	24.75	27.77
		0.4	1	22.71	20.76	17.53	14.10	12.13	14.17	17.60	20.74	22.72
		0.8	1	16.23	15.48	14.51	13.70	13.40	13.79	14.67	15.64	16.33

KI* at the angles 0 and 180 is greater than KI* at the angle 90. As a/c increases, KI* values along the crack front change less. KI* at the angle 180 is greater than KI* at the angle 0. Similar to inner and outer axial cracks case, KI* values increases as R/t increases.

As a/t increases, KI* increases for the same a/c value. But as a/c inreases, effect of a/t decreases.

3.1.4.Tension Applied-Partial Circumferential Inner Semi-elliptic Crack

Crack front angle 0 is the deepest point. Tensile load of magnitude 10Mpa is applied to the structure. Results are obtained for different R/t, a/t and a/c values. R is 50mm for all cases but a, c and t change. Results are obtained for the following ranges;

R/t = 5, 10 and 20

a/t = 0.2, 0.3 and 0.4

a/c = 0.2, 0.4 and 0.8

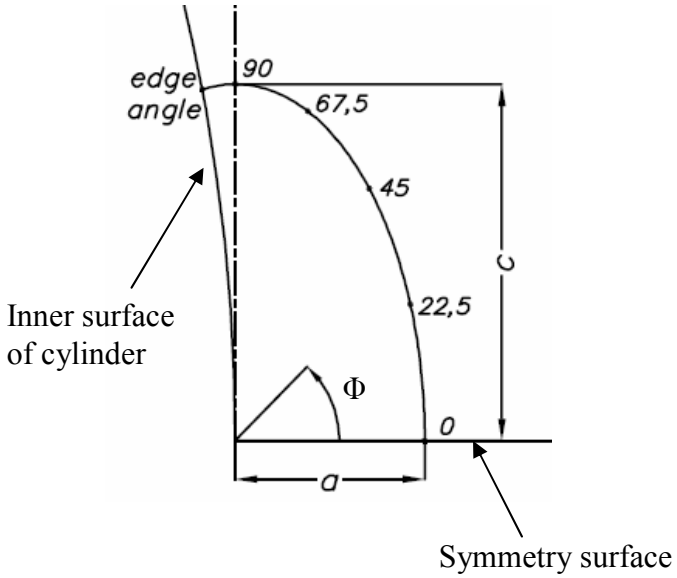

Figure 3.40 Crack front angles for Type4 and Type9

As it is mentioned in [7], because of the free-surface effect, SIF values along the crack front near the free surface calculated by FEM analyses, is not reliable.

One of the major assumptions of the linear elastic fracture mechanics (LEFM) is the continuity of the crack front. This assumption is no longer valid at

corner points of the crack, where the crack front intersects the free surface of the body. [7]

When analyzing 3D crack geometries, numerical values of fracture parameters at corner points are not reliable, and the use of quarter-point finite elements that model the square-root singularity of stresses and strains does not produce accurate results near such points. Asymptotical approach should be used at these points. [7]

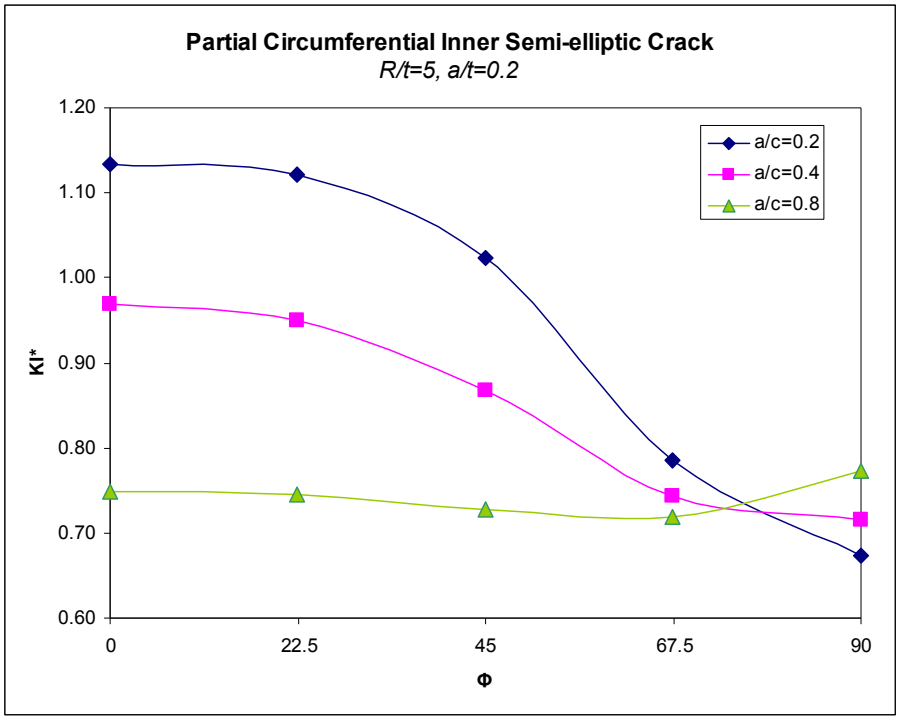

Figure 3.41 KI* versus Φ, Type4, R/t=5, a/t=0.2

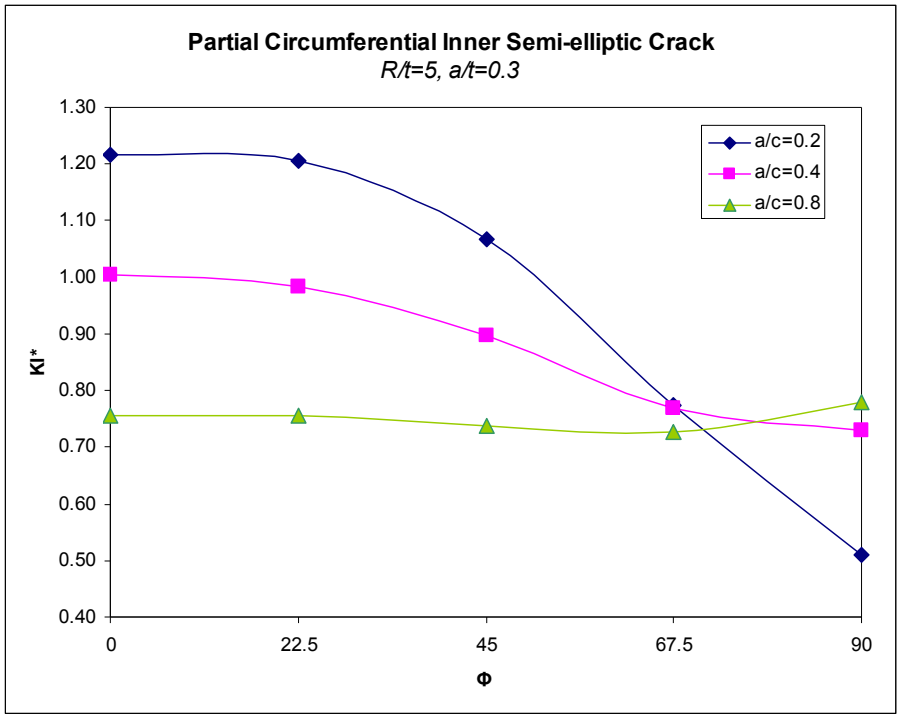

Figure 3.42 KI* versus Φ, Type4, R/t=5, a/t=0.3

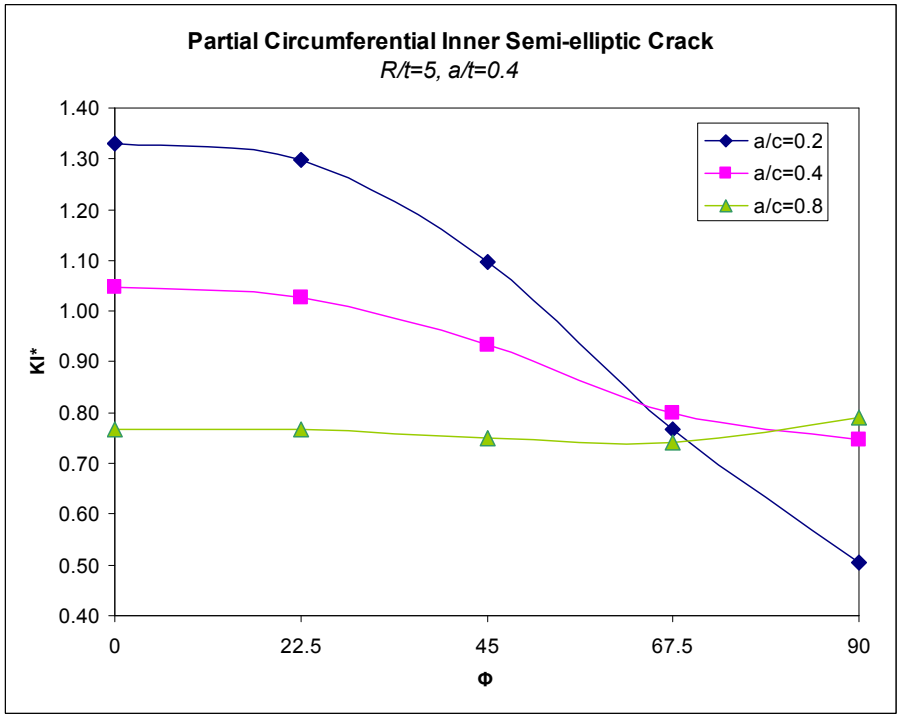

Figure 3.43 KI* versus Φ, Type4, R/t=5, a/t=0.4

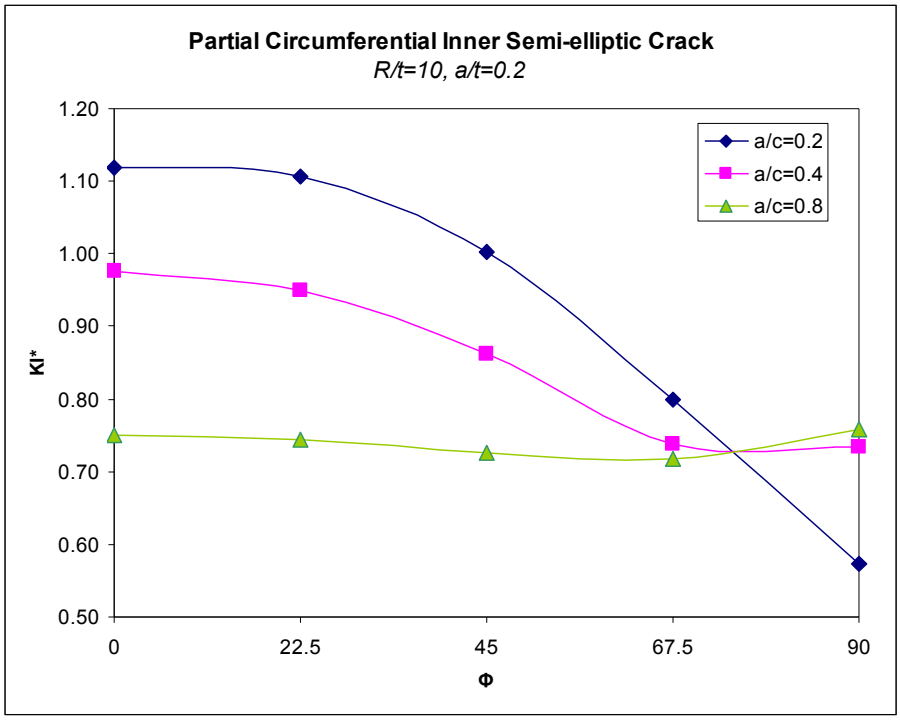

Figure 3.44 KI* versus Φ, Type4, R/t=10, a/t=0.2

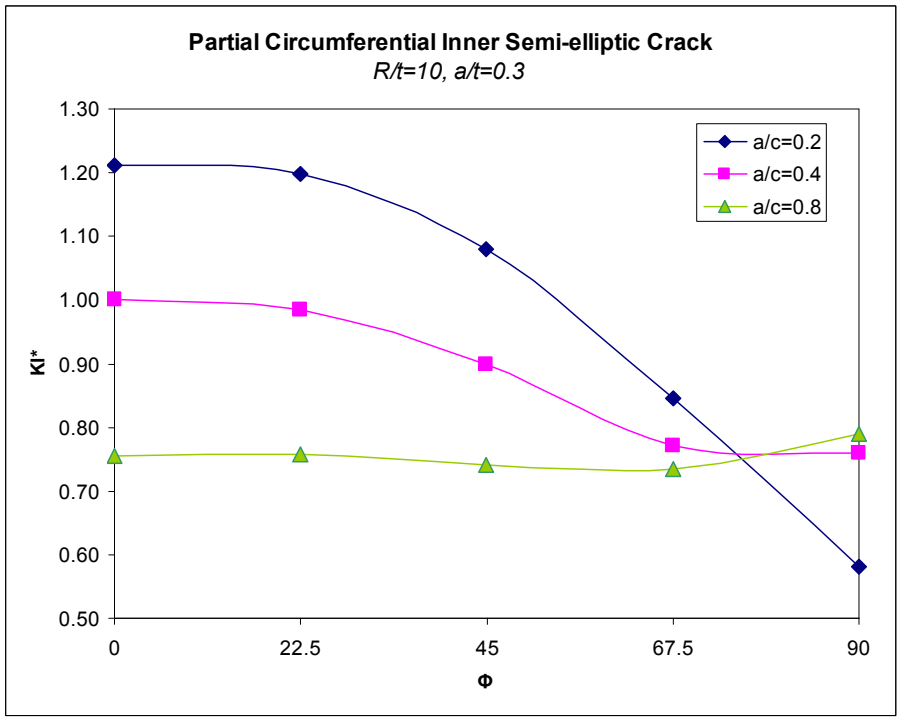

Figure 3.45 KI* versus Φ, Type4, R/t=10, a/t=0.3

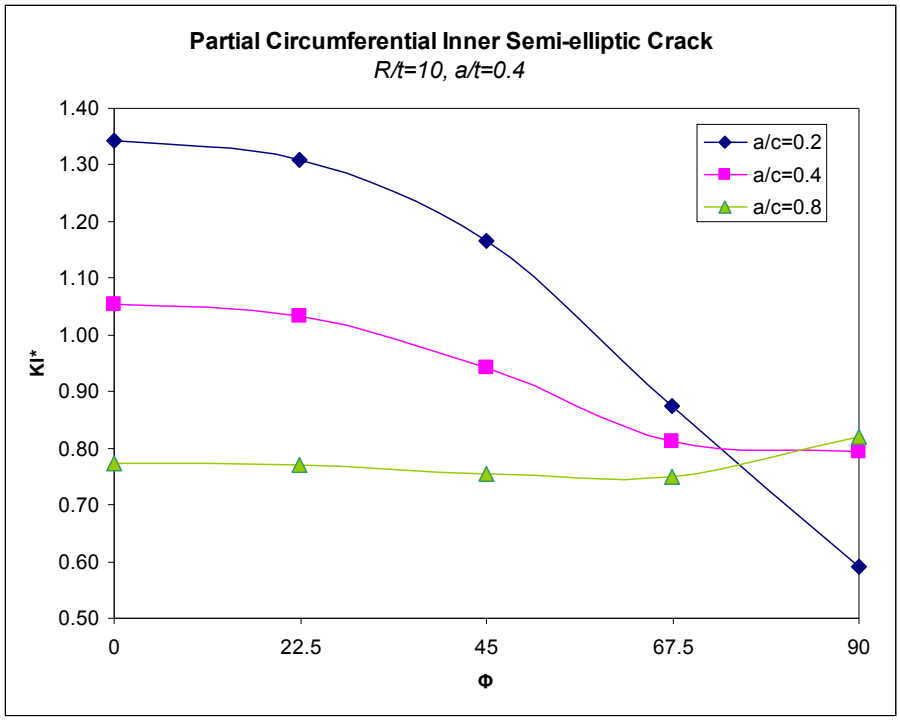

Figure 3.46 KI* versus Φ, Type4, R/t=10, a/t=0.4

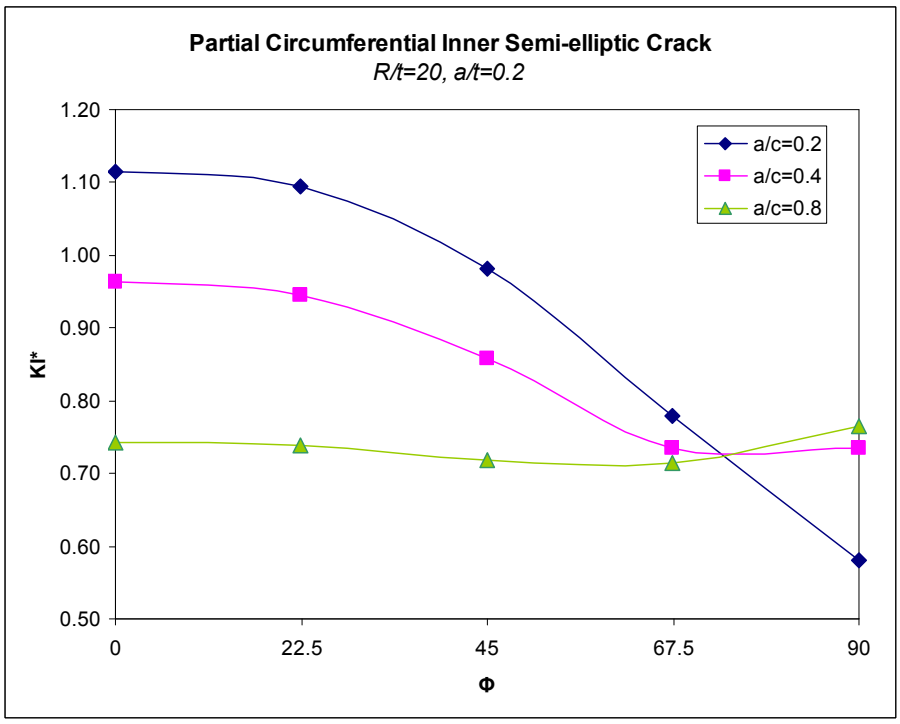

Figure 3.47 KI* versus Φ, Type4, R/t=20, a/t=0.2

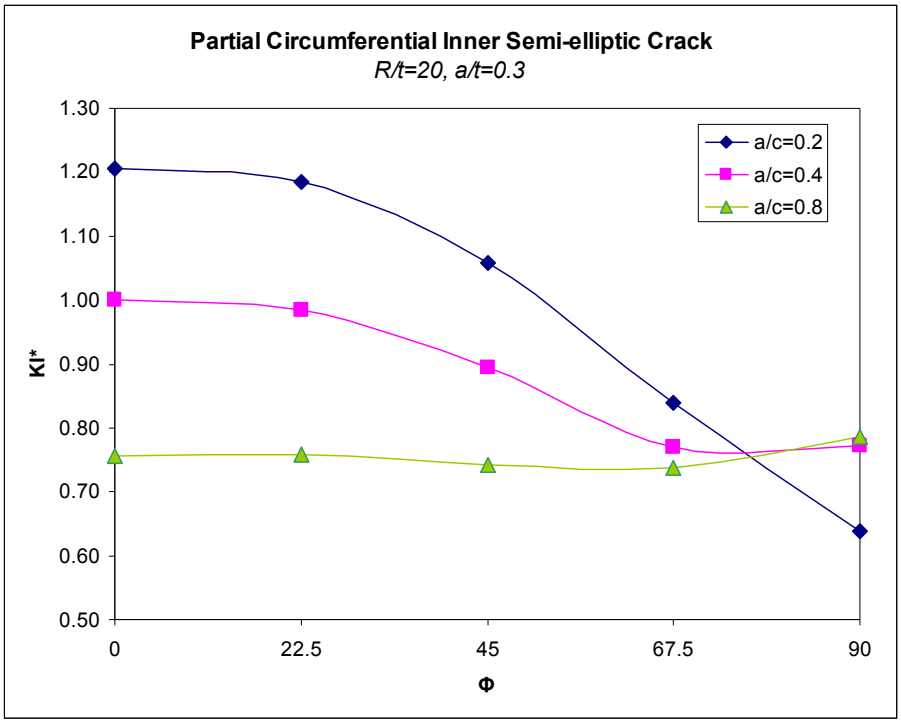

Figure 3.48 KI* versus Φ, Type4, R/t=20, a/t=0.3

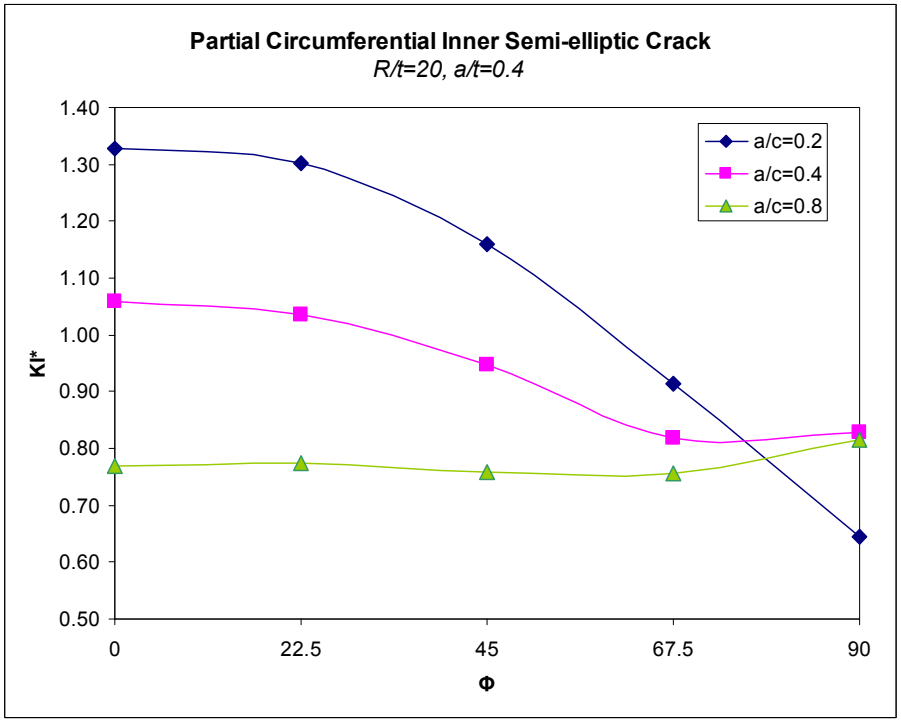

Figure 3.49 KI* versus Φ, Type4, R/t=20, a/t=0.4

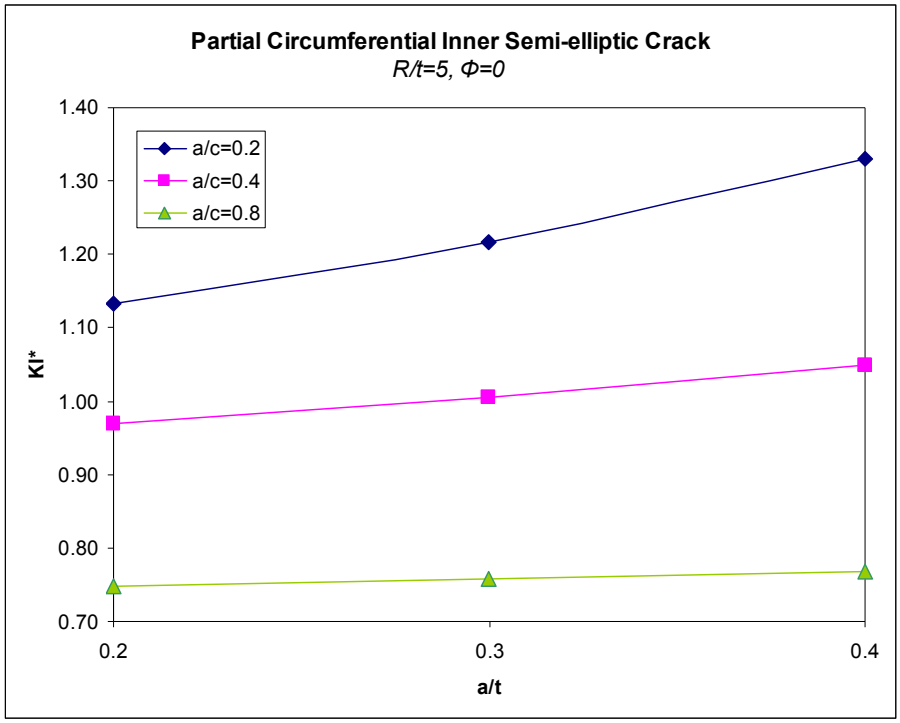

Figure 3.50 KI* at the deepest point versus a/t, Type4, R/t=5

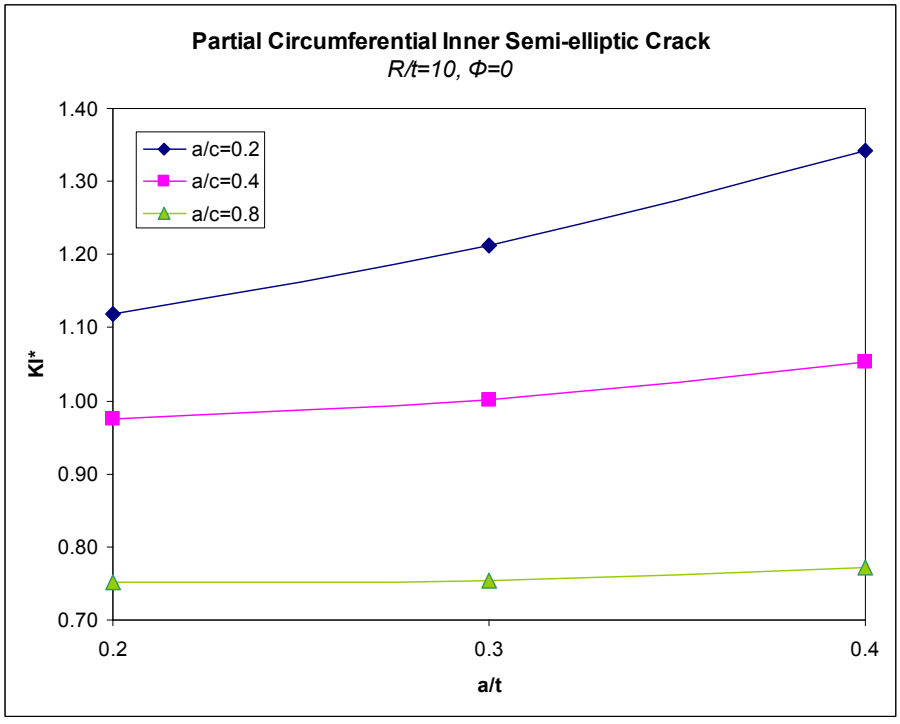

Figure 3.51 KI* at the deepest point versus a/t, Type4, R/t=10

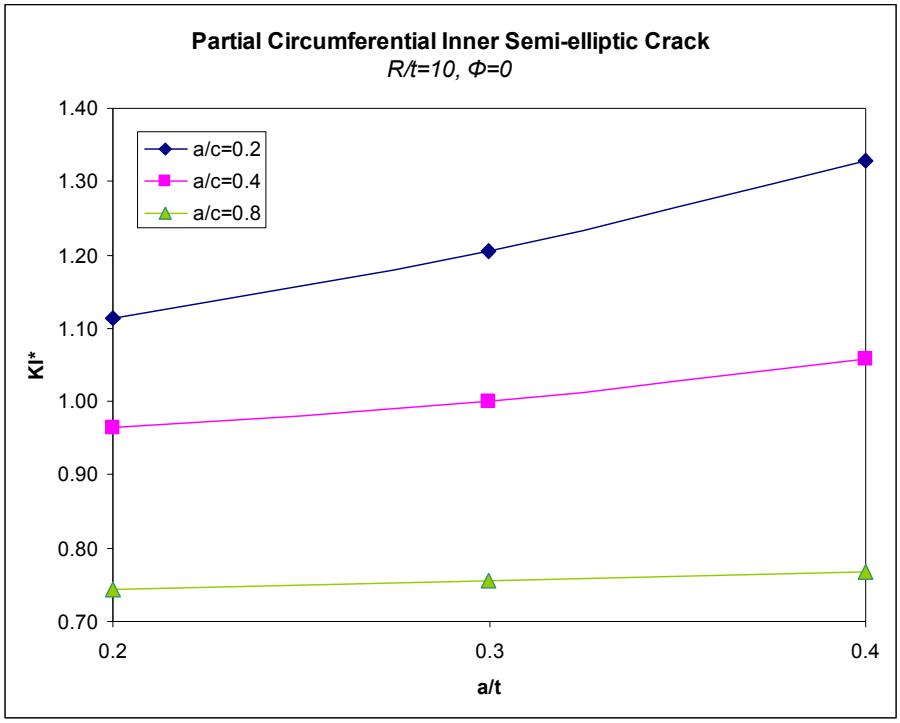

Figure 3.52 KI* at the deepest point versus a/t, Type4, R/t=20

Table 3.4 KI* for mechanical loaded partial inner circumferential crack

R/t	a/t	a/c	a (mm)	Φ=0	22.50	45	67.5	90
5	0.2	0.2	2	1.13	1.12	1.02	0.79	0.67
		0.4	2	0.97	0.95	0.87	0.74	0.72
		0.8	2	0.75	0.75	0.73	0.72	0.77
	0.3	0.2	3	1.22	1.21	1.07	0.77	0.51
		0.4	3	1.00	0.98	0.90	0.77	0.73
		0.8	3	0.76	0.76	0.74	0.73	0.78
	0.4	0.2	4	1.33	1.30	1.10	0.77	0.50
		0.4	4	1.05	1.03	0.93	0.80	0.75
		0.8	4	0.77	0.77	0.75	0.74	0.79
10	0.2	0.2	1	1.12	1.11	1.00	0.80	0.57
		0.4	1	0.98	0.95	0.86	0.74	0.73
		0.8	1	0.75	0.74	0.72	0.72	0.76
	0.3	0.2	1.5	1.21	1.20	1.08	0.85	0.58
		0.4	1.5	1.00	0.98	0.90	0.77	0.76
		0.8	1.5	0.75	0.76	0.74	0.73	0.79
	0.4	0.2	2	1.34	1.31	1.17	0.87	0.59
		0.4	2	1.05	1.03	0.94	0.81	0.79
		0.8	2	0.77	0.77	0.75	0.75	0.82
20	0.2	0.2	0.5	1.11	1.10	0.98	0.78	0.58
		0.4	0.5	0.96	0.94	0.86	0.73	0.74
		0.8	0.5	0.74	0.74	0.72	0.71	0.76
	0.3	0.2	0.8	1.21	1.18	1.06	0.84	0.64
		0.4	0.8	1.00	0.98	0.89	0.77	0.77
		0.8	0.8	0.76	0.76	0.74	0.74	0.79
	0.4	0.2	1	1.33	1.30	1.16	0.91	0.64
		0.4	1	1.06	1.04	0.95	0.82	0.83
		0.8	1	0.77	0.77	0.76	0.76	0.81

KI* at the deepest point is greater than KI* at the surface point for the cases a/c is equal to 0.2 and 0.4. For the cases a/c is equal to 0.8, KI* values along the crack front are almost constant. R/t, does not affect KI* values so much, compared for the cases with same a/t and a/c.

As a/t increases, KI* increases for the same a/c value. But as a/c inreases, effect of a/t decreases.

3.1.5.Tension Applied-Partial Circumferential Outer Semi-elliptic Crack

Crack front angle 0 is the deepest point. Tensile load of magnitude 10Mpa is applied to the structure. Results are obtained for different R/t, a/t and a/c values. R is 50mm for all cases but a, c and t change. Results are obtained for the following ranges;

R/t = 5, 10 and 20

a/t = 0.2, 0.3 and 0.4

a/c = 0.2, 0.4 and 0.8

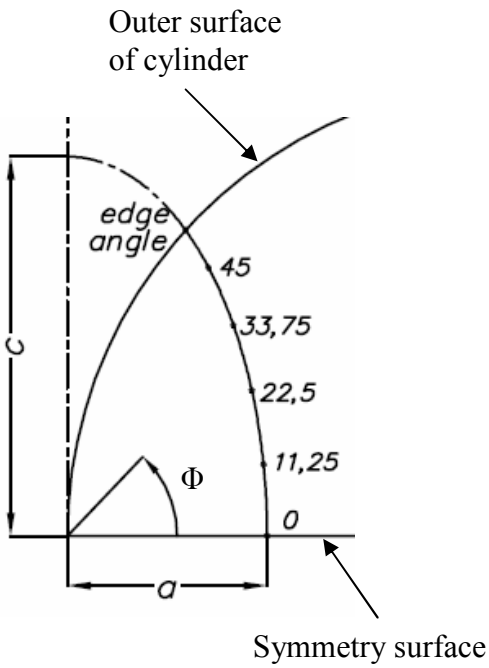

Figure 3.53 Crack front angles for Type5 and Type10

As it is expressed in partial circumferential Inner Semi-elliptic crack analysis, the calculated SIF values at the edge point are not reliable. Therefore edge point results are not considered in this study.

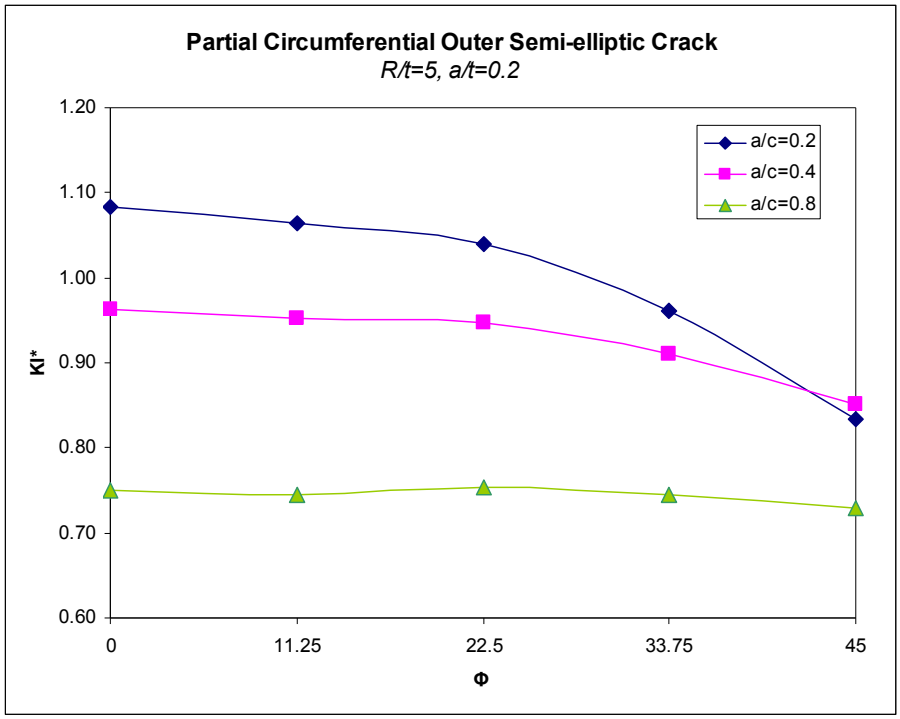

Figure 3.54 KI* versus Φ, Type5, R/t=5, a/t=0.2

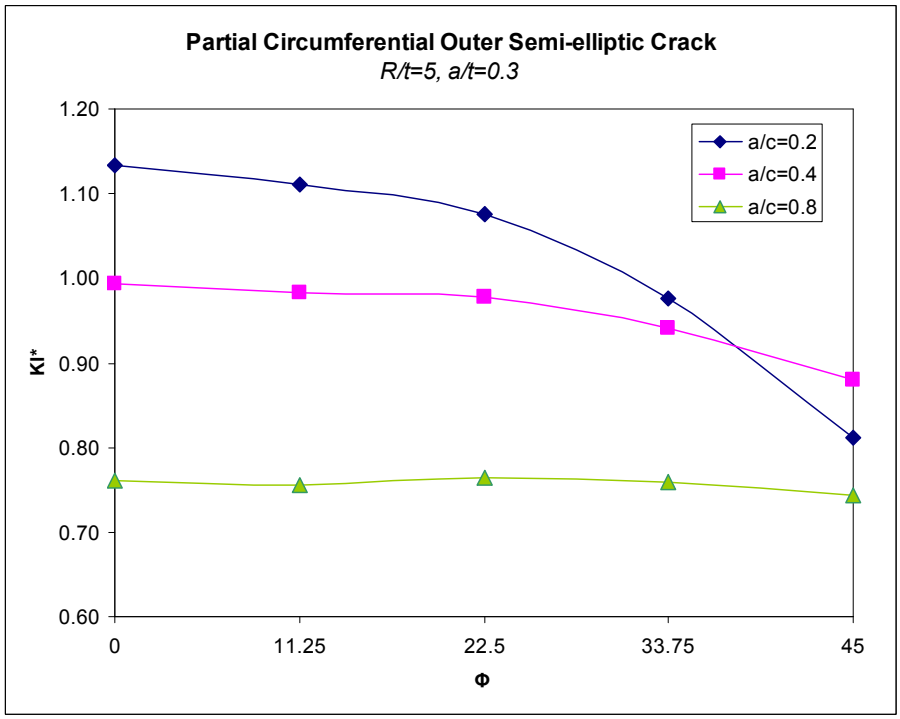

Figure 3.55 KI* versus Φ, Type5, R/t=5, a/t=0.3

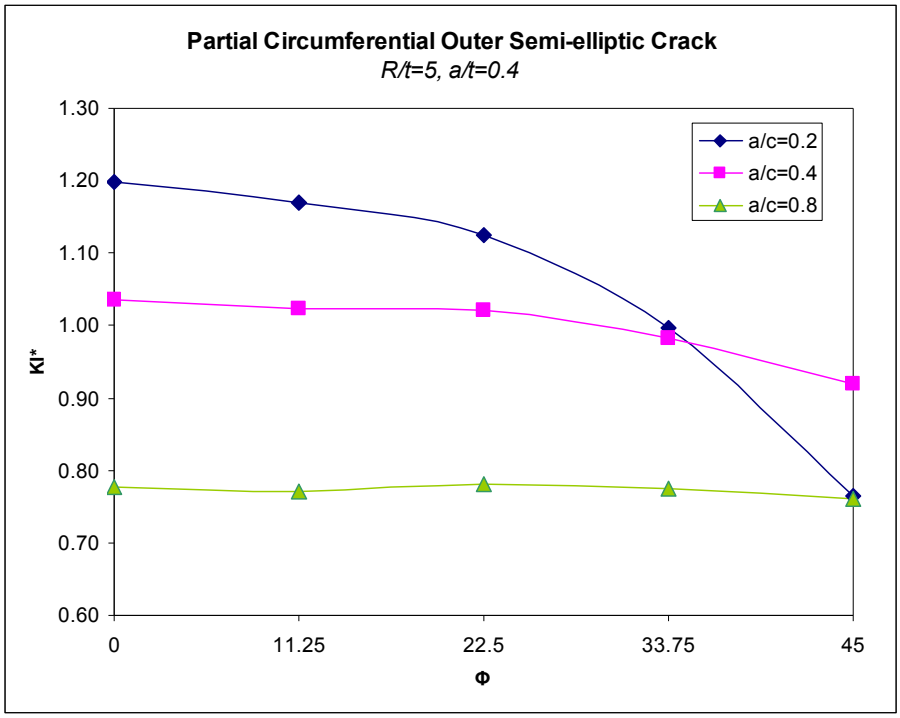

Figure 3.56 KI* versus Φ, Type5, R/t=5, a/t=0.4

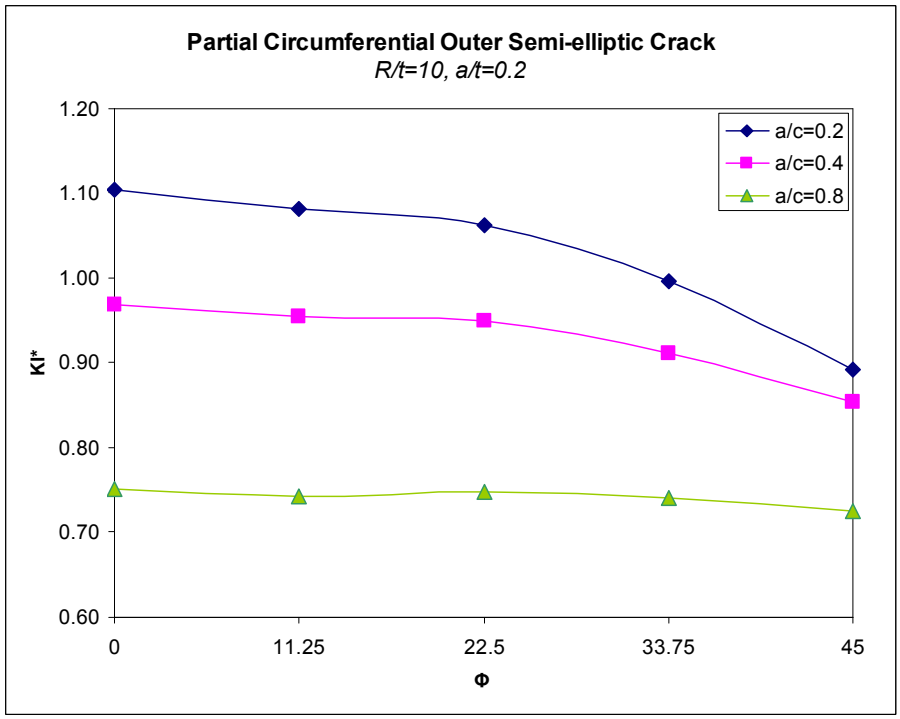

Figure 3.57 KI* versus Φ, Type5, R/t=10, a/t=0.2

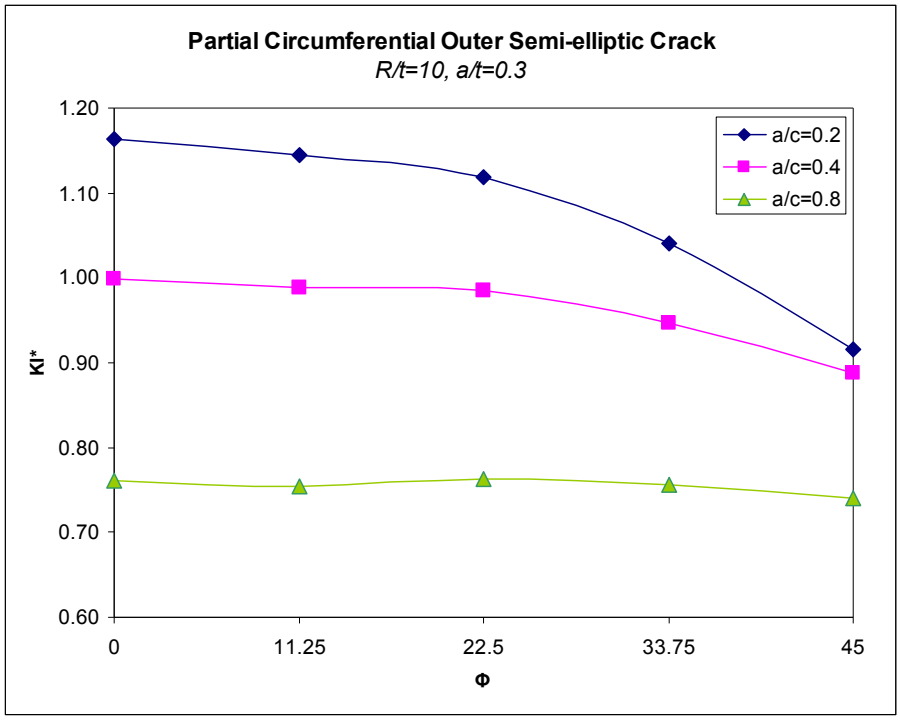

Figure 3.58 KI* versus Φ, Type5, R/t=10, a/t=0.3

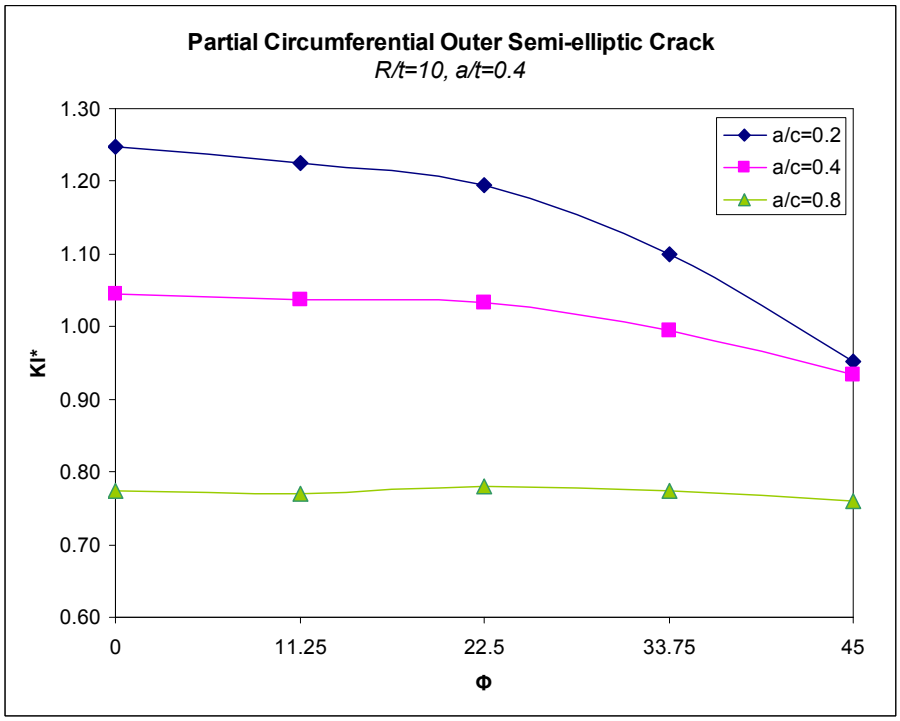

Figure 3.59 KI* versus Φ, Type5, R/t=10, a/t=0.4

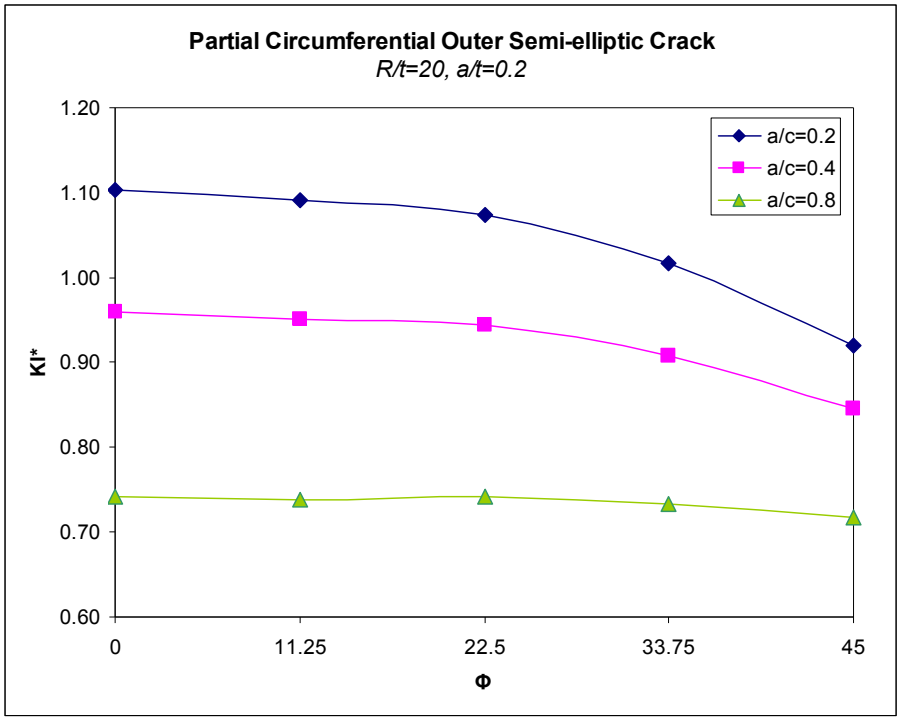

Figure 3.60 KI* versus Φ, Type5, R/t=20, a/t=0.2

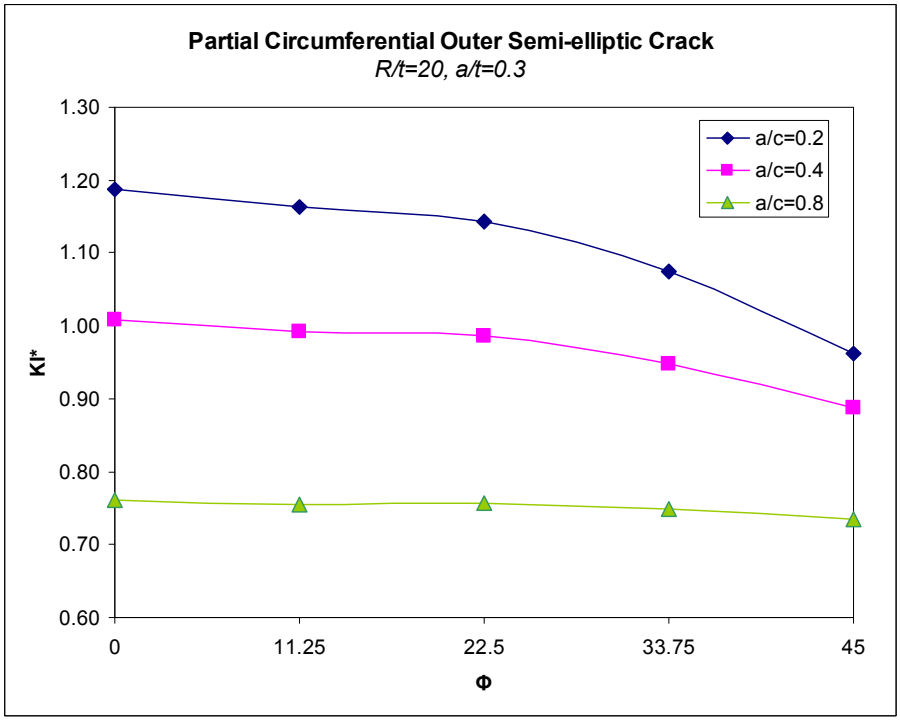

Figure 3.61 KI* versus Φ, Type5, R/t=20, a/t=0.3

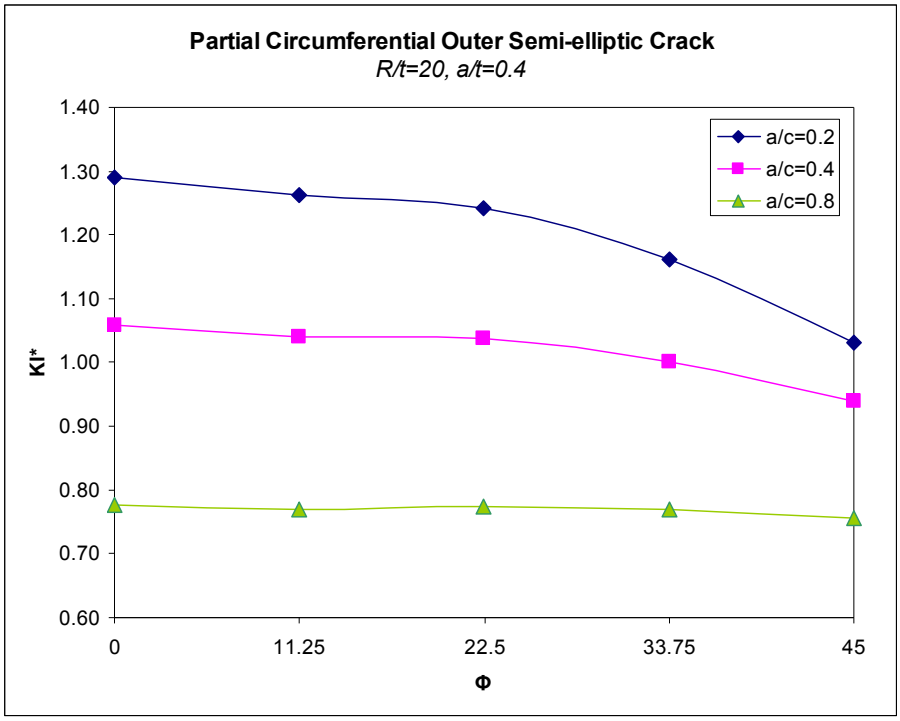

Figure 3.62 KI* versus Φ, Type5, R/t=20, a/t=0.4

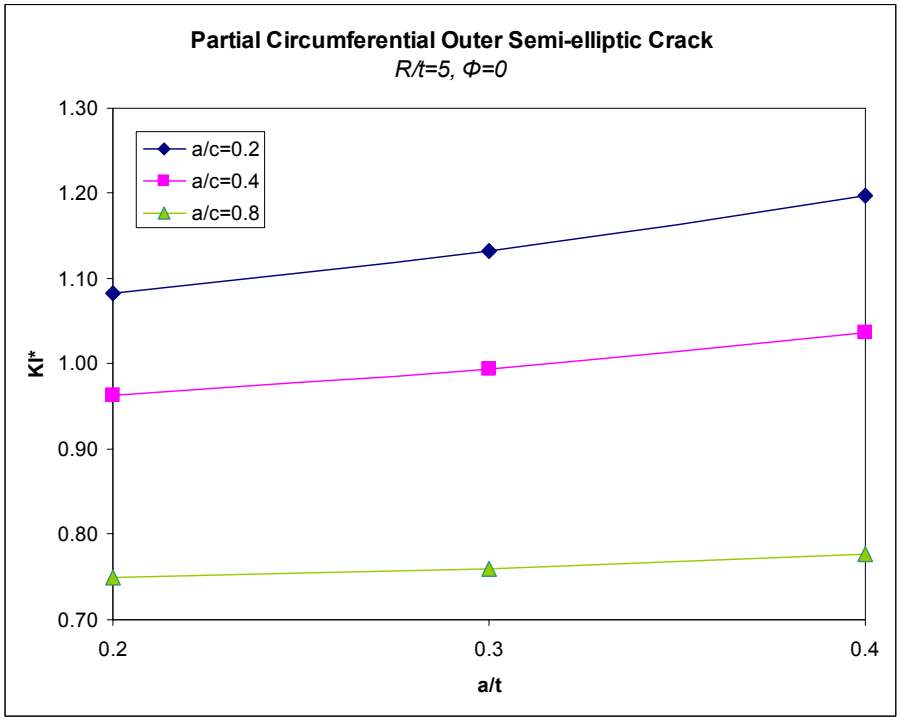

Figure 3.63 KI* at the deepest point versus a/t, Type5, R/t=5

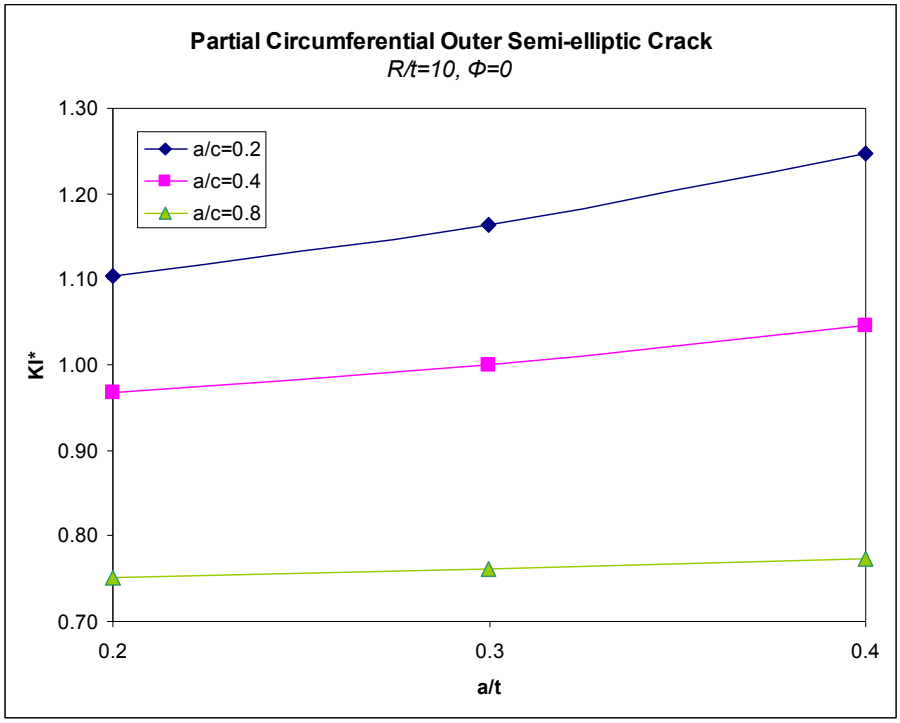

Figure 3.64 KI* at the deepest point versus a/t, Type5, R/t=10

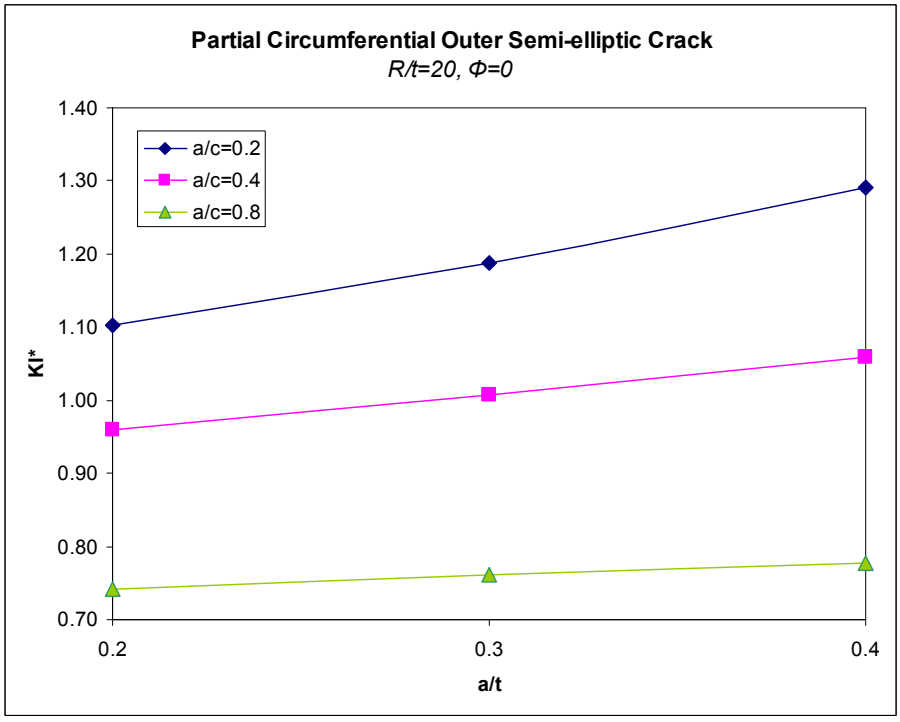

Figure 3.65 KI* at the deepest point versus a/t, Type5, R/t=20

Table 3.5 KI* for mechanical loaded partial outer circumferential crack

R/t	a/t	a/c	a (mm)	Φ=0	11.25	22.5	33.75	45
5	0.2	0.2	2	1.08	1.06	1.04	0.96	0.83
		0.4	2	0.96	0.95	0.95	0.91	0.85
		0.8	2	0.75	0.74	0.75	0.75	0.73
	0.3	0.2	3	1.13	1.11	1.08	0.98	0.81
		0.4	3	0.99	0.98	0.98	0.94	0.88
		0.8	3	0.76	0.76	0.77	0.76	0.74
	0.4	0.2	4	1.20	1.17	1.12	1.00	0.76
		0.4	4	1.04	1.02	1.02	0.98	0.92
		0.8	4	0.78	0.77	0.78	0.78	0.76
10	0.2	0.2	1	1.10	1.08	1.06	1.00	0.89
		0.4	1	0.97	0.95	0.95	0.91	0.85
		0.8	1	0.75	0.74	0.75	0.74	0.73
	0.3	0.2	1.5	1.16	1.14	1.12	1.04	0.91
		0.4	1.5	1.00	0.99	0.98	0.95	0.89
		0.8	1.5	0.76	0.76	0.76	0.76	0.74
	0.4	0.2	2	1.25	1.23	1.19	1.10	0.95
		0.4	2	1.05	1.04	1.03	0.99	0.93
		0.8	2	0.77	0.77	0.78	0.77	0.76
20	0.2	0.2	0.5	1.10	1.09	1.07	1.02	0.92
		0.4	0.5	0.96	0.95	0.94	0.91	0.85
		0.8	0.5	0.74	0.74	0.74	0.73	0.72
	0.3	0.2	0.8	1.19	1.16	1.14	1.08	0.96
		0.4	0.8	1.01	0.99	0.99	0.95	0.89
		0.8	0.8	0.76	0.75	0.76	0.75	0.73
	0.4	0.2	1	1.29	1.26	1.24	1.16	1.03
		0.4	1	1.06	1.04	1.04	1.00	0.94
		0.8	1	0.78	0.77	0.78	0.77	0.76

KI* at the deepest point is greater than KI* at the surface point for the cases a/c is equal to 0.2 and 0.4. For the cases a/c is equal to 0.8, KI* values along the crack front are almost constant. R/t, does not affect KI* values so much, compared for the cases with same a/t and a/c.

As a/t increases, KI* increases for the same a/c value. But as a/c inreases, effect of a/t decreases.

3.1.6.Tension Applied-Circumferential Embedded Crack

Crack front angle 0 is closer to the outer surface of the cylinder. Tensile load of magnitude 10Mpa is applied to the structure. Results are obtained for different R/t, a/t and a/c values. R is 50mm for all cases but a, c and t change. Results are obtained for the following ranges;

R/t = 5, 10 and 20

a/t = 0.2, 0.3 and 0.4

a/c = 0.2, 0.4 and 0.8

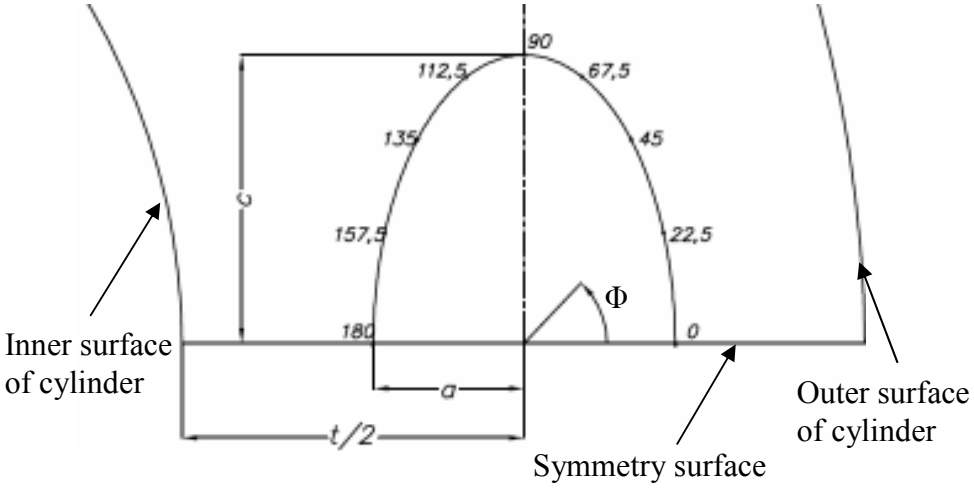

Figure 3.66 Crack front angles for Type6

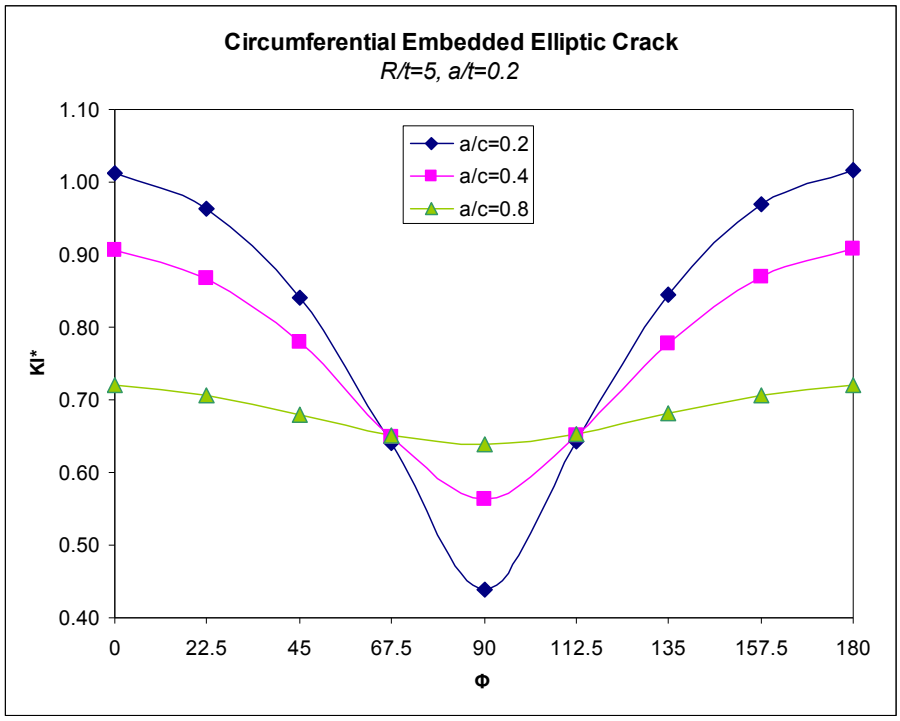

Figure 3.67 KI* versus Φ, Type6, R/t=5, a/t=0.2

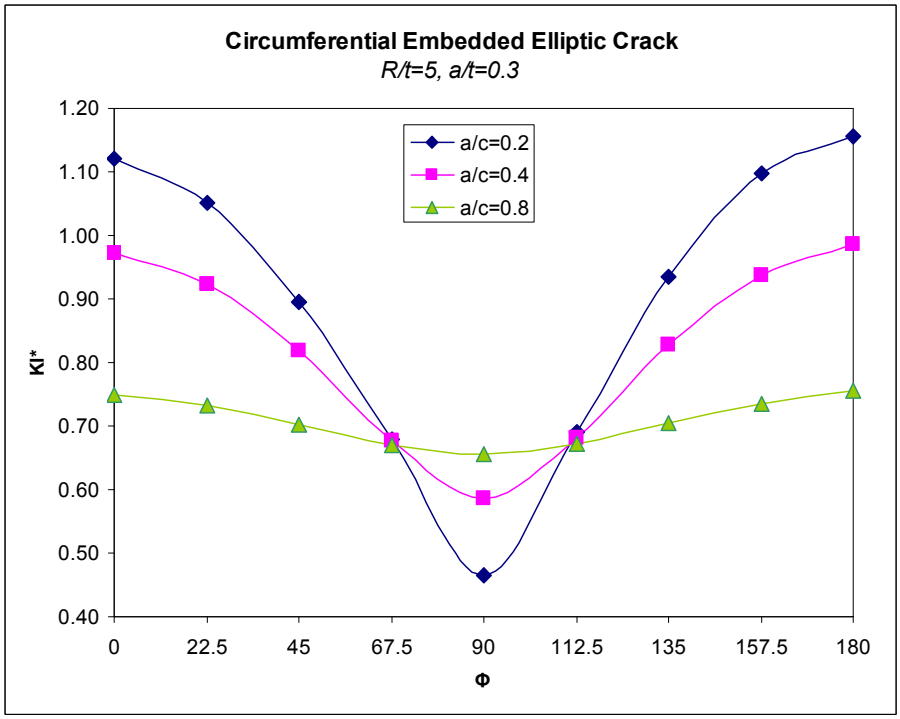

Figure 3.68 KI* versus Φ, Type6, R/t=5, a/t=0.3

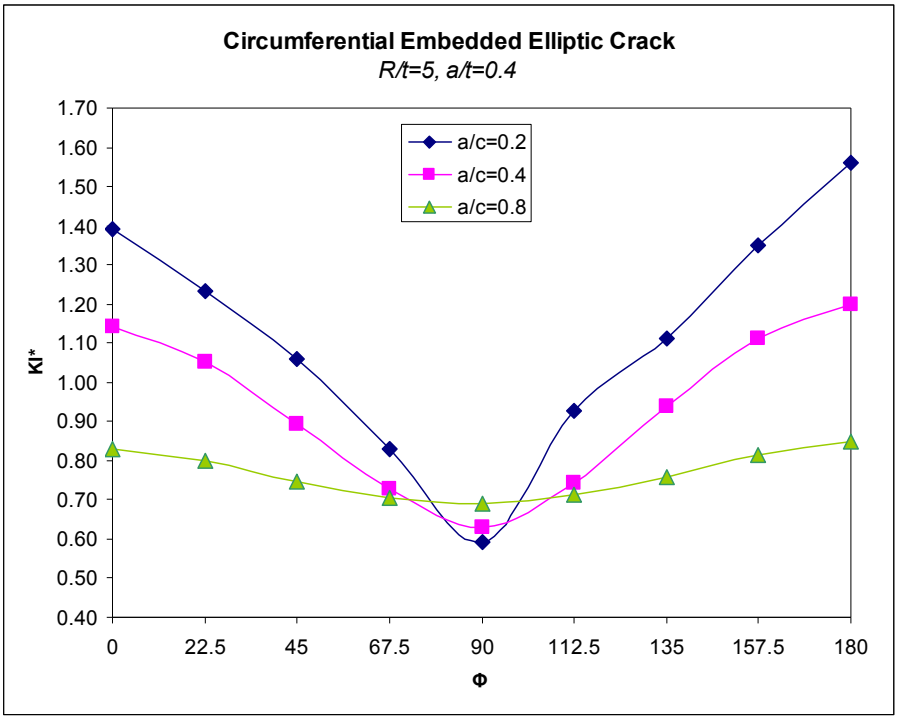

Figure 3.69 KI* versus Φ, Type6, R/t=5, a/t=0.4

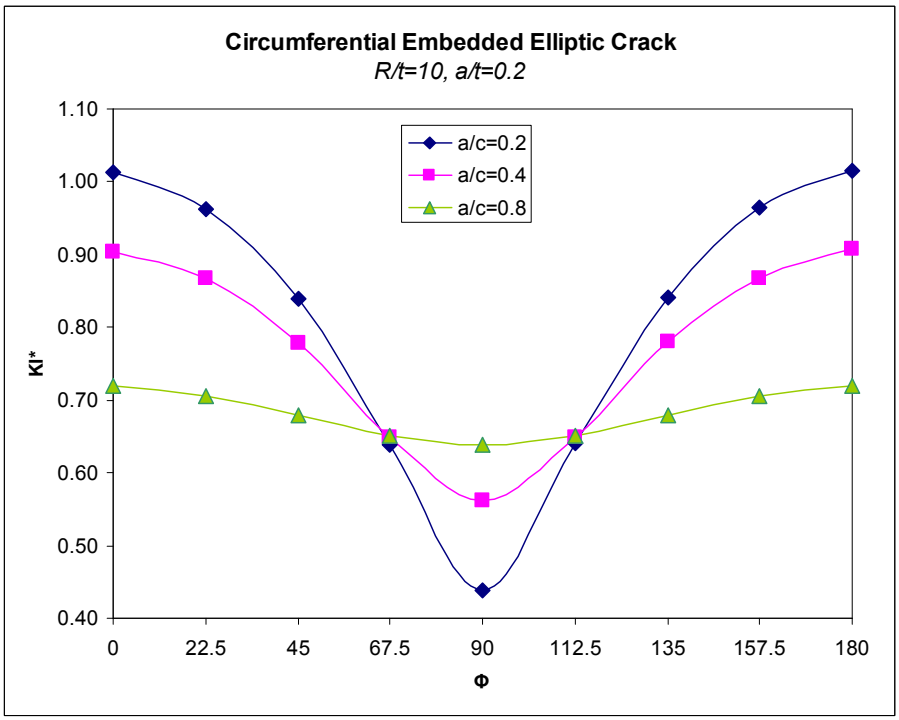

Figure 3.70 KI* versus Φ, Type6, R/t=10, a/t=0.2

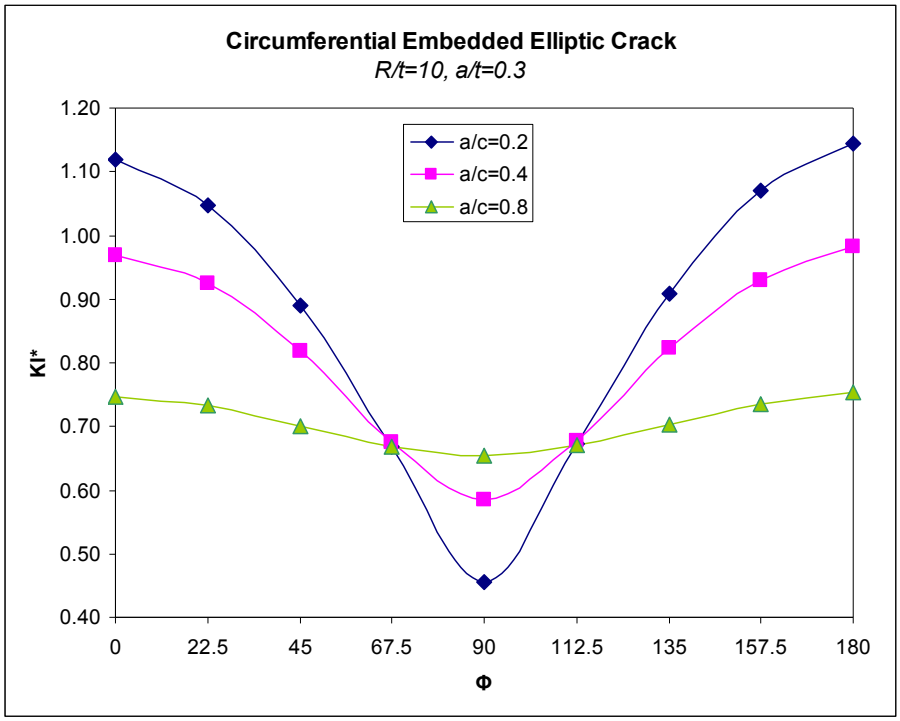

Figure 3.71 KI* versus Φ, Type6, R/t=10, a/t=0.3

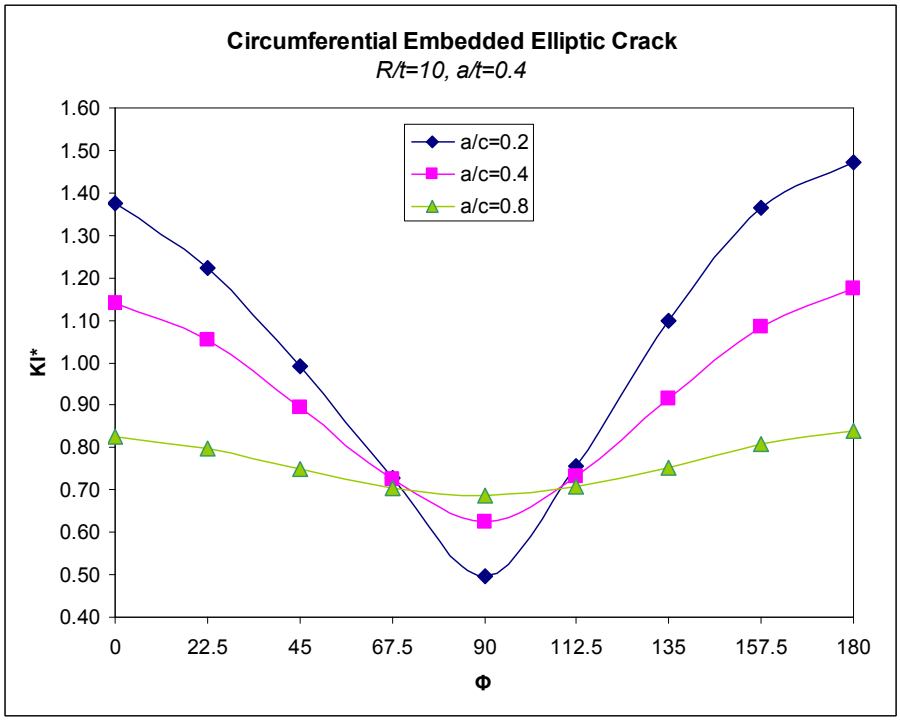

Figure 3.72 KI* versus Φ, Type6, R/t=10, a/t=0.4

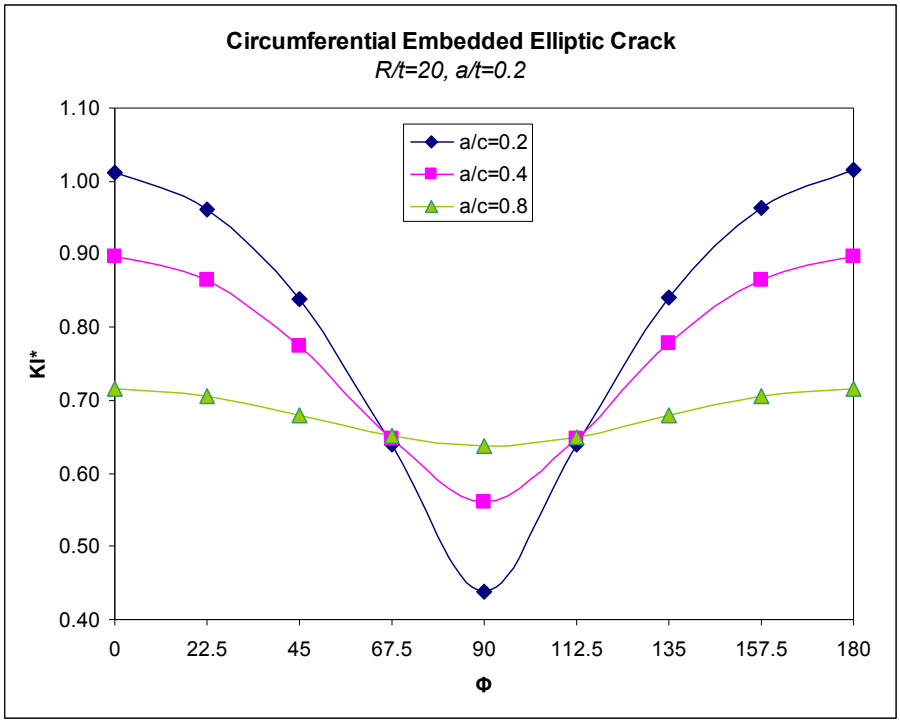

Figure 3.73 KI* versus Φ, Type6, R/t=20, a/t=0.2

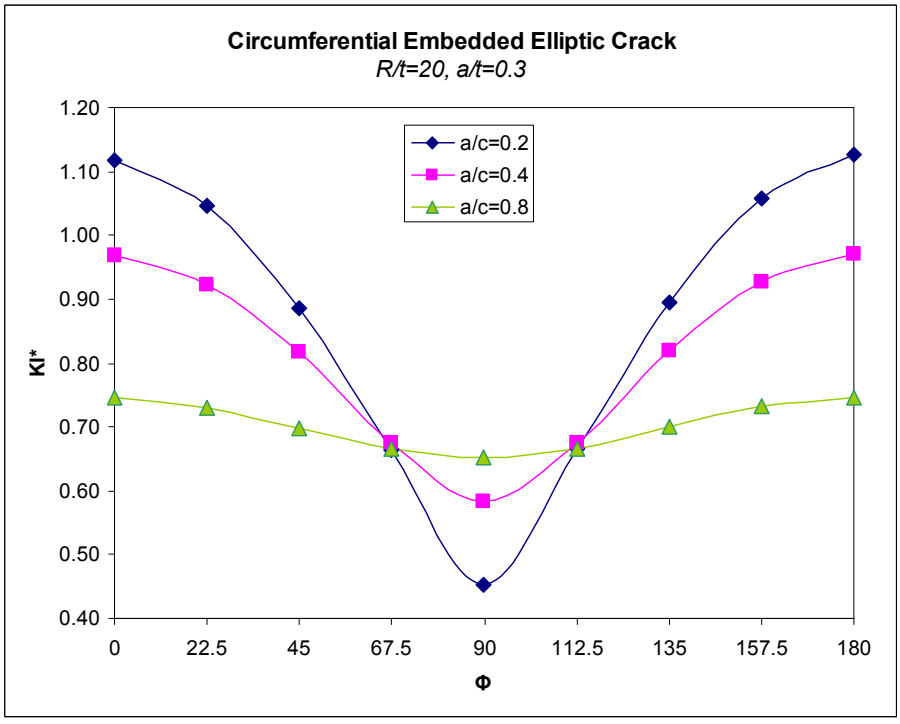

Figure 3.74 KI* versus Φ, Type6, R/t=20, a/t=0.3

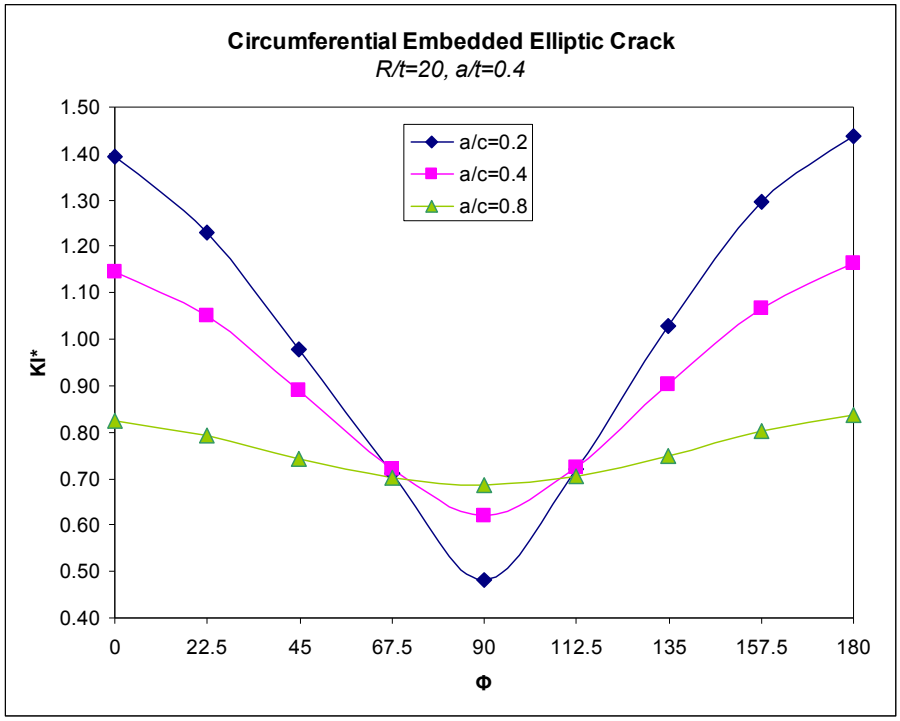

Figure 3.75 KI* versus Φ, Type6, R/t=20, a/t=0.4

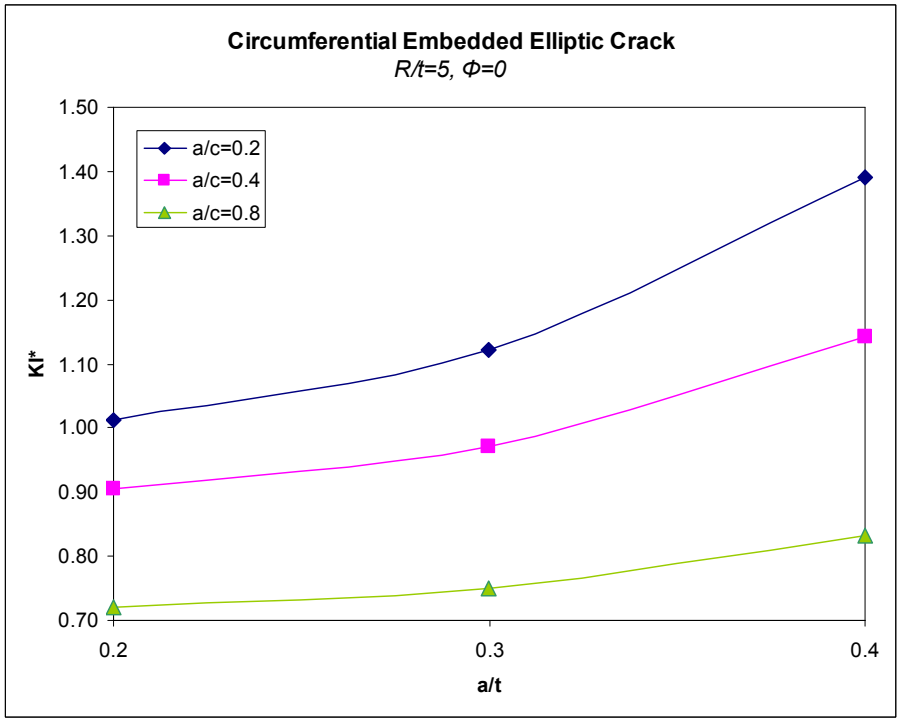

Figure 3.76 KI* at Φ=0 versus a/t, Type6, R/t=5

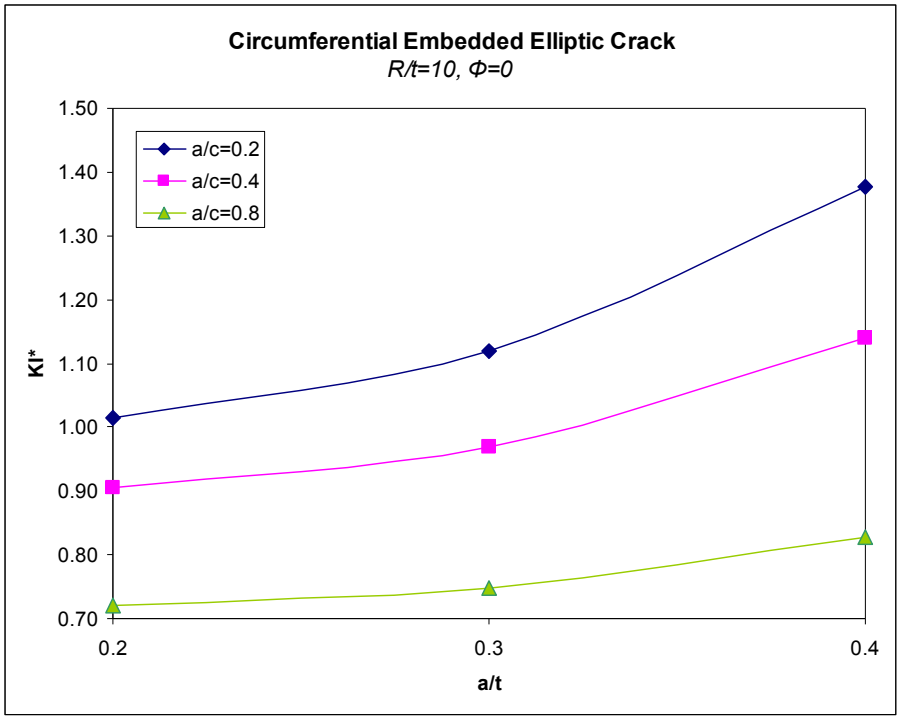

Figure 3.77 KI* at Φ=0 versus a/t, Type6, R/t=10

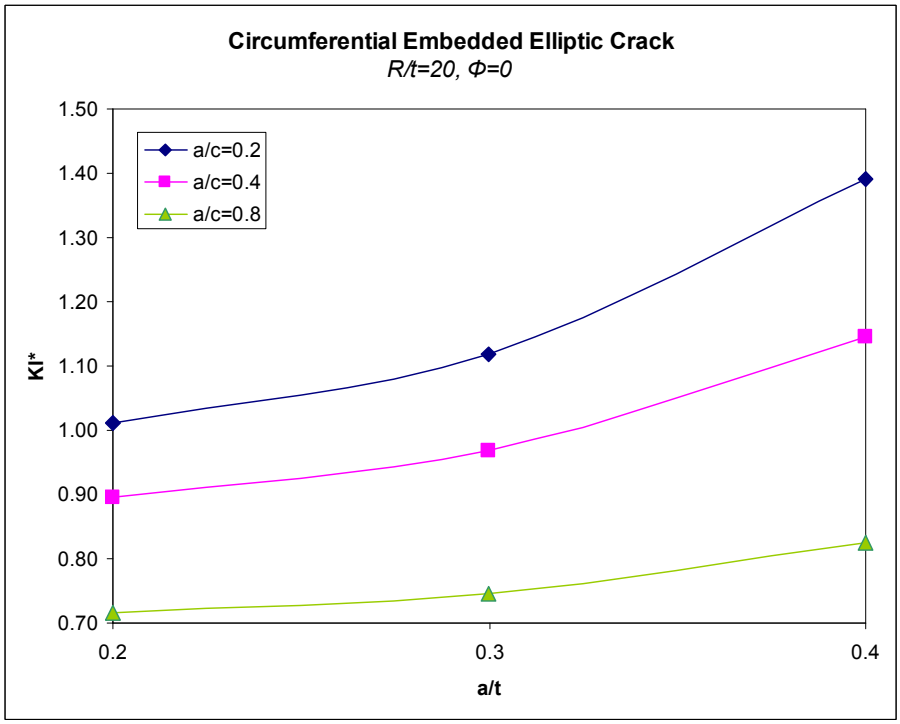

Figure 3.78 KI* at Φ=0 versus a/t, Type6, R/t=20

Table 3.6 KI* for mechanical loaded embedded circumferential crack

R/t	a/t	a/c	a (mm)	Φ=0	22.50	45	67.50	90	112.50	135	157.50	180
5	0.2	0.2	2	1.01	0.96	0.84	0.64	0.44	0.64	0.84	0.97	1.02
		0.4	2	0.91	0.87	0.78	0.65	0.56	0.65	0.78	0.87	0.91
		0.8	2	0.72	0.71	0.68	0.65	0.64	0.65	0.68	0.71	0.72
	0.3	0.2	3	1.12	1.05	0.90	0.68	0.46	0.69	0.94	1.10	1.16
		0.4	3	0.97	0.92	0.82	0.68	0.59	0.68	0.83	0.94	0.99
		0.8	3	0.75	0.73	0.70	0.67	0.66	0.67	0.71	0.74	0.76
	0.4	0.2	4	1.39	1.23	1.06	0.83	0.59	0.93	1.11	1.35	1.56
		0.4	4	1.14	1.05	0.89	0.73	0.63	0.74	0.94	1.11	1.20
		0.8	4	0.83	0.80	0.75	0.71	0.69	0.71	0.76	0.81	0.85
10	0.2	0.2	1	1.01	0.96	0.84	0.64	0.44	0.64	0.84	0.96	1.02
		0.4	1	0.90	0.87	0.78	0.65	0.56	0.65	0.78	0.87	0.91
		0.8	1	0.72	0.70	0.68	0.65	0.64	0.65	0.68	0.71	0.72
	0.3	0.2	1.5	1.12	1.05	0.89	0.67	0.46	0.67	0.91	1.07	1.14
		0.4	1.5	0.97	0.92	0.82	0.68	0.58	0.68	0.82	0.93	0.98
		0.8	1.5	0.75	0.73	0.70	0.67	0.66	0.67	0.70	0.73	0.75
	0.4	0.2	2	1.38	1.22	0.99	0.73	0.50	0.76	1.10	1.36	1.47
		0.4	2	1.14	1.06	0.89	0.72	0.62	0.73	0.92	1.09	1.17
		0.8	2	0.83	0.80	0.75	0.70	0.69	0.71	0.75	0.81	0.84
20	0.2	0.2	0.5	1.01	0.96	0.84	0.64	0.44	0.64	0.84	0.96	1.02
		0.4	0.5	0.90	0.86	0.78	0.65	0.56	0.65	0.78	0.87	0.90
		0.8	0.5	0.72	0.71	0.68	0.65	0.64	0.65	0.68	0.71	0.72
	0.3	0.2	0.8	1.12	1.05	0.89	0.66	0.45	0.67	0.90	1.06	1.13
		0.4	0.8	0.97	0.92	0.82	0.67	0.58	0.68	0.82	0.93	0.97
		0.8	0.8	0.75	0.73	0.70	0.67	0.65	0.67	0.70	0.73	0.75
	0.4	0.2	1	1.39	1.23	0.98	0.71	0.48	0.72	1.03	1.30	1.44
		0.4	1	1.15	1.05	0.89	0.72	0.62	0.72	0.90	1.07	1.16
		0.8	1	0.83	0.79	0.74	0.70	0.68	0.70	0.75	0.80	0.84

KI* at the angles 0 and 180 is greater than KI* at the angle 90. As a/c increases, KI* values along the crack front change less. R/t, does not affect KI* values so much, compared for the cases with same a/t and a/c.

As a/t increases, KI* increases for the same a/c value. But as a/c inreases, effect of a/t decreases.

3.2.THERMAL LOADING

3.2.1.Thermally loaded-Partial Axial Inner Semi-elliptic Crack

Crack front angle 0 is the deepest point and angle 90 is the surface point. Steady-state thermal load is applied to the structure. Inside temperature is lower than the outer temperature. Inner temperature is applied -100°C and outer temperature is applied 100°C. Results are obtained for different R/t, a/t and a/c values. R is 50mm for all cases but a, c and t change. Results are obtained for the following ranges;

R/t = 5, 10 and 20

a/t = 0.2, 0.4 and 0.6

a/c = 0.2, 0.4 and 0.8

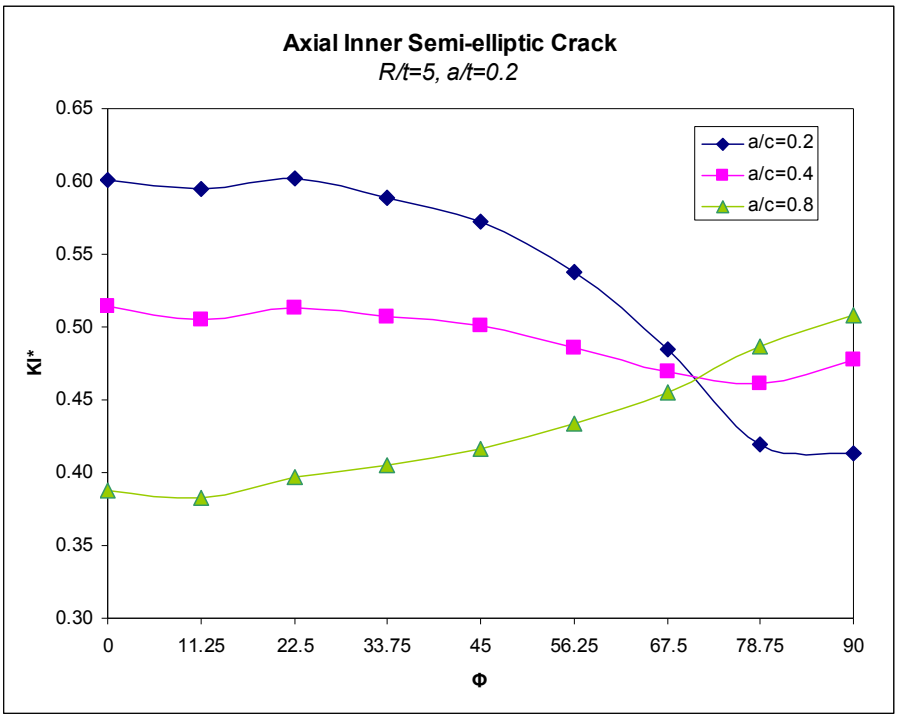

Figure 3.79 KI* versus Φ, Type7, R/t=5, a/t=0.2

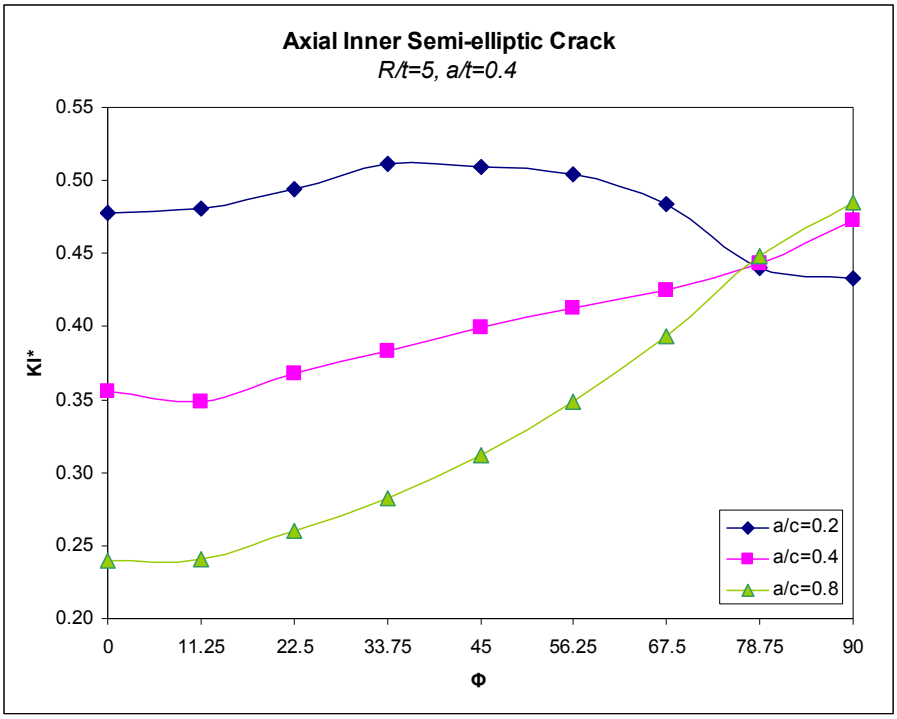

Figure 3.80 KI* versus Φ, Type7, R/t=5, a/t=0.4

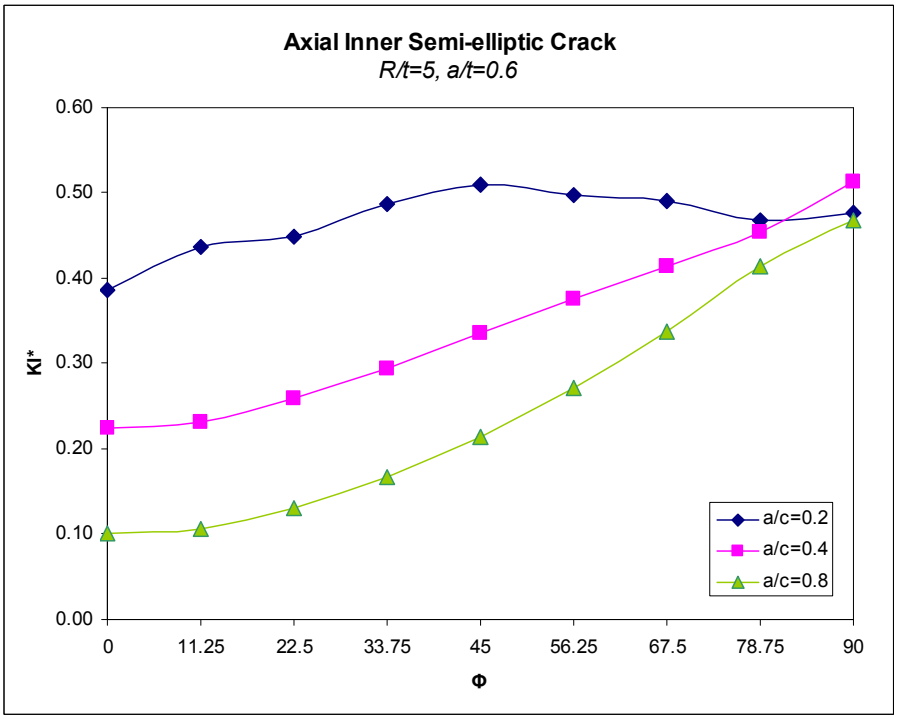

Figure 3.81 KI* versus Φ, Type7, R/t=5, a/t=0.6

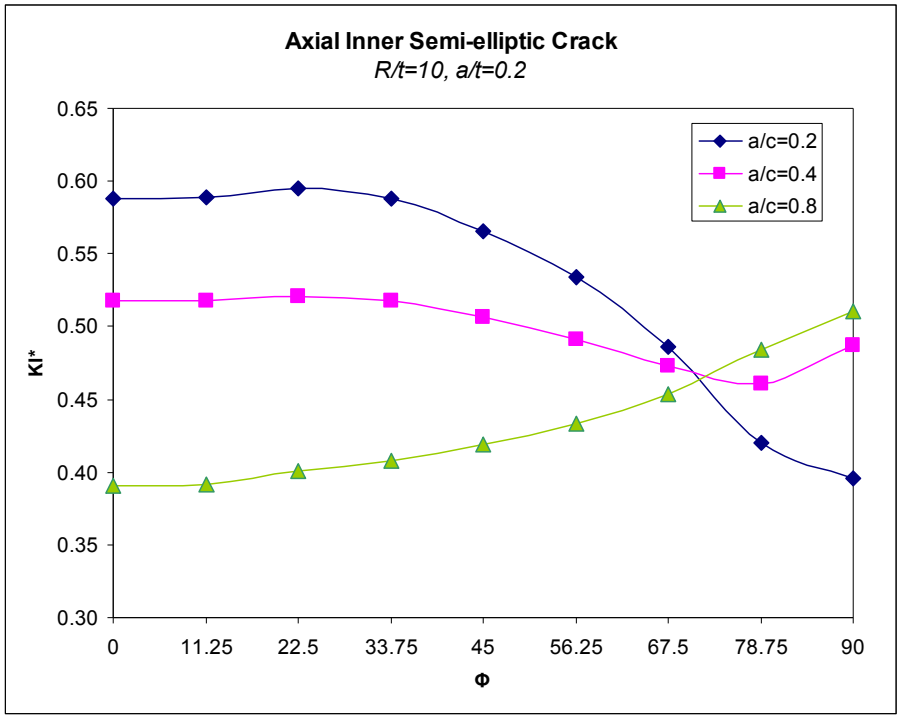

Figure 3.82 KI* versus Φ, Type7, R/t=10, a/t=0.2

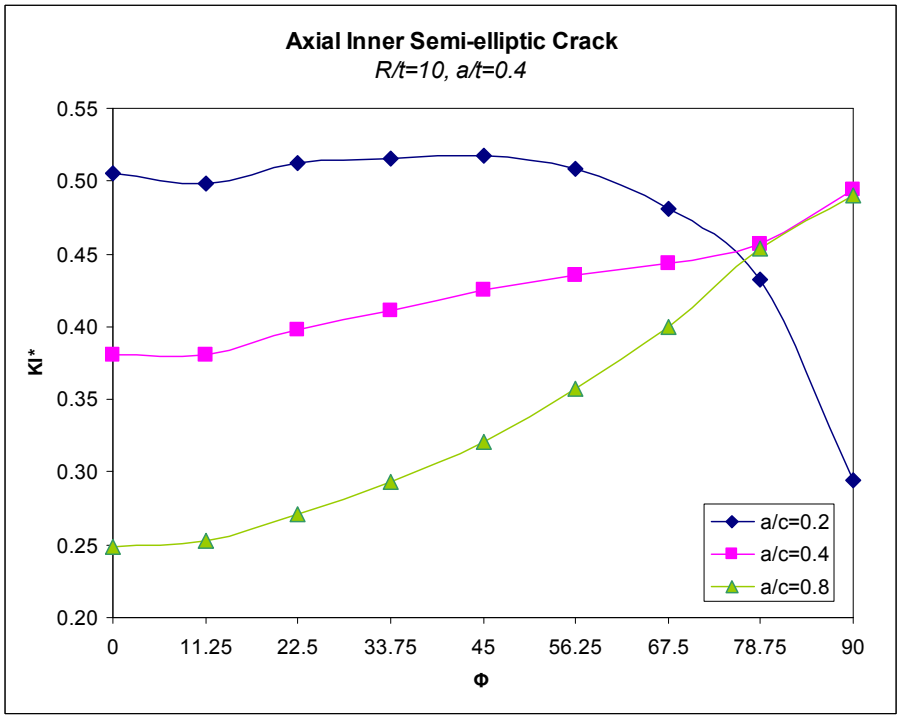

Figure 3.83 KI* versus Φ, Type7, R/t=10, a/t=0.4

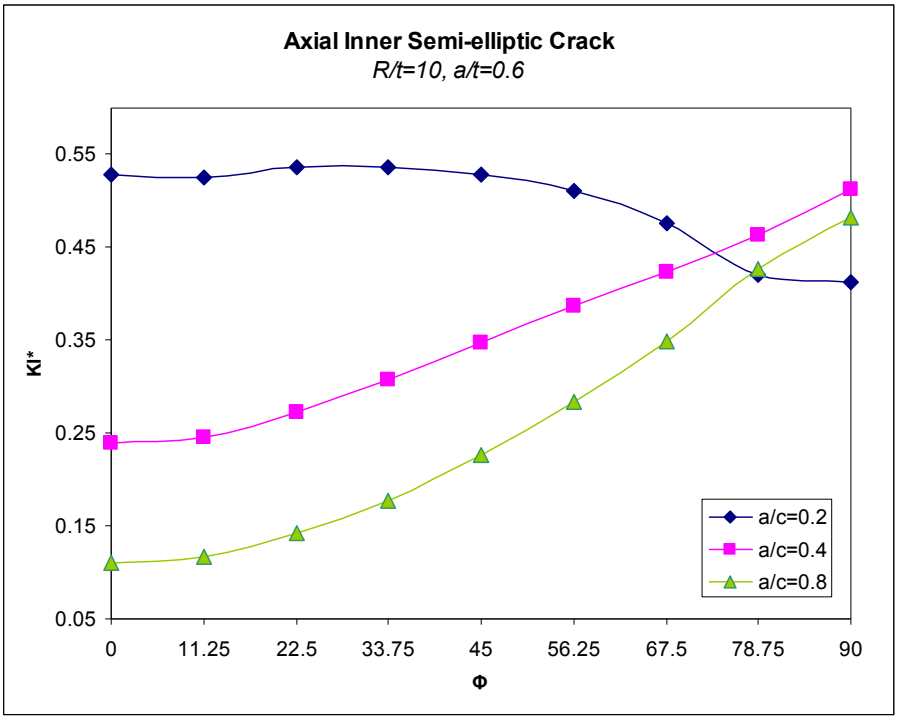

Figure 3.84 KI* versus Φ, Type7, R/t=10, a/t=0.6

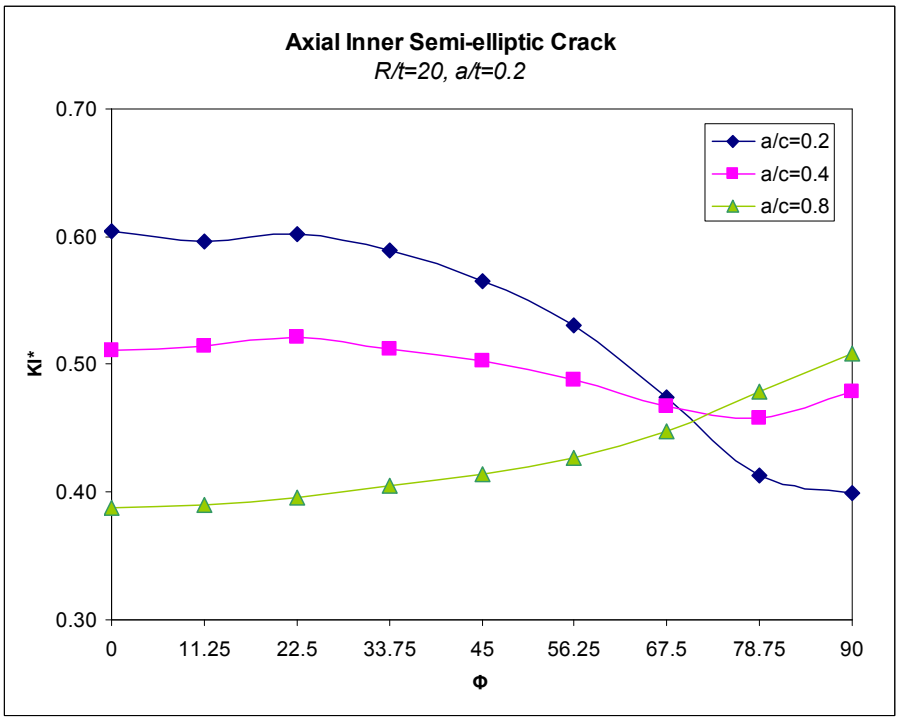

Figure 3.85 KI* versus Φ, Type7, R/t=20, a/t=0.2

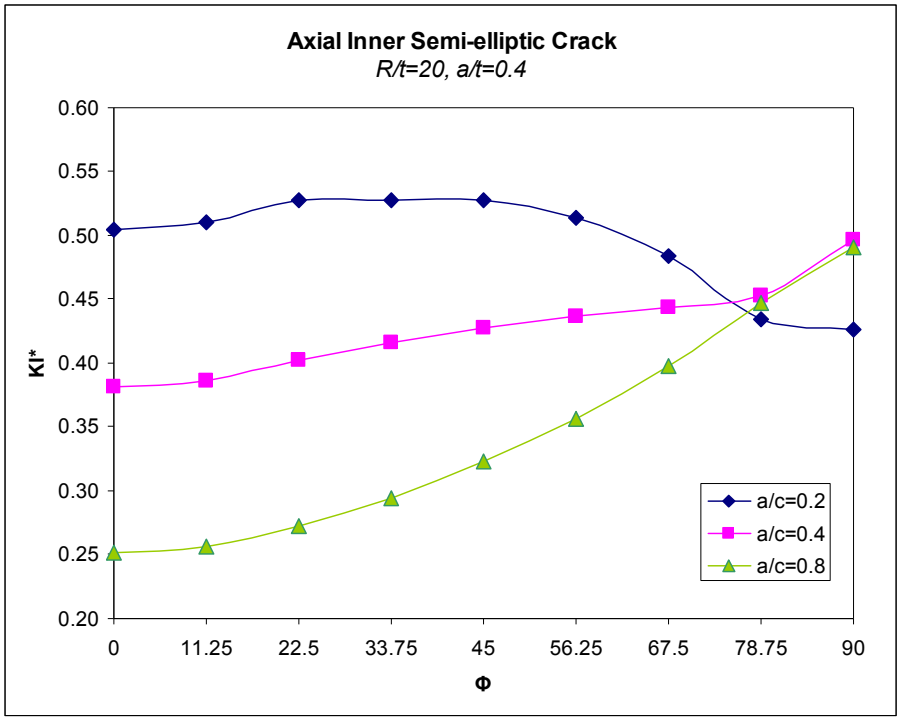

Figure 3.86 KI* versus Φ, Type7, R/t=20, a/t=0.4

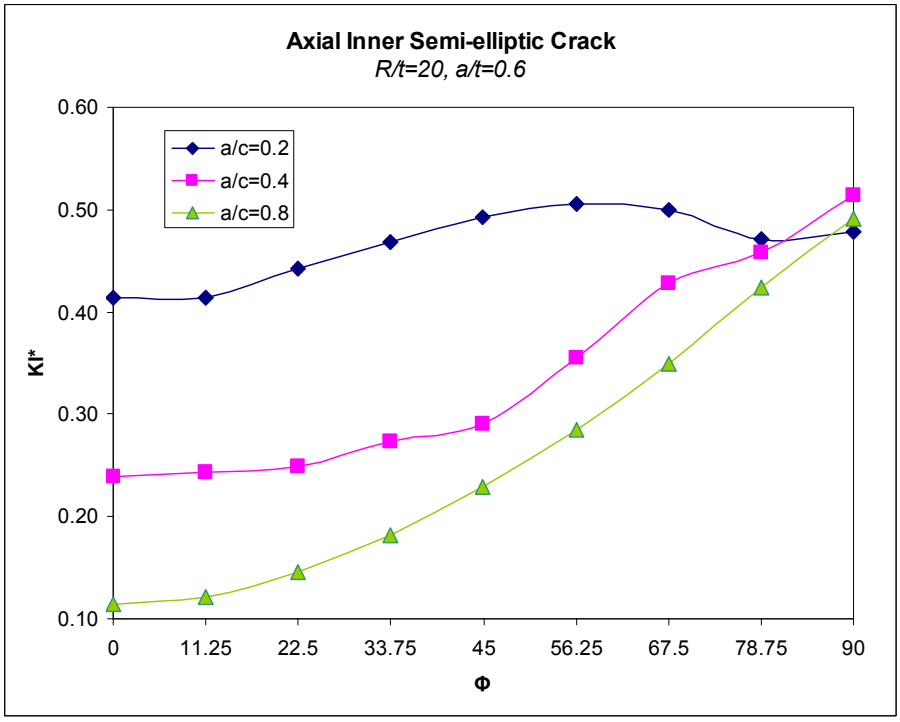

Figure 3.87 KI* versus Φ, Type7, R/t=20, a/t=0.6

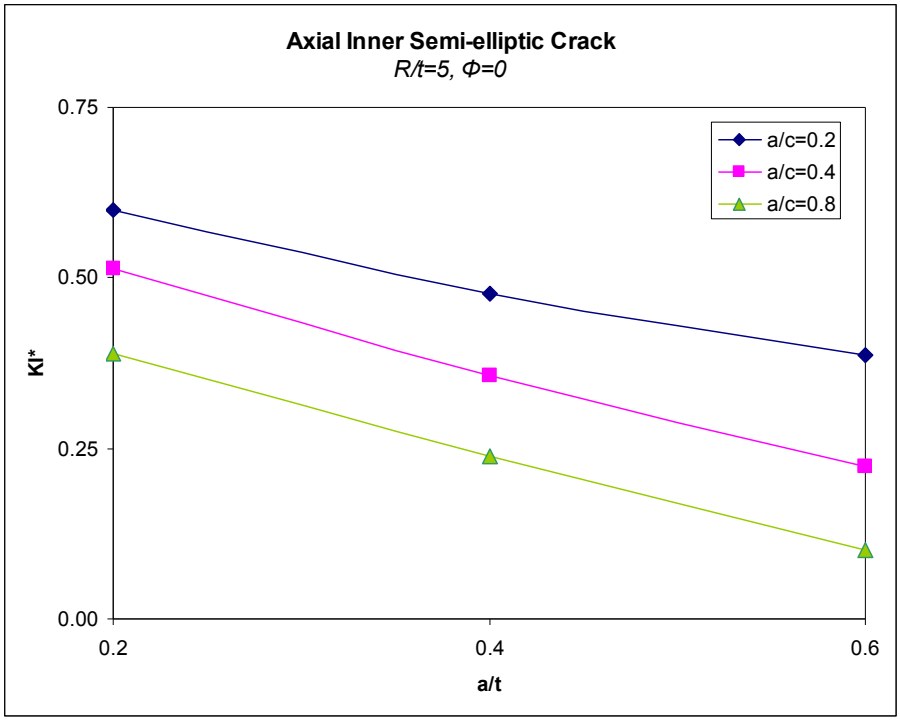

Figure 3.88 KI* at the deepest point versus a/t, Type7, R/t=5

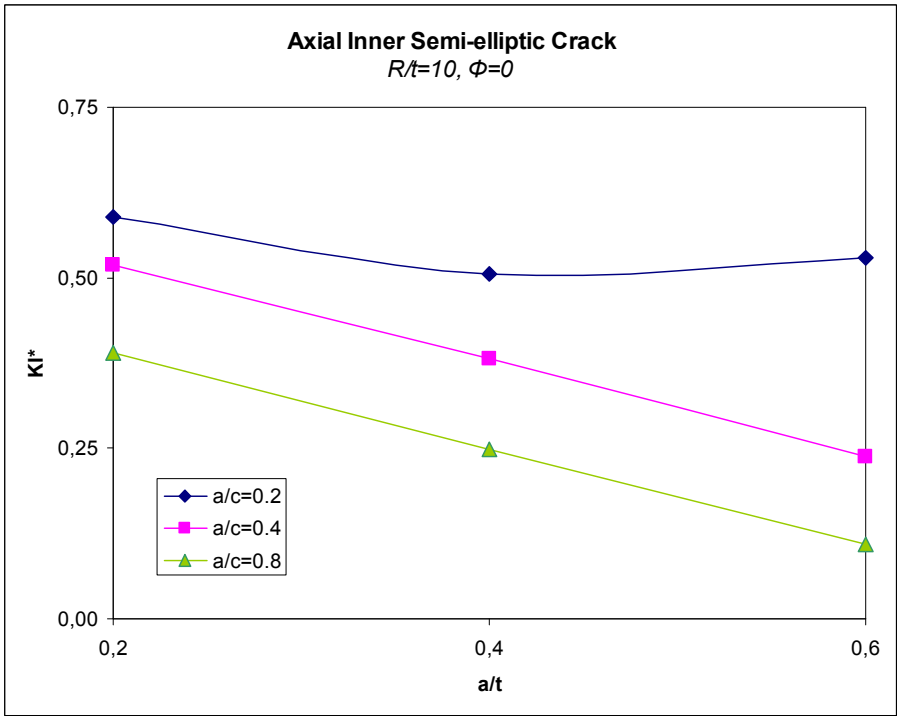

Figure 3.89 KI* at the deepest point versus a/t, Type7, R/t=10

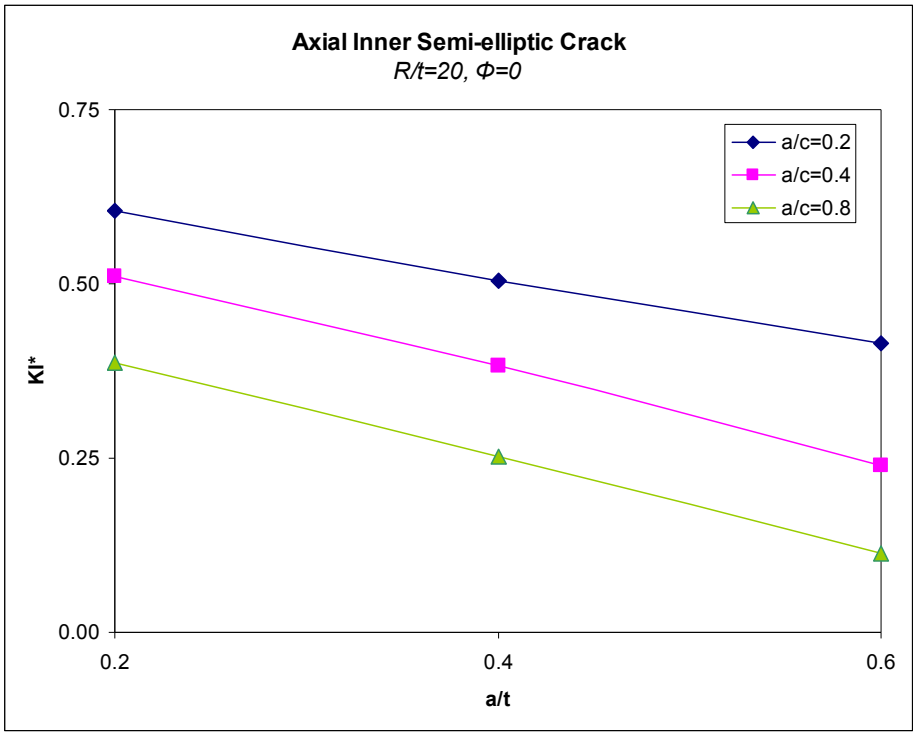

Figure 3.90 KI* at the deepest point versus a/t, Type7, R/t=20

Table 3.7 KI* for thermal loaded partial inner axial crack

R/t	a/t	a/c	a (mm)	Φ=0	11.25	22.5	33.75	45	56.25	67.5	78.75	90
5	0.2	0.2	2	0.60	0.60	0.60	0.59	0.57	0.54	0.48	0.42	0.41
		0.4	2	0.51	0.50	0.51	0.51	0.50	0.49	0.47	0.46	0.48
		0.8	2	0.39	0.38	0.40	0.40	0.42	0.43	0.45	0.49	0.51
	0.4	0.2	4	0.48	0.48	0.49	0.51	0.51	0.50	0.48	0.44	0.43
		0.4	4	0.36	0.35	0.37	0.38	0.40	0.41	0.43	0.44	0.47
		0.8	4	0.24	0.24	0.26	0.28	0.31	0.35	0.39	0.45	0.48
	0.6	0.2	6	0.39	0.44	0.45	0.49	0.51	0.50	0.49	0.47	0.48
		0.4	6	0.22	0.23	0.26	0.29	0.33	0.38	0.41	0.45	0.51
		0.8	6	0.10	0.11	0.13	0.17	0.21	0.27	0.34	0.41	0.47
10	0.2	0.2	1	0.59	0.59	0.60	0.59	0.57	0.53	0.49	0.42	0.40
		0.4	1	0.52	0.52	0.52	0.52	0.51	0.49	0.47	0.46	0.49
		0.8	1	0.39	0.39	0.40	0.41	0.42	0.43	0.45	0.48	0.51
	0.4	0.2	2	0.51	0.50	0.51	0.52	0.52	0.51	0.48	0.43	0.29
		0.4	2	0.38	0.38	0.40	0.41	0.43	0.44	0.44	0.46	0.49
		0.8	2	0.25	0.25	0.27	0.29	0.32	0.36	0.40	0.45	0.49
	0.6	0.2	3	0.53	0.53	0.54	0.54	0.53	0.51	0.48	0.42	0.41
		0.4	3	0.24	0.25	0.27	0.31	0.35	0.39	0.42	0.46	0.51
		0.8	3	0.11	0.12	0.14	0.18	0.23	0.28	0.35	0.43	0.48
20	0.2	0.2	0.5	0.60	0.60	0.60	0.59	0.56	0.53	0.47	0.41	0.40
		0.4	0.5	0.51	0.51	0.52	0.51	0.50	0.49	0.47	0.46	0.48
		0.8	0.5	0.39	0.39	0.40	0.40	0.41	0.43	0.45	0.48	0.51
	0.4	0.2	1	0.50	0.51	0.53	0.53	0.53	0.51	0.48	0.43	0.43
		0.4	1	0.38	0.39	0.40	0.42	0.43	0.44	0.44	0.45	0.50
		0.8	1	0.25	0.26	0.27	0.29	0.32	0.36	0.40	0.45	0.49
	0.6	0.2	1.5	0.41	0.41	0.44	0.47	0.49	0.51	0.50	0.47	0.48
		0.4	1.5	0.24	0.24	0.25	0.27	0.29	0.35	0.43	0.46	0.51
		0.8	1.5	0.11	0.12	0.15	0.18	0.23	0.28	0.35	0.42	0.49

KI* at the deepest point is greater than KI* at the surface point for the cases a/c and a/t is small. As a/c and a/t increases, KI* at surface point is greater than KI* at the deepest point.

As a/t increases, crack propagates at the surface point rather than deepest point.

3.2.2.Thermally loaded-Partial Axial Outer Semi-elliptic Crack

Crack front angle 0 is the deepest point and angle 90 is the surface point. Steady-state thermal load is applied to the structure. Inside temperature is higher than the outer temperature. Inner temperature is applied 100°C and outer temperature is applied -100°C. Results are obtained for different R/t, a/t and a/c values. R is 50mm for all cases but a, c and t change. Results are obtained for the following ranges;

R/t = 5, 10 and 20

a/t = 0.2, 0.4 and 0.6

a/c = 0.2, 0.4 and 0.8

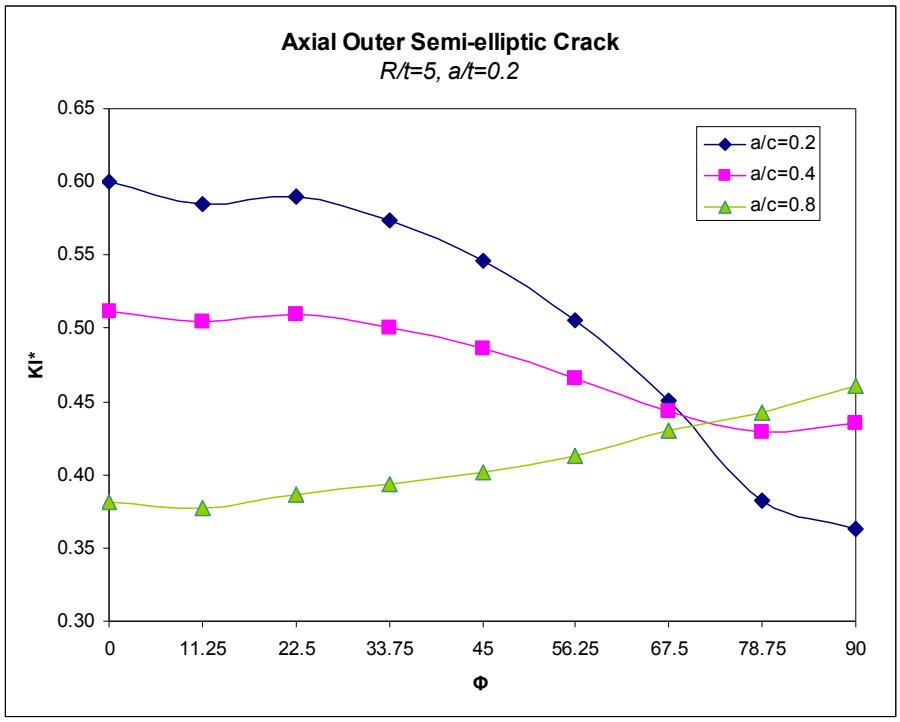

Figure 3.91 KI* versus Φ, Type8, R/t=5, a/t=0.2

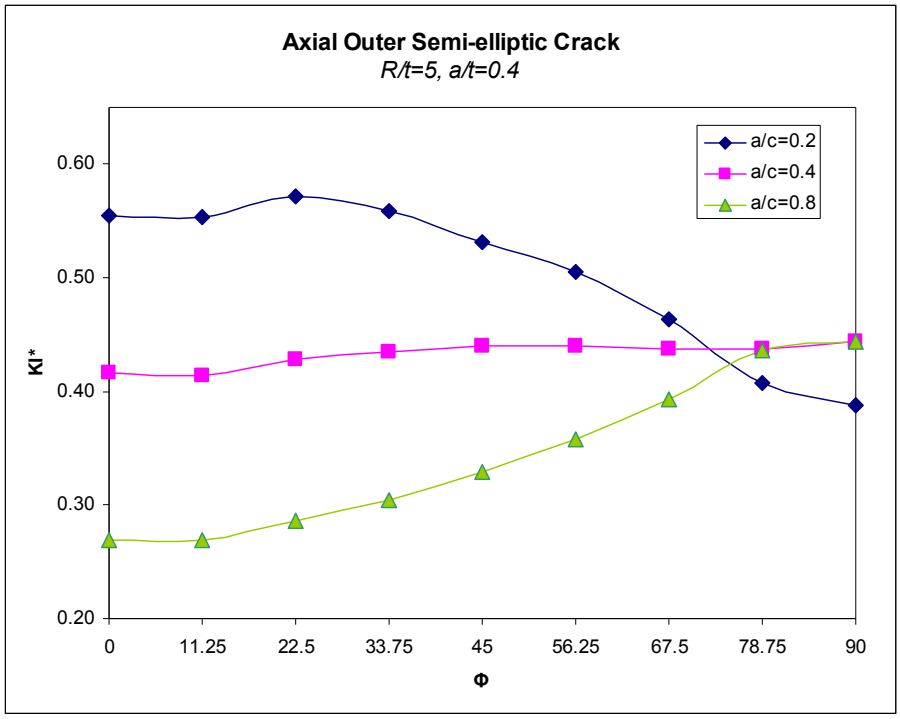

Figure 3.92 KI* versus Φ, Type8, R/t=5, a/t=0.4

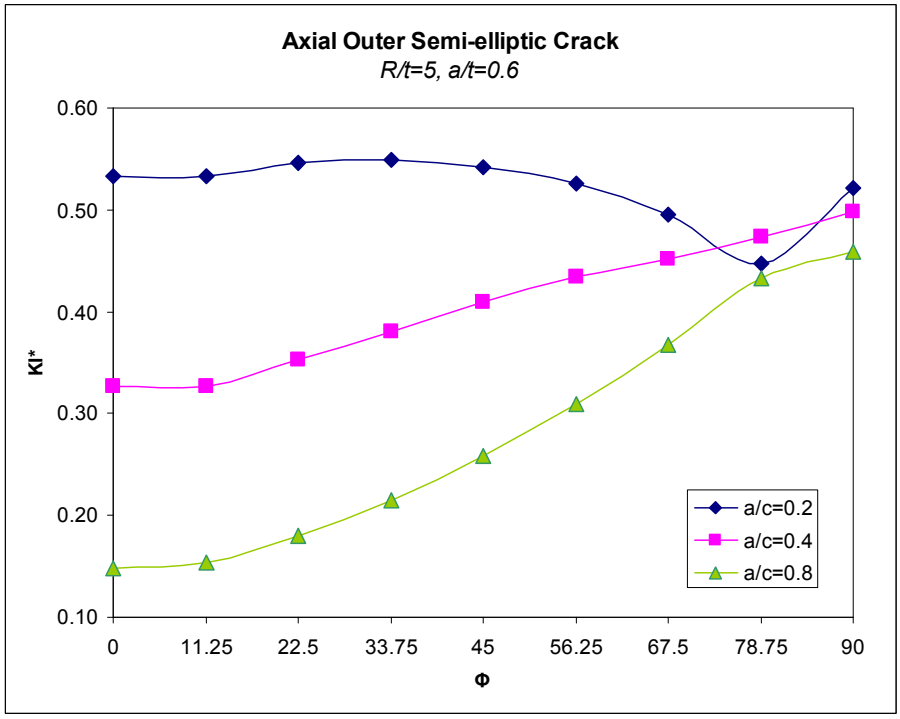

Figure 3.93 KI* versus Φ, Type8, R/t=5, a/t=0.6

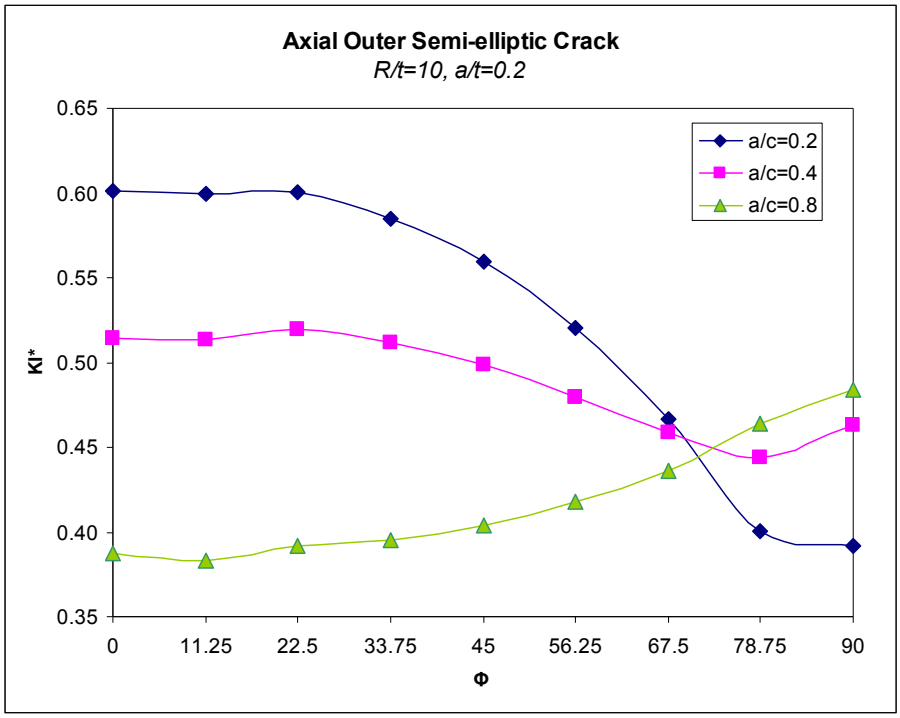

Figure 3.94 KI* versus Φ, Type8, R/t=10, a/t=0.2

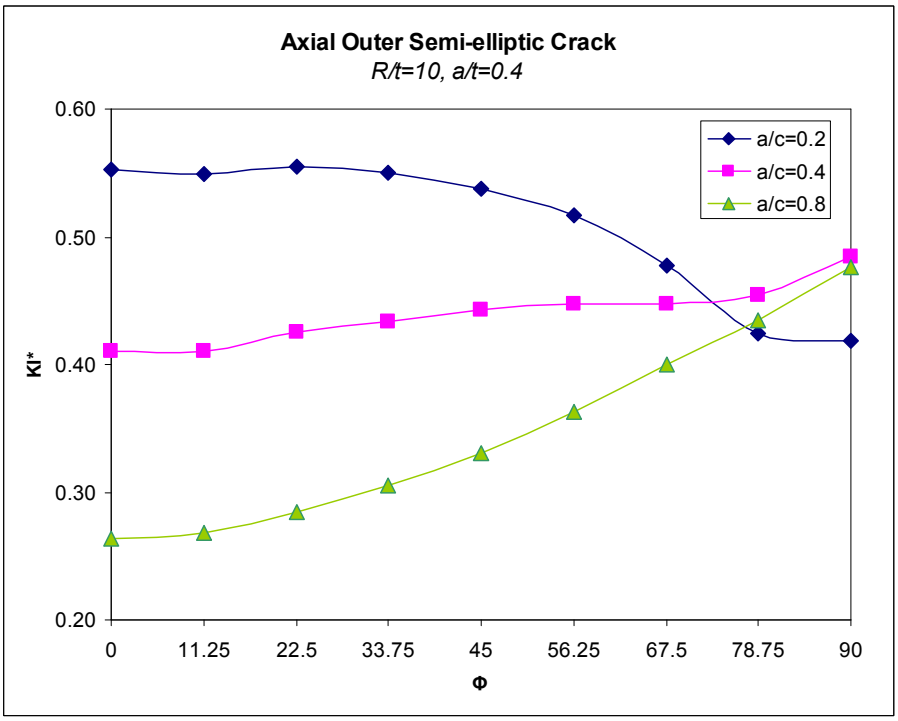

Figure 3.95 KI* versus Φ, Type8, R/t=10, a/t=0.4

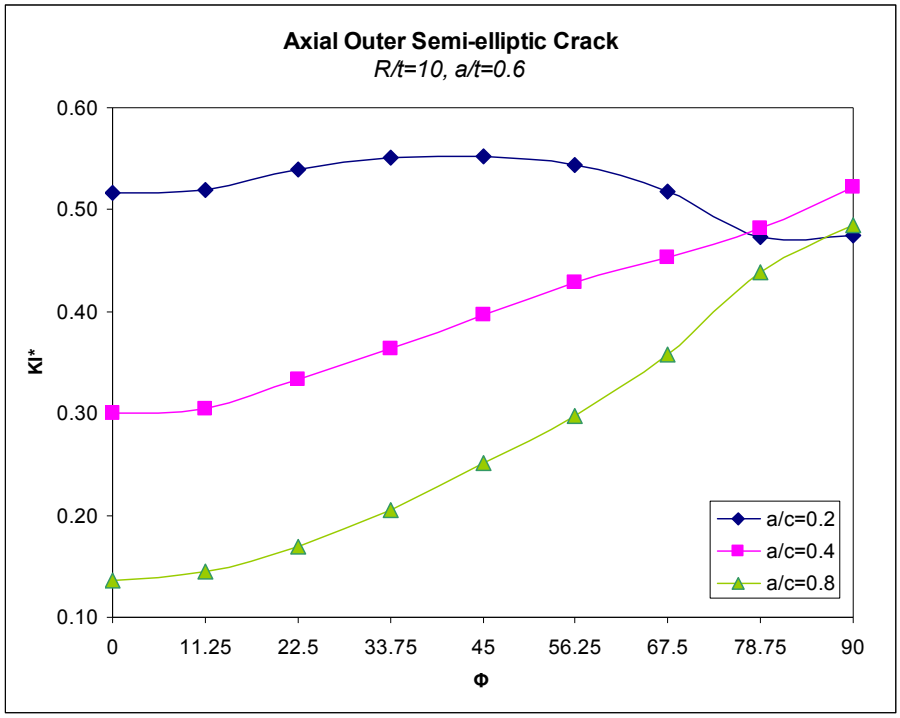

Figure 3.96 KI* versus Φ, Type8, R/t=10, a/t=0.6

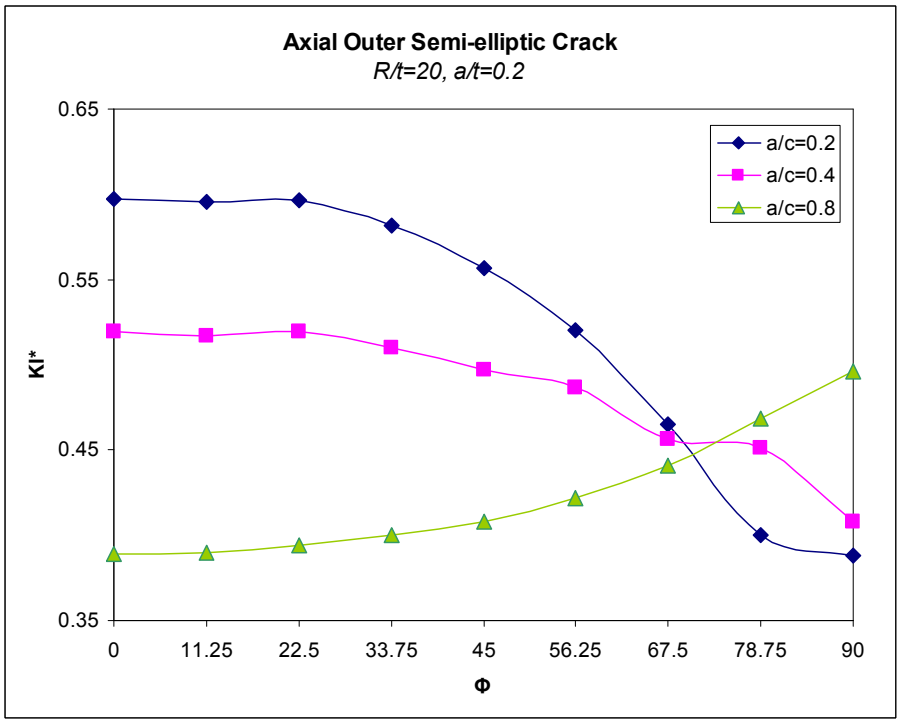

Figure 3.97 KI* versus Φ, Type8, R/t=20, a/t=0.2

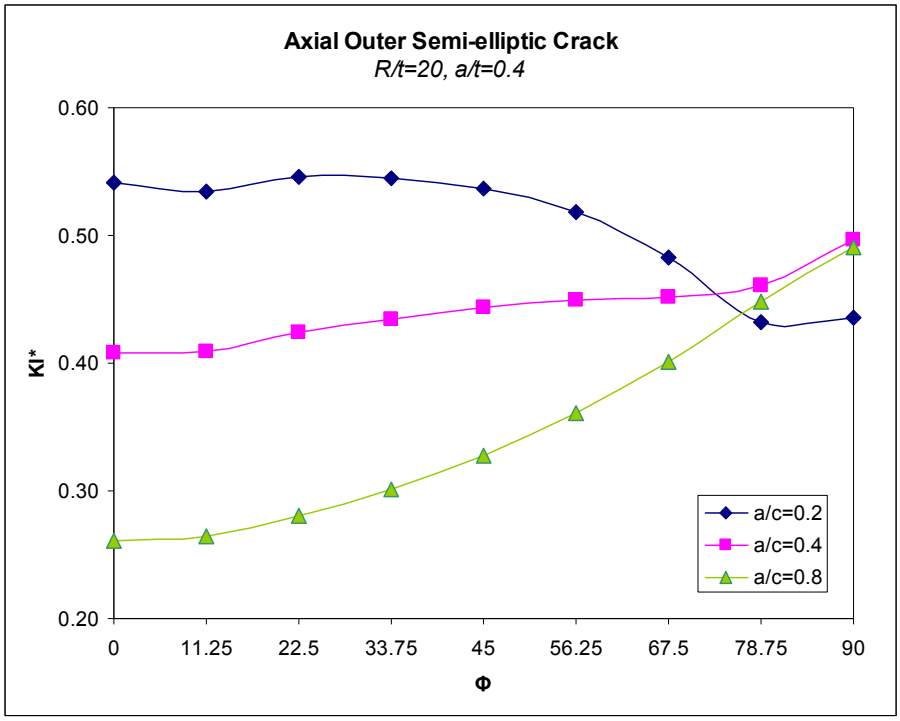

Figure 3.98 KI* versus Φ, Type8, R/t=20, a/t=0.4

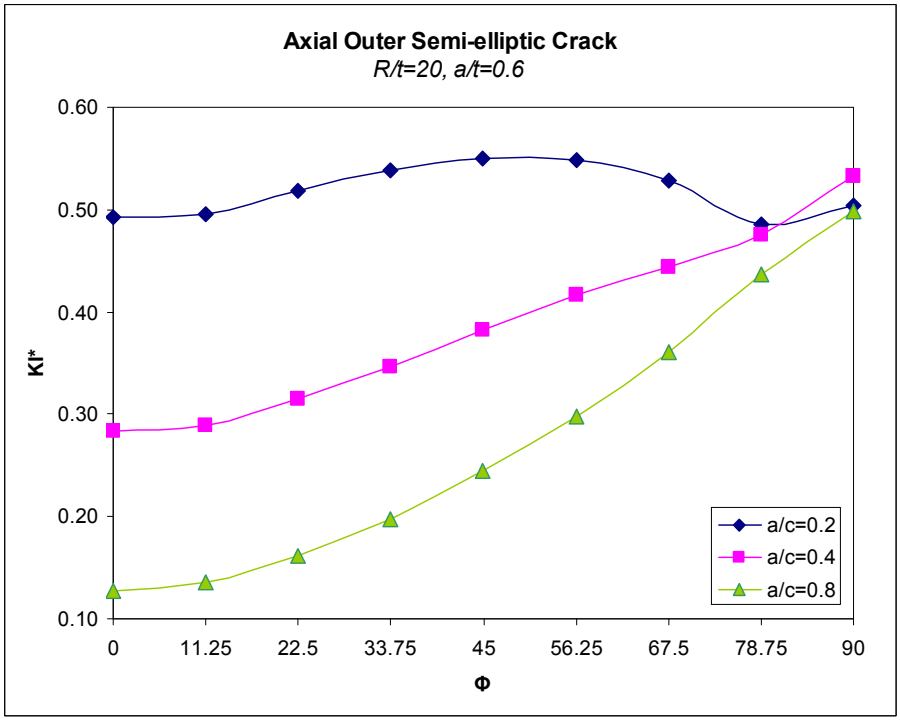

Figure 3.99 KI* versus Φ, Type8, R/t=20, a/t=0.6

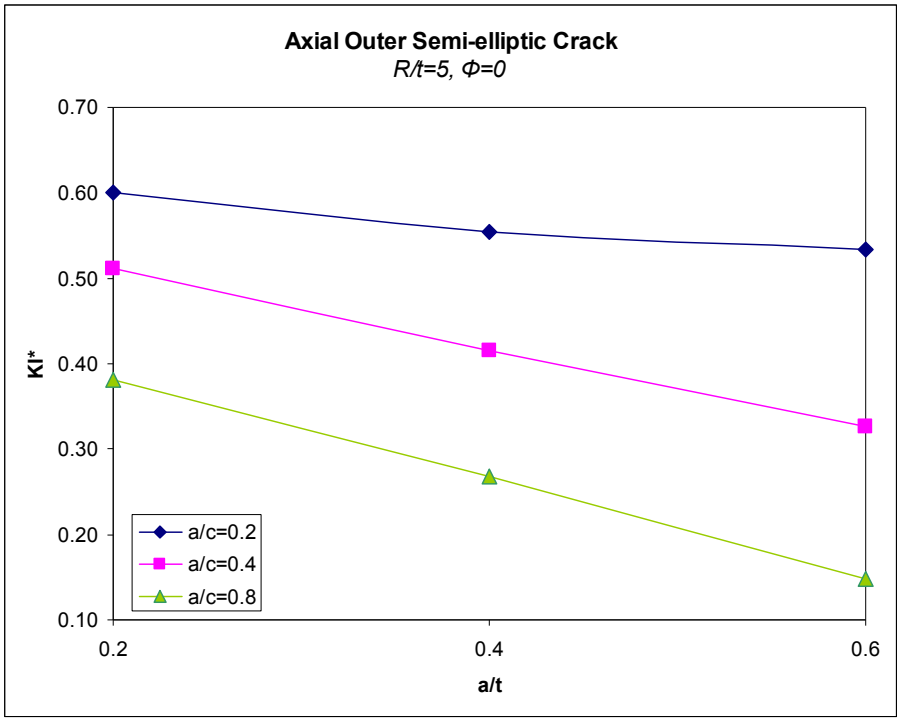

Figure 3.100 KI* at the deepest point versus a/t, Type8, R/t=5

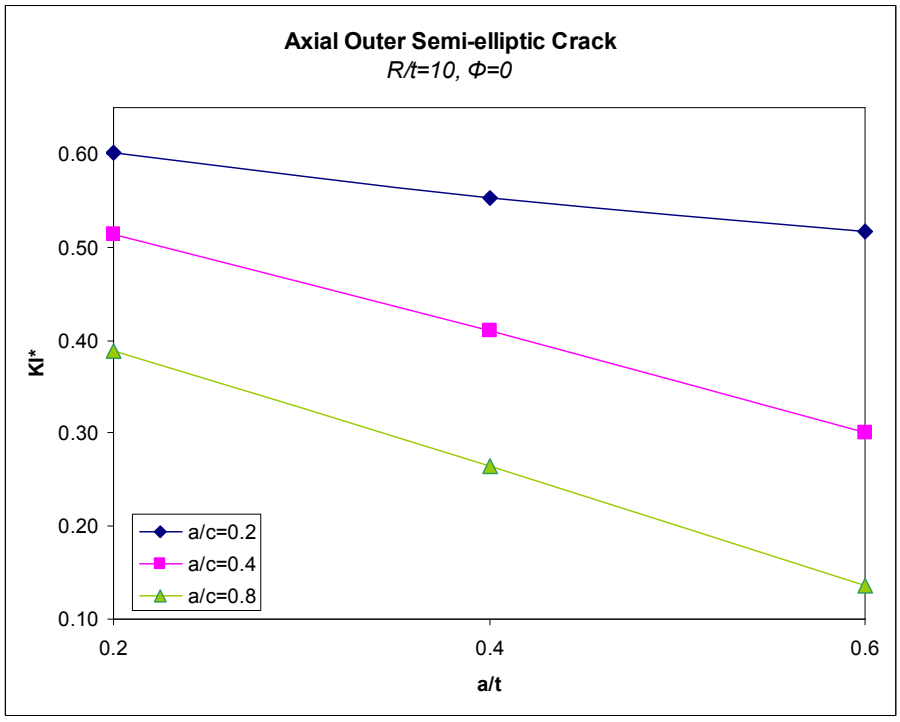

Figure 3.101 KI* at the deepest point versus a/t, Type8, R/t=10

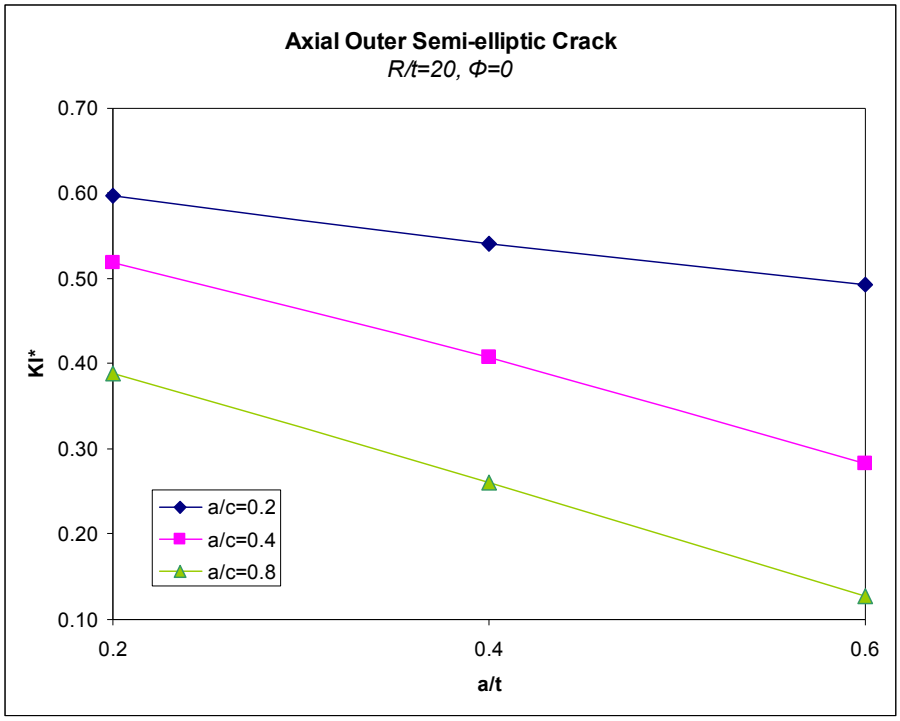

Figure 3.102 KI* at the deepest point versus a/t, Type8, R/t=20

Table 3.8 KI* for thermal loaded partial outer axial crack

R/t	a/t	a/c	a (mm)	Φ=0	11.25	22.5	33.75	45	56.25	67.5	78.75	90
5	0.2	0.2	2	0.60	0.59	0.59	0.57	0.55	0.51	0.45	0.38	0.36
		0.4	2	0.51	0.50	0.51	0.50	0.49	0.47	0.44	0.43	0.44
		0.8	2	0.38	0.38	0.39	0.39	0.40	0.41	0.43	0.44	0.46
	0.4	0.2	4	0.55	0.55	0.57	0.56	0.53	0.50	0.46	0.41	0.39
		0.4	4	0.42	0.41	0.43	0.43	0.44	0.44	0.44	0.44	0.44
		0.8	4	0.27	0.27	0.29	0.30	0.33	0.36	0.39	0.44	0.44
	0.6	0.2	6	0.53	0.53	0.55	0.55	0.54	0.53	0.49	0.45	0.52
		0.4	6	0.33	0.33	0.35	0.38	0.41	0.43	0.45	0.47	0.50
		0.8	6	0.15	0.15	0.18	0.21	0.26	0.31	0.37	0.43	0.46
10	0.2	0.2	1	0.60	0.60	0.60	0.58	0.56	0.52	0.47	0.40	0.39
		0.4	1	0.51	0.51	0.52	0.51	0.50	0.48	0.46	0.44	0.46
		0.8	1	0.39	0.38	0.39	0.40	0.40	0.42	0.44	0.46	0.48
	0.4	0.2	2	0.55	0.55	0.56	0.55	0.54	0.52	0.48	0.42	0.42
		0.4	2	0.41	0.41	0.43	0.43	0.44	0.45	0.45	0.45	0.48
		0.8	2	0.26	0.27	0.28	0.30	0.33	0.36	0.40	0.44	0.48
	0.6	0.2	3	0.52	0.52	0.54	0.55	0.55	0.54	0.52	0.47	0.47
		0.4	3	0.30	0.30	0.33	0.36	0.40	0.43	0.45	0.48	0.52
		0.8	3	0.14	0.14	0.17	0.20	0.25	0.30	0.36	0.44	0.48
20	0.2	0.2	0.5	0.60	0.60	0.60	0.58	0.56	0.52	0.46	0.40	0.39
		0.4	0.5	0.52	0.52	0.52	0.51	0.50	0.49	0.46	0.45	0.41
		0.8	0.5	0.39	0.39	0.39	0.40	0.41	0.42	0.44	0.47	0.50
	0.4	0.2	1	0.54	0.53	0.55	0.54	0.54	0.52	0.48	0.43	0.44
		0.4	1	0.41	0.41	0.42	0.43	0.44	0.45	0.45	0.46	0.50
		0.8	1	0.26	0.26	0.28	0.30	0.33	0.36	0.40	0.45	0.49
	0.6	0.2	1.5	0.49	0.50	0.52	0.54	0.55	0.55	0.53	0.49	0.50
		0.4	1.5	0.28	0.29	0.31	0.35	0.38	0.42	0.44	0.48	0.53
		0.8	1.5	0.13	0.14	0.16	0.20	0.24	0.30	0.36	0.44	0.50

Similar to the thermal loaded inner axial crack case, KI* at the deepest point is greater than KI* at the surface point for the cases a/c and a/t is small. As a/c and a/t increases, KI* at surface point is greater than KI* at the deepest point.

As a/t increases, crack propagates at the surface point rather than deepest point.

3.2.3.Thermally loaded- Circumferential Inner Semi-elliptic Crack

Crack front angle 0 is the deepest point. Steady-state thermal load is applied to the structure. Inside temperature is lower than the outer temperature. Inner temperature is applied -100°C and outer temperature is applied 100°C. Results are obtained for different R/t, a/t and a/c values. R is 50mm for all cases but a, c and t change. Results are obtained for the following ranges;

R/t = 5, 10 and 20

a/t = 0.2, 0.3 and 0.4

a/c = 0.2, 0.4 and 0.8

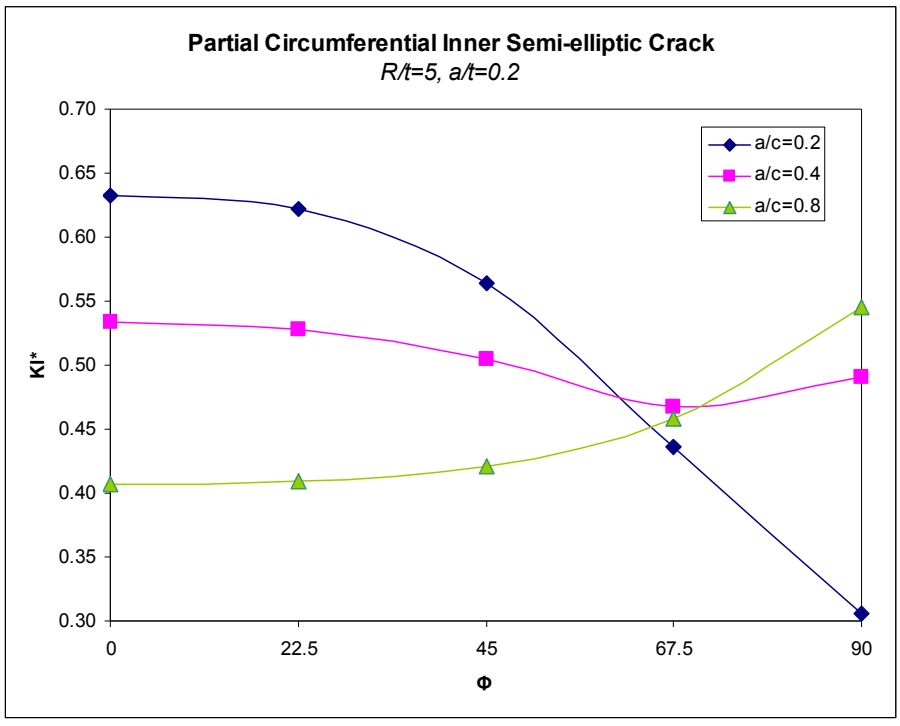

Figure 3.103 KI* versus Φ, Type9, R/t=5, a/t=0.2

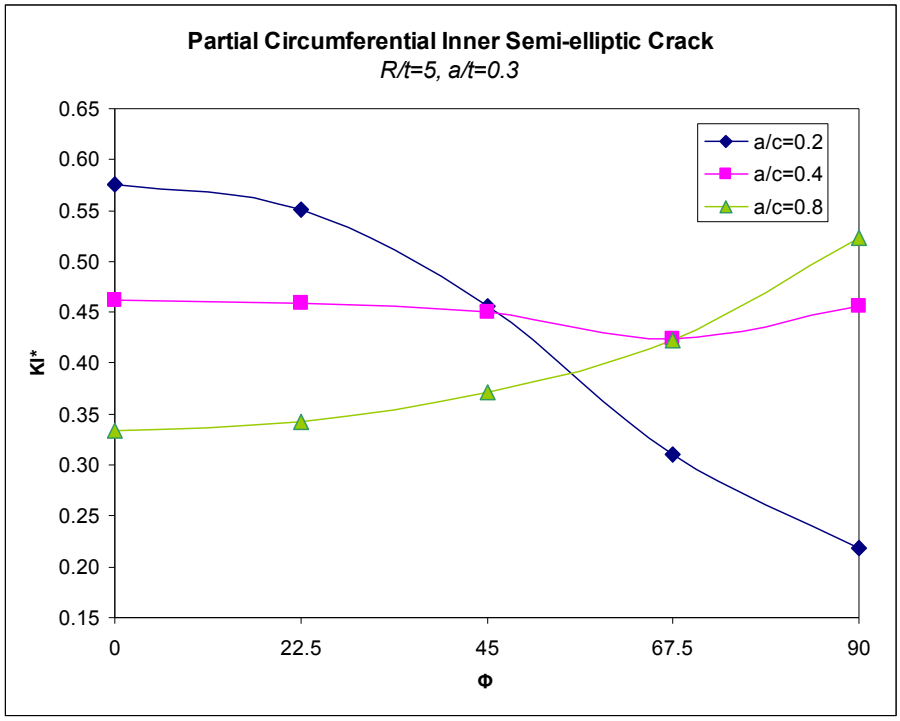

Figure 3.104 KI* versus Φ, Type9, R/t=5, a/t=0.3

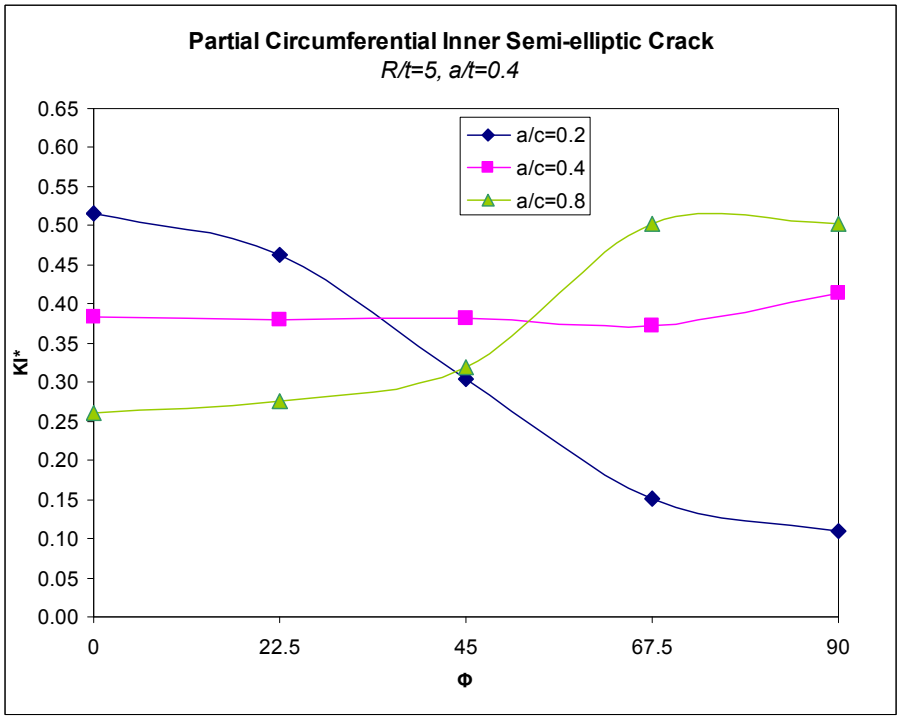

Figure 3.105 KI* versus Φ, Type9, R/t=5, a/t=0.4

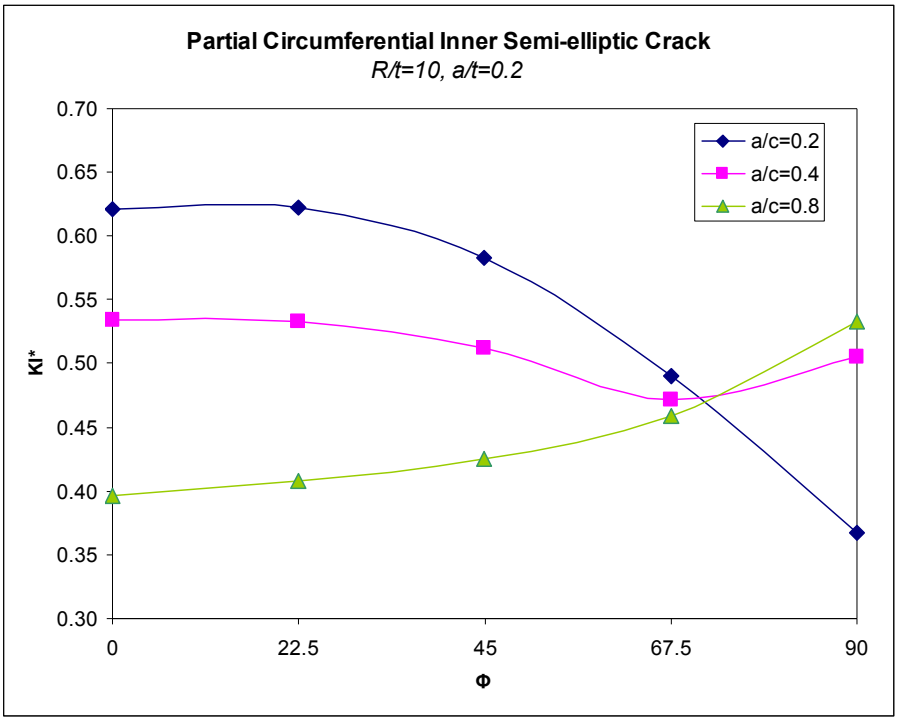

Figure 3.106 KI* versus Φ, Type9, R/t=10, a/t=0.2

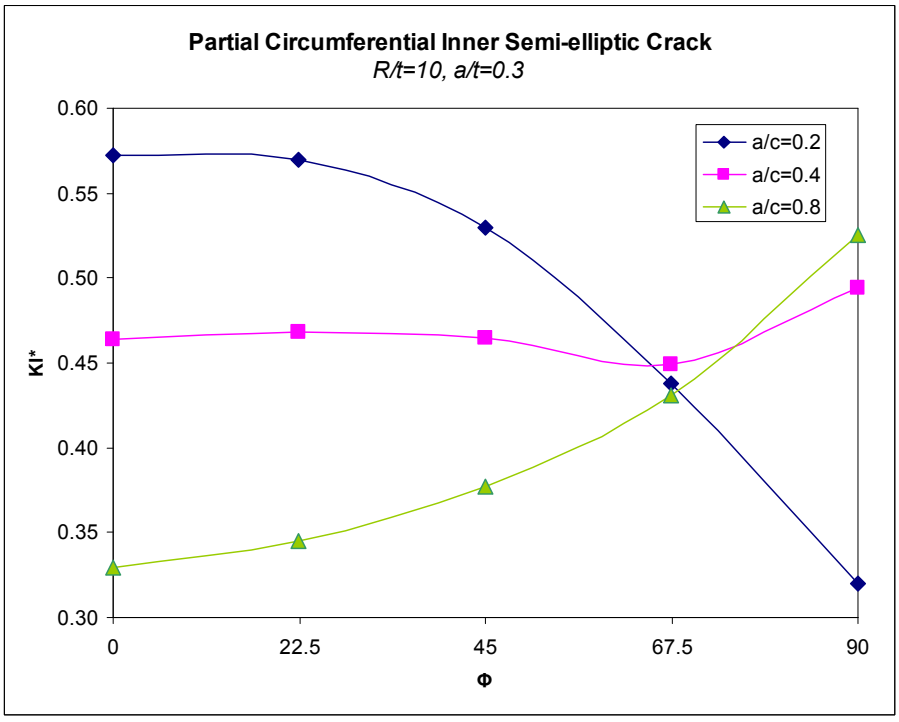

Figure 3.107 KI* versus Φ, Type9, R/t=10, a/t=0.3

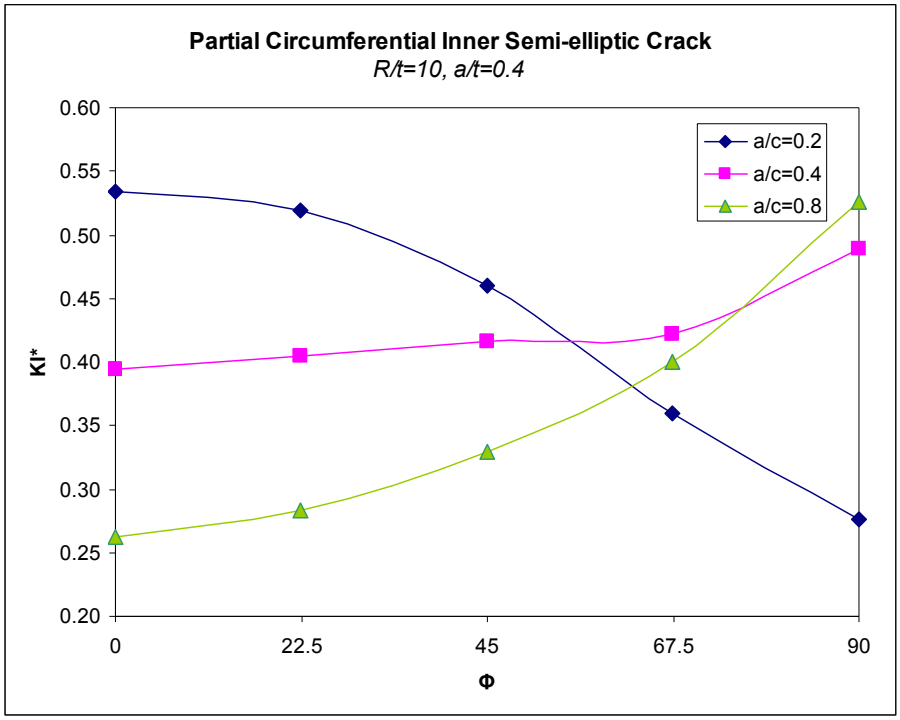

Figure 3.108 KI* versus Φ, Type9, R/t=10, a/t=0.4

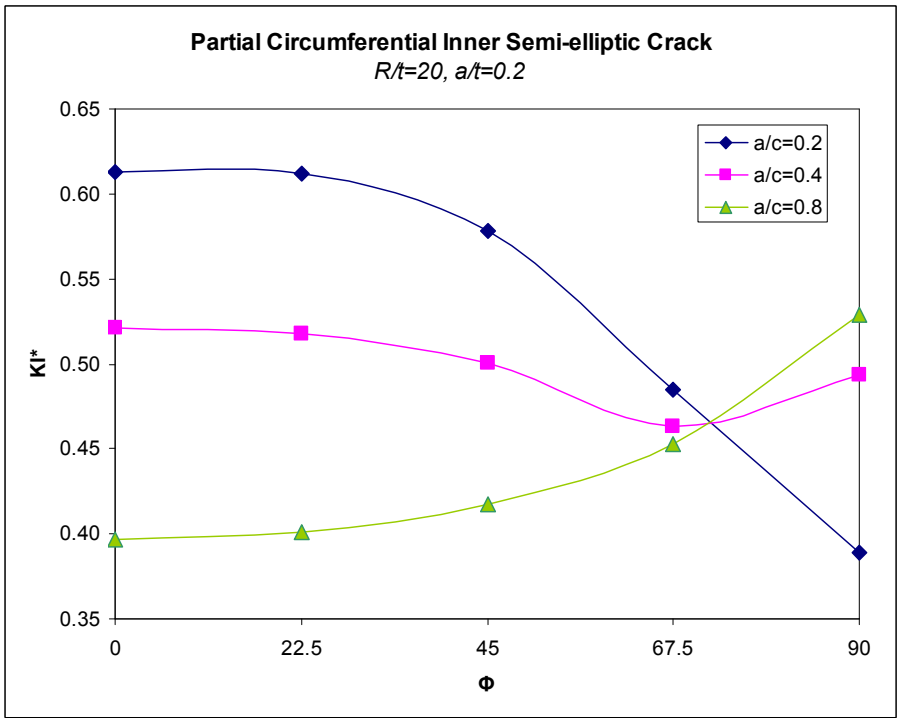

Figure 3.109 KI* versus Φ, Type9, R/t=20, a/t=0.2

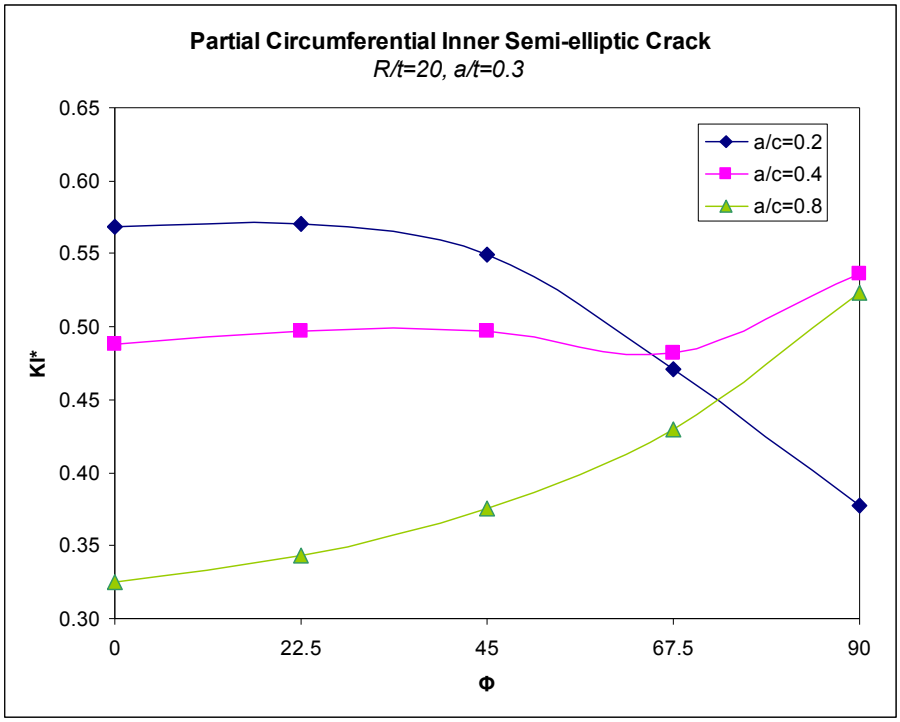

Figure 3.110 KI* versus Φ, Type9, R/t=20, a/t=0.3

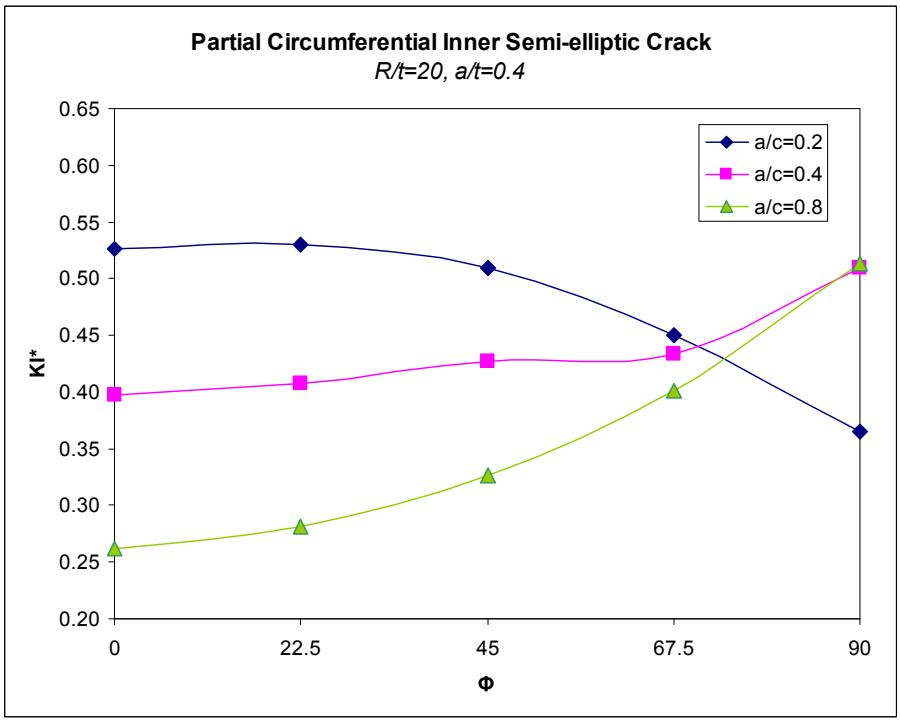

Figure 3.111 KI* versus Φ, Type9, R/t=20, a/t=0.4

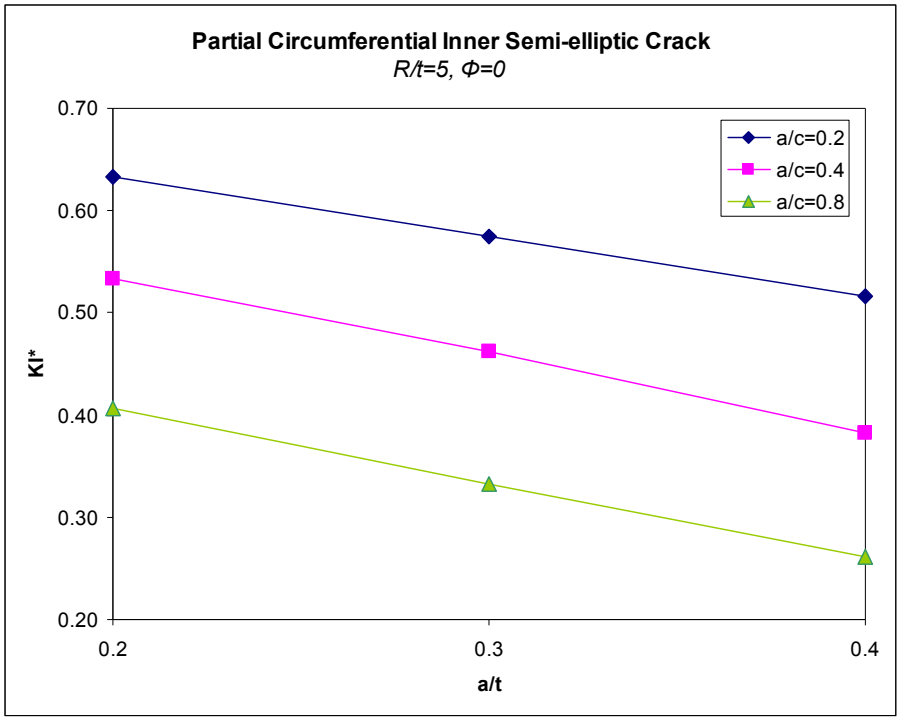

Figure 3.112 KI* at the deepest point versus a/t, Type9, R/t=5

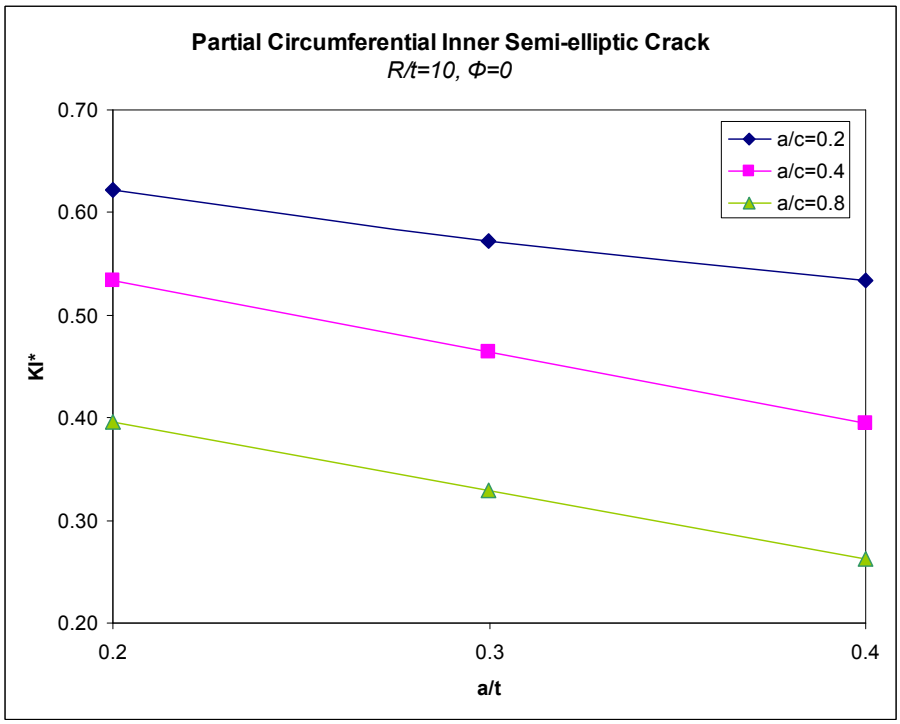

Figure 3.113 KI* at the deepest point versus a/t, Type9, R/t=10

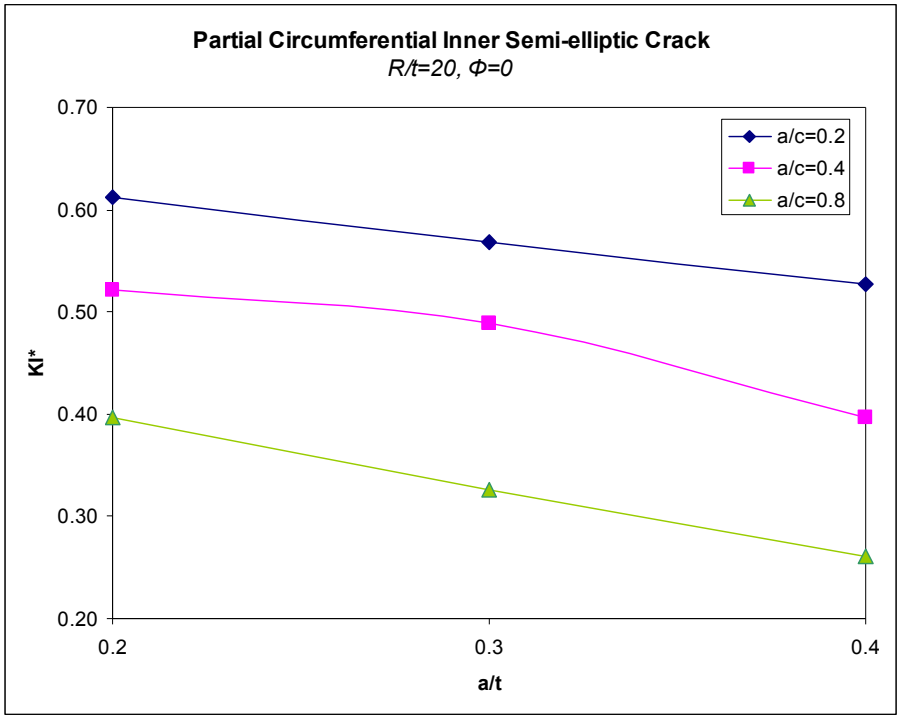

Figure 3.114 KI* at the deepest point versus a/t, Type9, R/t=20

Table 3.9 KI* for thermal loaded partial inner circumferential crack

R/t	a/t	a/c	a (mm)	Φ=0	22.50	45	67.50	90
5	0.2	0.2	2	0.63	0.62	0.56	0.44	0.31
		0.4	2	0.53	0.53	0.50	0.47	0.49
		0.8	2	0.41	0.41	0.42	0.46	0.55
	0.3	0.2	3	0.58	0.55	0.46	0.31	0.22
		0.4	3	0.46	0.46	0.45	0.42	0.46
		0.8	3	0.33	0.34	0.37	0.42	0.52
	0.4	0.2	4	0.52	0.46	0.30	0.15	0.11
		0.4	4	0.38	0.38	0.38	0.37	0.41
		0.8	4	0.26	0.28	0.32	0.50	0.50
10	0.2	0.2	1	0.62	0.62	0.58	0.49	0.37
		0.4	1	0.53	0.53	0.51	0.47	0.51
		0.8	1	0.40	0.41	0.43	0.46	0.53
	0.3	0.2	1.5	0.57	0.57	0.53	0.44	0.32
		0.4	1.5	0.46	0.47	0.46	0.45	0.49
		0.8	1.5	0.33	0.35	0.38	0.43	0.53
	0.4	0.2	2	0.53	0.52	0.46	0.36	0.28
		0.4	2	0.39	0.41	0.42	0.42	0.49
		0.8	2	0.26	0.28	0.33	0.40	0.53
20	0.2	0.2	0.5	0.61	0.61	0.58	0.48	0.39
		0.4	0.5	0.52	0.52	0.50	0.46	0.49
		0.8	0.5	0.40	0.40	0.42	0.45	0.53
	0.3	0.2	0.8	0.57	0.57	0.55	0.47	0.38
		0.4	0.8	0.49	0.50	0.50	0.48	0.54
		0.8	0.8	0.33	0.34	0.38	0.43	0.52
	0.4	0.2	1	0.53	0.53	0.51	0.45	0.37
		0.4	1	0.40	0.41	0.43	0.43	0.51
		0.8	1	0.26	0.28	0.33	0.40	0.51

As a/c increases, KI* at surface points become larger than KI* at deepest point. As a/t increases, KI* decreases for same R/t and a/c values.

3.2.4.Thermally loaded-Circumferential Outer Semi-elliptic Crack

Crack front angle 0 is the deepest point. Steady-state thermal load is applied to the structure. Inside temperature is higher than the outer temperature. Inner temperature is applied 100°C and outer temperature is applied -100°C. Results are obtained for different R/t, a/t and a/c values. R is 50mm for all cases but a, c and t change. Results are obtained for the following ranges;

R/t = 5, 10 and 20

a/t = 0.2, 0.3 and 0.4

a/c = 0.2, 0.4 and 0.8

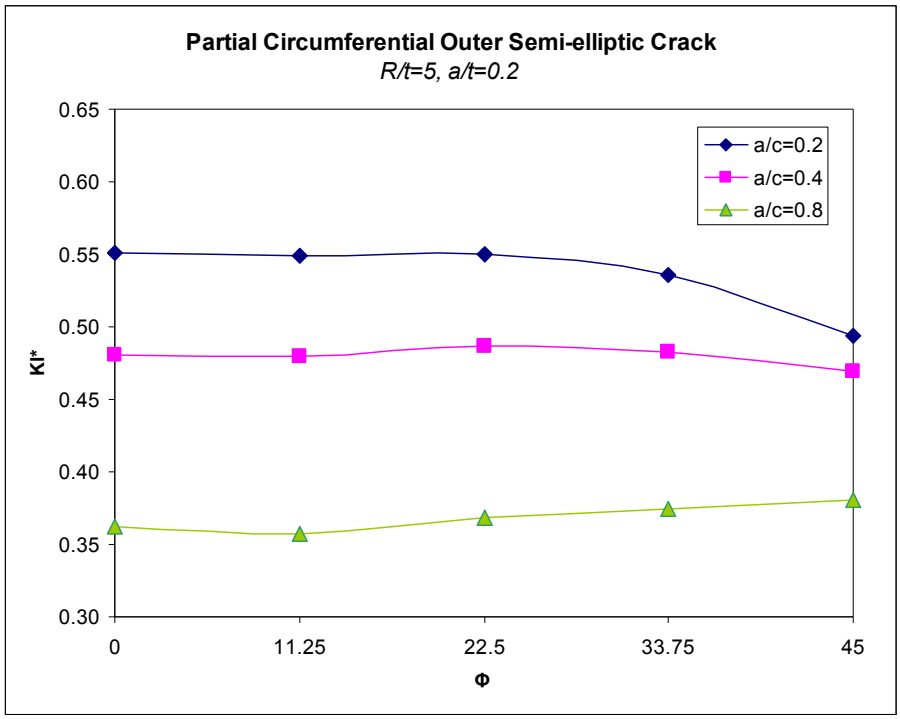

Figure 3.115 KI* versus Φ, Type10, R/t=5, a/t=0.2

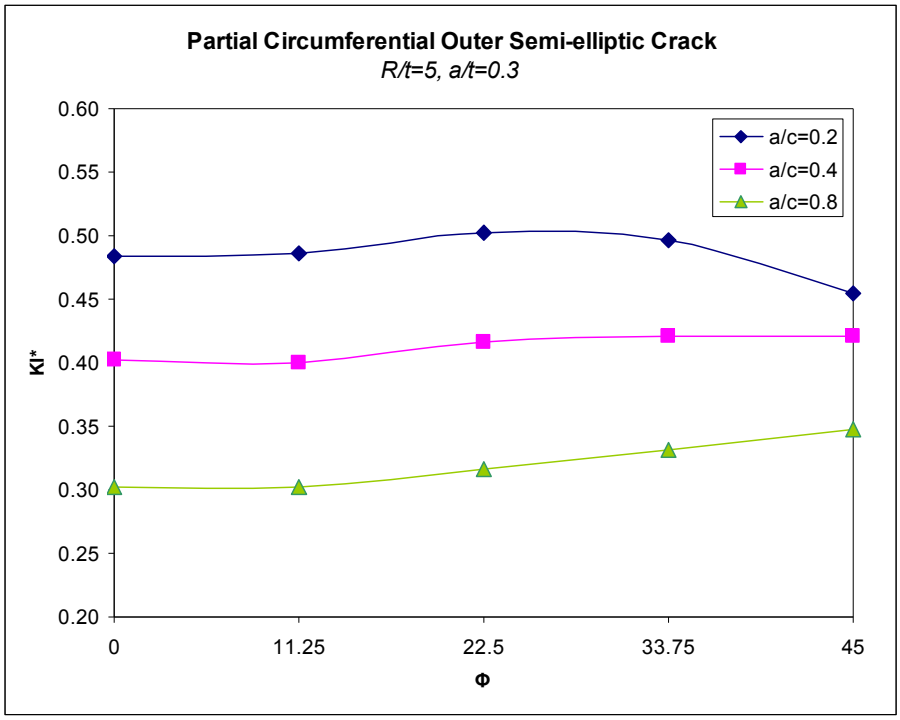

Figure 3.116 KI* versus Φ, Type10, R/t=5, a/t=0.3

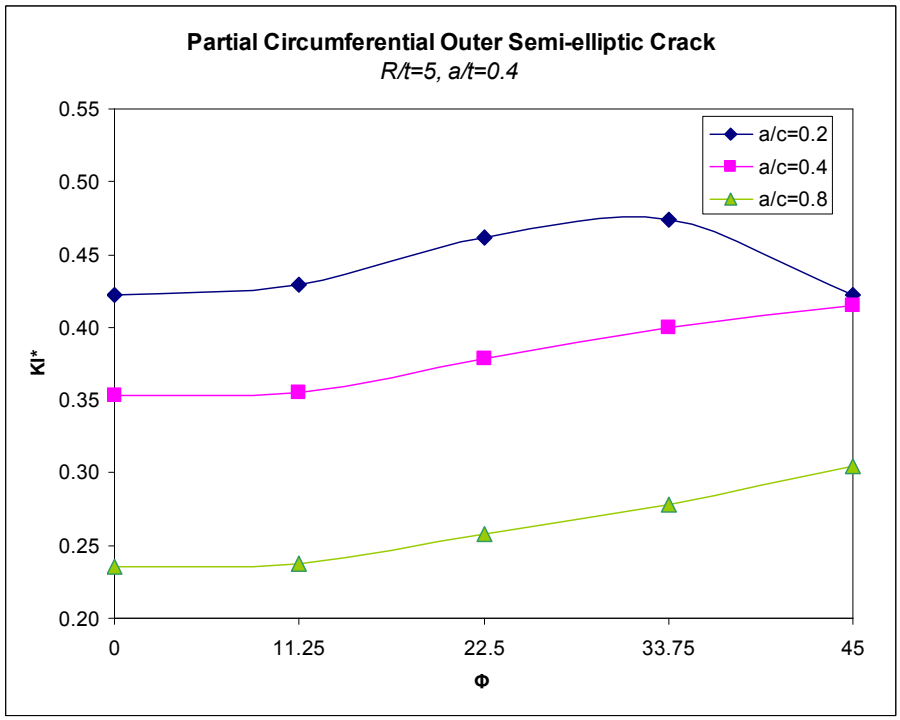

Figure 3.117 KI* versus Φ, Type10, R/t=5, a/t=0.4

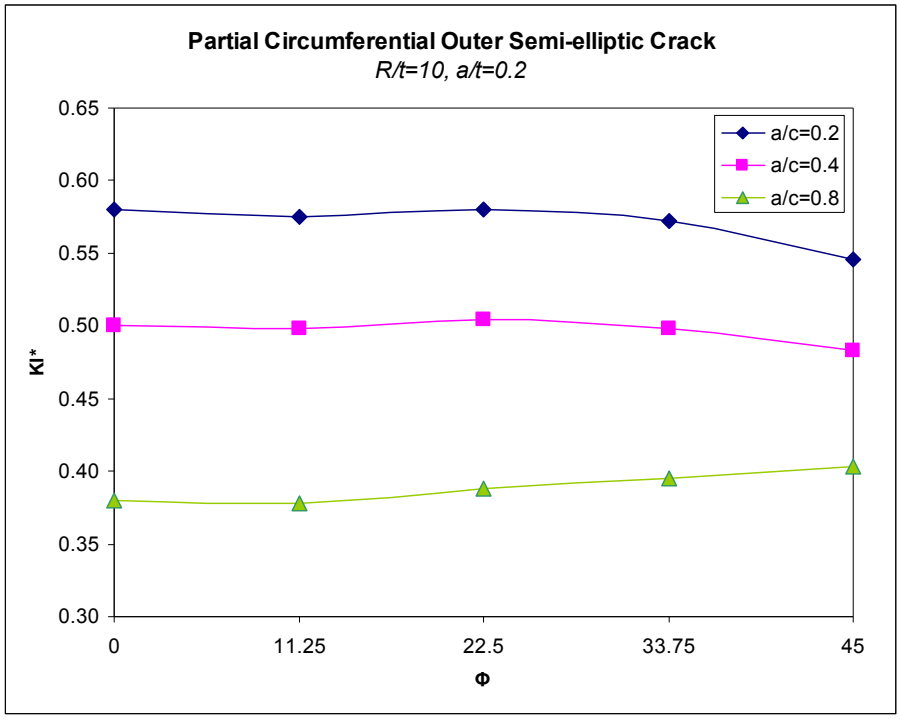

Figure 3.118 KI* versus Φ, Type10, R/t=10, a/t=0.2

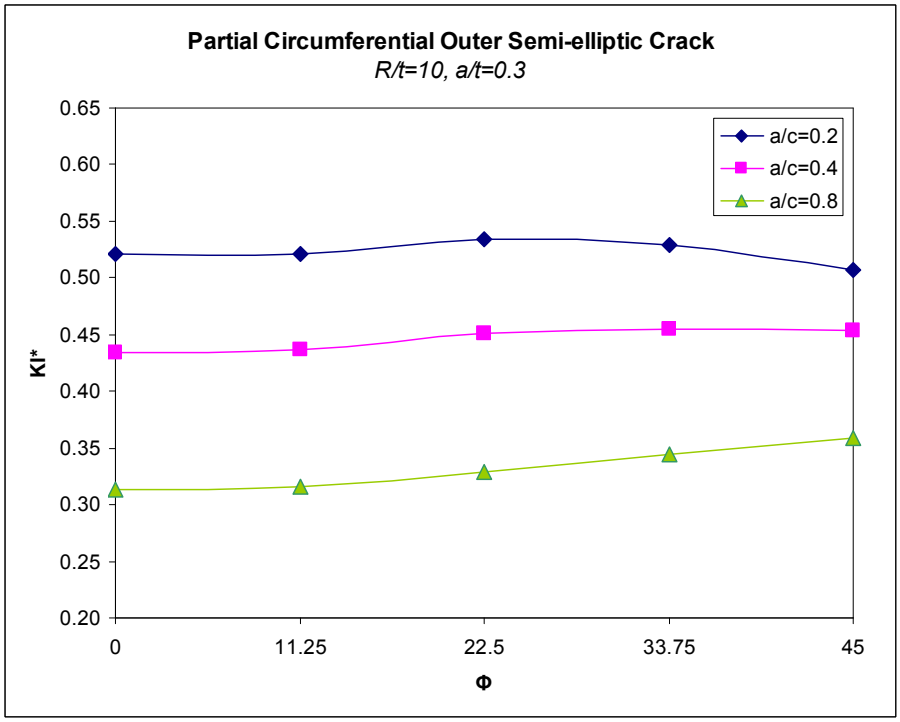

Figure 3.119 KI* versus Φ, Type10, R/t=10, a/t=0.3

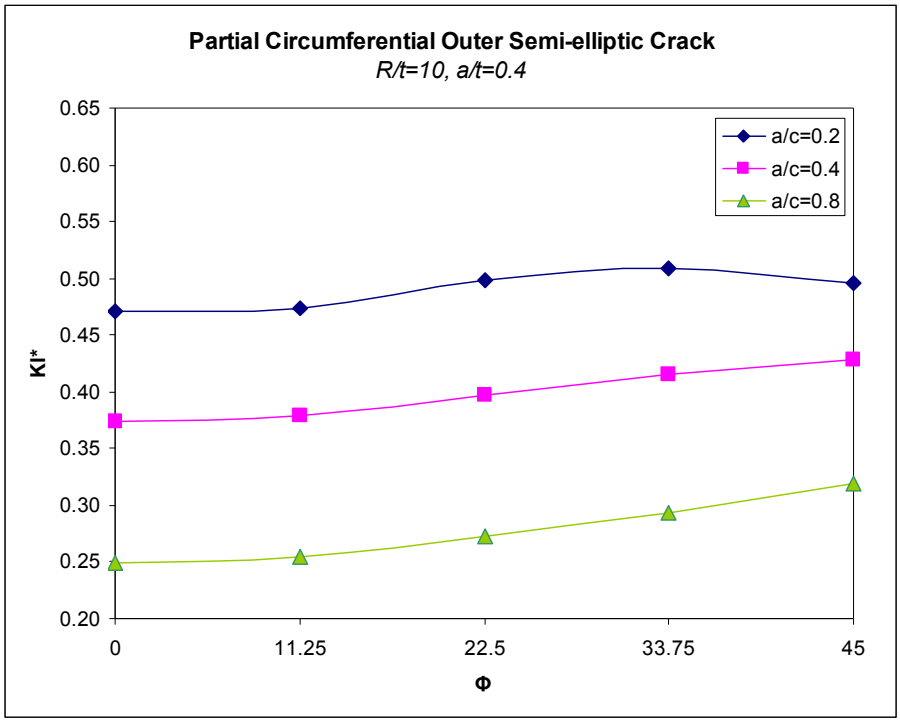

Figure 3.120 KI* versus Φ, Type10, R/t=10, a/t=0.4

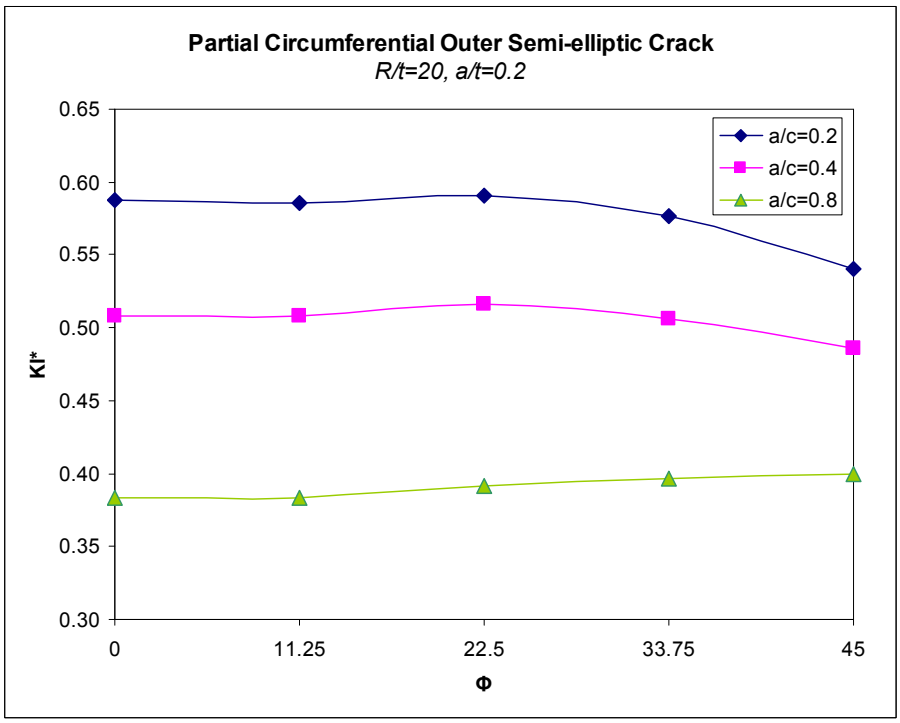

Figure 3.121 KI* versus Φ, Type10, R/t=20, a/t=0.2

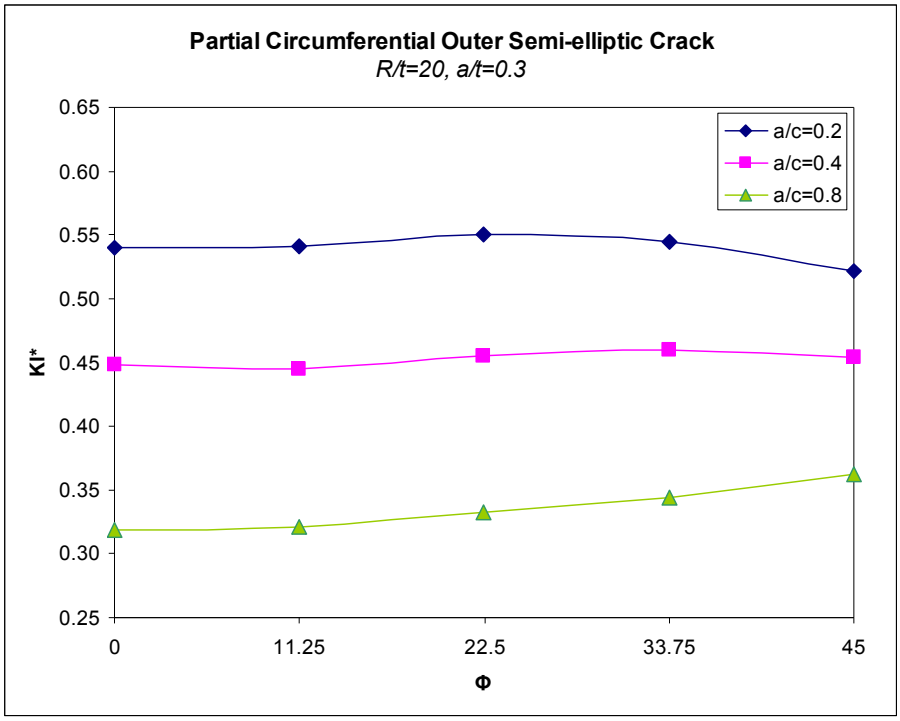

Figure 3.122 KI* versus Φ, Type10, R/t=20, a/t=0.3

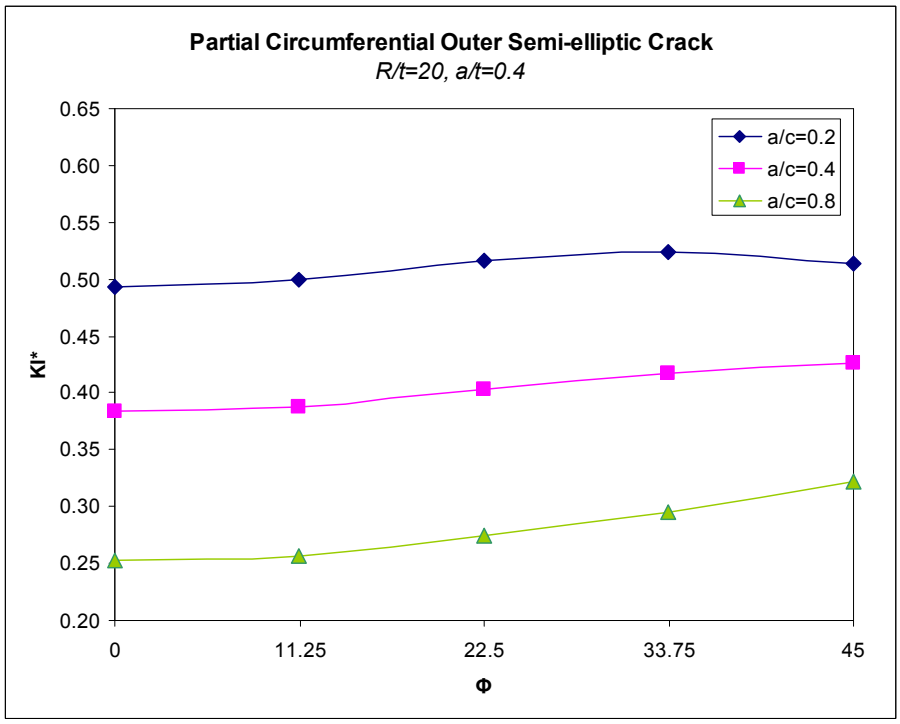

Figure 3.123 KI* versus Φ, Type10, R/t=20, a/t=0.4

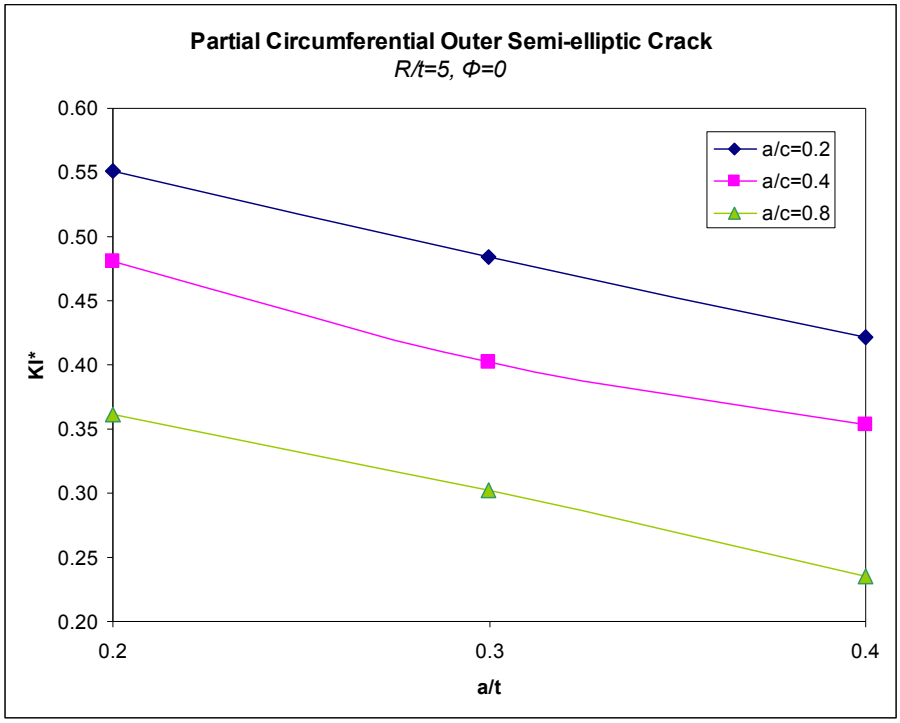

Figure 3.124 KI* at the deepest point versus a/t, Type10, R/t=5

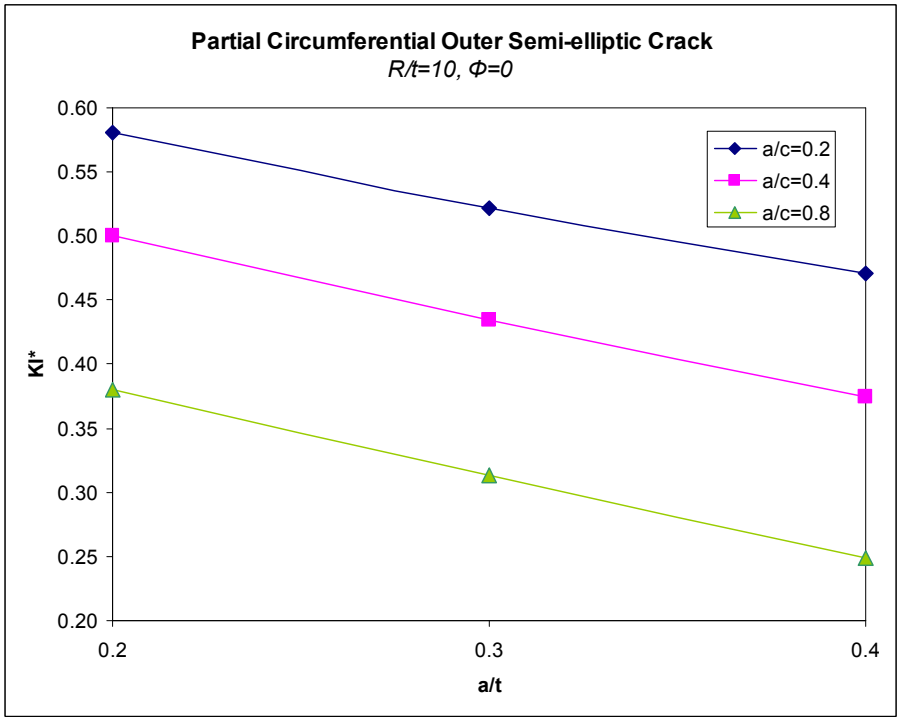

Figure 3.125 KI* at the deepest point versus a/t, Type10, R/t=10

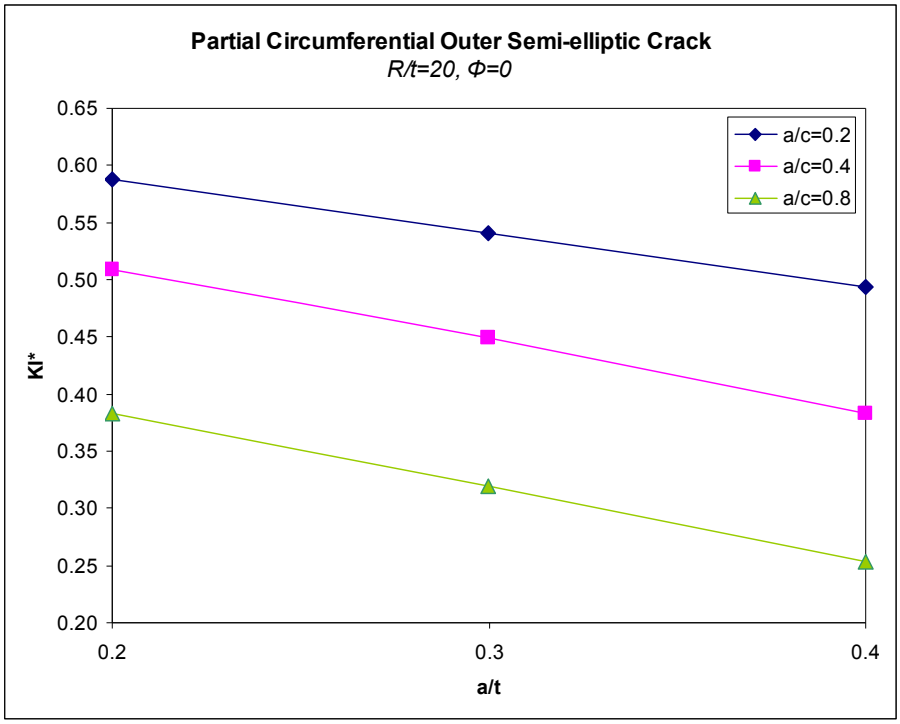

Figure 3.126 KI* at the deepest point versus a/t, Type10, R/t=20

Table 3.10 KI* for thermal loaded partial outer circumferential crack

R/t	a/t	a/c	a (mm)	Φ=0	11.25	22.5	33.75	45
5	0.2	0.2	2	0.55	0.55	0.55	0.54	0.49
		0.4	2	0.48	0.48	0.49	0.48	0.47
		0.8	2	0.36	0.36	0.37	0.37	0.38
	0.3	0.2	3	0.48	0.49	0.50	0.50	0.45
		0.4	3	0.40	0.40	0.42	0.42	0.42
		0.8	3	0.30	0.30	0.32	0.33	0.35
	0.4	0.2	4	0.42	0.43	0.46	0.47	0.42
		0.4	4	0.35	0.36	0.38	0.40	0.42
		0.8	4	0.24	0.24	0.26	0.28	0.30
10	0.2	0.2	1	0.58	0.57	0.58	0.57	0.55
		0.4	1	0.50	0.50	0.50	0.50	0.48
		0.8	1	0.38	0.38	0.39	0.40	0.40
	0.3	0.2	1.5	0.52	0.52	0.53	0.53	0.51
		0.4	1.5	0.43	0.44	0.45	0.46	0.45
		0.8	1.5	0.31	0.32	0.33	0.34	0.36
	0.4	0.2	2	0.47	0.47	0.50	0.51	0.50
		0.4	2	0.37	0.38	0.40	0.42	0.43
		0.8	2	0.25	0.25	0.27	0.29	0.32
20	0.2	0.2	0.5	0.59	0.59	0.59	0.58	0.54
		0.4	0.5	0.51	0.51	0.52	0.51	0.49
		0.8	0.5	0.38	0.38	0.39	0.40	0.40
	0.3	0.2	0.8	0.54	0.54	0.55	0.54	0.52
		0.4	0.8	0.45	0.45	0.46	0.46	0.45
		0.8	0.8	0.32	0.32	0.33	0.34	0.36
	0.4	0.2	1	0.49	0.50	0.52	0.52	0.51
		0.4	1	0.38	0.39	0.40	0.42	0.43
		0.8	1	0.25	0.26	0.27	0.29	0.32

As a/c increases, KI* at surface points become larger than KI* at deepest point. As a/t increases, KI* decreases for same R/t and a/c values.

CHAPTER 4

DISCUSSION

The results are obtained for different R/t, a/t and a/c values. As it can be seen from the graphics, while R/t increases, KI* values increases for the inner pressure applied cases. For tensile and thermal load applied cases the values do not change so much. Also when R/t and a/t is constant, KI* decreases as a/c increases.

In most cases maximum KI* is at the deepest point. But in some cases maximum KI* can be at surface point depending on the geometry and the loading. Crack propagates at the point which has the maximum KI*. In Figure 4.1, a crack propagating at the surface point is shown.

In inner surface semi-elliptic crack cases, as a/c gets closer to 1 (means circular crack), KI* of the surface point increases, while KI* of the deepest point decreases. This explains that why cracks propagate to an elliptic shape. When a/c is 1, KI* of surface points forces the crack propagate at the surface and when crack gets an elliptic shape KI* of the surface point decreases and stops propagating at surface.

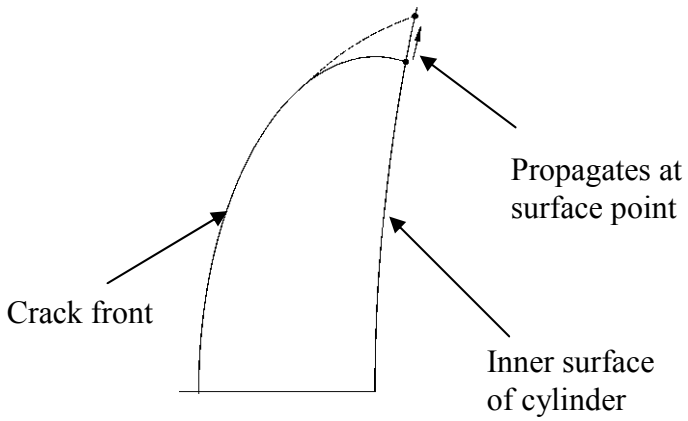

Figure 4.1 Propagation of a circumferential inner crack

The model used in this study is verified with four different cases. The first one was embedded semi-elliptic crack in an infinite medium. Results from closed formulas and ANSYS were compared. The results matched almost exactly.

For the other cases, ANSYS results were matched with some a/c and R/t values, and for other a/c and R/t values the results were parallel but different. Each case considered in this study was valid for spesific a/c and R/t ranges. As these values get out of the specified range, the results obtained from this study get invalid. So, these results are case dependent. This is because of the nature of the problem. At the moment, there is no generalized exact formula for all types of cracks. It is believed that this study was able to create a generalized crack model with an acceptable error. APDL codes are generated to achieve this result. Finite element analysis is a computer dependent method. Therefore in the following years, due to the development in computer technology, this method will also develope.

CHAPTER 5

CONCLUSION AND FUTURE WORK

APDL codes are developed for ten cases in this study. Six of them are for mechanical loading and the remaining four of them are for thermal loading of different geometries. Thermal load has not been applied to the geometries containing embedded cracks. The results are obtained for different R/t, a/c and a/t values. Ten APDL codes are developed to solve each ten geometries with different R/t, a/c and a/t values. This goal is achieved mostly. But for some cases, mostly the cases with sharp elliptical path (e.g. a/c=0.2), meshing can not be done with a straightforward way. Special effort is needed. Element sizes are aligned according to the geometry.

This thesis study can be extended by the following subjects

- In this thesis study, homogeneous isotropic material is considered. In the future, FGM (Functionally Graded Material) can also be considered.
- Elasto-plastic fracture mechanics can be considered with these crack types.
- This work can be extended with different dimensions of structure and crack.
- Conical shapes can also be considered.

REFERENCES

[1] Gery Wilkowsky, Leak-Before-Break: What Does It Really Mean? Journal of Pressure Vessel Technology, August 2000, Volume 122, Issue 3, pp. 267-272

[2] A. Zahoor, Closed Form expressions for Fracture Mechanics Analysis of Cracked pipes. Journal of Pressure Vessel Technology 1985, vol.107, pp.203-205.

[3] Raju IS, Newman Jr C. Stress intensity factors for internal and external surface crack in cylindrical vessels. Journal of Pressure Vessel Technology 1982, vol.104, 293–8.

[4] A.R.Shahani, S.M.Nabavi, Closed form stress intensity factors for a semi-elliptical crack in a thick-walled cylinder under thermal stress. International Journal of Fatigue 28, 2006, pp.926-933

[5] A.R.Shahani, S.M.Nabavi, Transient Thermal stress intensity factors for an internal longitudinal semi-elliptical crack in a thick-walled cylinder. Engineering Fracture Mechanics 74, 2007, pp.2585-2602

[6] A.R.Shahani, S.M.Nabavi, Calculation of stress intensity factors for a longitudinal semi-elliptical crack in a finite-length thick-walled cylinder. Fatigue and Fracture of Engineering Materials and Structures 31, 2008, pp.85-94

[7] A.R.Shahani, S.E. Habibi, Stress intensity factors in a hollow cylinder containing a circumferential semi-elliptical crack subjected to combined loading. International journal of Fatigue, 29, 2007, pp. 128-140

[8] Naoki Miura, Yukio Takahashi, Hiroshi Shibamoto, Kazuhiko Inoue, Comparison of stress intensity factor solutions for cylinders with axial and circumferential cracks, Nuclear Engineering and Design 238, 2008, pp.423-434

[9] B.Acar, Finite Element Analysis of Fracture Mechanics Problems, Master Thesis, June 1997

[10] G.Atalay, A Computational Elastic Fracture Analysis of Cylindrical and Conical Structures, September 2002

[11] Ö.İnan, Three Dimensional Fracture Analysis of FGM Coatings, September 2004

[12] B.Sabuncuoğlu, Fatigue Crack Growth Analysis Models for Functionally Graded Materials, January 2006

[13] S.Köşker, Three Dimensional Mixed Mode Fracture Analysis of Functionally Graded Materials, September 2007

[14] Release 11.0 Documentation for ANSYS

[15] Fracture Mechanics: Fundamentals and Applications, Anderson, T.L., 2005